RESEARCH AND MODELLING IN CIVIL ENGINEERING 2019

EDITED BY **JACEK KATZER**
KRZYSZTOF CICHOCKI
AND **JACEK DOMSKI**

KOSZALIN UNIVERSITY OF TECHNOLOGY

KOSZALIN UNIVERSITY OF TECHNOLOGY

RESEARCH AND MODELLING
IN CIVIL ENGINEERING
2019

Edited by
Jacek Katzer, Krzysztof Cichocki and Jacek Domski

KOSZALIN 2019

Table of contents

Preface

This monograph was created as the scientific outcome of the "4th Central European Civil Engineering Meeting 2019" (CECEM 2019) which took place at Koszalin University of Technology (Faculty of Civil Engineering, Environmental and Geodetic Sciences) in Poland, 3-7 June 2019. The meeting was organized by an international scientific society "Research and Modelling in Civil Engineering" in cooperation with Koszalin University of Technology. Researchers representing four countries (Bulgaria, Czech Republic, Portugal and Poland) were attending the meeting. The meeting was organized as an ERASMUS+ event. CECEM 2019 had both staff training (STT) and teaching (STA) character and was a great opportunity to share knowledge and experience in the field of civil and structural engineering. The week-long programme included round table discussions, presentations, problem solving cases, lab visits, workshops and social events. The main objectives of CECEM 2019 included peer-learning, networking, transfer of knowledge and sharing research experiences and best practices. Participants brought into the discussion examples from their own institutions and present best practices and innovative approaches to the issues addressed.

The meeting was following the "1st Central European Civil Engineering Meeting 2016" (CECEM 2016), the "2nd Central European Civil Engineering Meeting 2017" (CECEM 2017) and the "3rd Central European Civil Engineering Meeting 2018" (CECEM 2018). All meetings took place at Koszalin University of Technology (Faculty of Civil Engineering, Environmental and Geodetic Sciences) in Poland. The 1st CECEM 2016 (21 - 23 June 2016) attracted researchers from Czech Republic and Ukraine. The 2nd CECEM 2017 (5 - 9 June 2017) attracted researchers from Czech Republic, Slovakia, Romania and Poland. The 3rd CECEM 2018 (4 - 8 June 2018) attracted researchers from Czech Republic, Slovakia, Spain, Poland and Vietnam.

During CECEM 2019 multiple scientific presentations were delivered and discussed. Organizers decided to prepare a monograph as the outcome of the meeting to prevent these high quality presentations from perishing. Willing authors prepared extended versions of their papers for publication. After very careful analyses and peer-review process 9 chapters were accepted for the final version of the monograph. The inclusion of a chapter in the monograph was free of charge for the authors. The peer-reviewing, editing and printing costs were covered by Faculty of Civil Engineering, Environmental and Geodetic Sciences at Koszalin University of Technology.

The 5th CECEM 2020 will take place in Olsztyn (Poland), 1 - 5 June 2020. It will be hosted by University of Warmia and Mazury in Olsztyn. Colleagues from partner and non-partner institutions are encouraged to take part in the event. Contact

person: prof. Jacek Katzer (cecem@cecem.eu). All details concerning the 5th CECEM 2020, previous meetings and an international scientific society "Research and Modelling in Civil Engineering" are available at the meeting website: www.cecem.eu. Free electronic versions of the current and previous monographs are also available there.

Editors
Jacek Katzer, Krzysztof Cichocki and Jacek Domski

cecem@cecem.eu
www.cecem.eu

1. Thermally loaded concrete specimens: fractal dimensions of fracture surface and mechanical fracture parameters

Iva Rozsypalová[1], Tomáš Trčka[2], Petr Frantík[1], Hana Šimonová[1], Barbora Svobodová[1], Petr Daněk[1], Zbyněk Keršner[13]

[1] *Brno University of Technology, Faculty of Civil Engineering, Brno, Czech Republic, iva.rozsypalova@vutbr.cz, orcid.org/0000-0003-3109-3820, kitnarf@centrum.cz, orcid.org/0000-0003-0141-2966, simonova.h@vutbr.cz, orcid.org/0000-0003-1537-6388, BaraKory@seznam.cz, orcid.org/0000-0001-7922-0847, petr.danek@vutbr.cz, orcid.org/0000-0001-8489-9452, kersner.z@fce.vutbr.cz, orcid.org/0000-0003-4724-6166*

[2] *Brno University of Technology, Faculty of Electrical Engineering and Communication, Brno, Czech Republic, xtrcka03@gmail.com, orcid.org/0000-0002-3704-9532*

Abstract: The chapter deals primarily with the fractal dimension of fracture surfaces of fractured concrete specimens after thermal loading. These specimens were obtained from experimental concrete panels after extensive fire experiments. The panels were exposed on one side to heat from a furnace at nominal maximum temperatures of 550, 600, 800 and 1000 °C. Reference specimens unexposed to heat load were also tested. Specimens with nominal dimensions of $100 \times 100 \times 400$ mm and a 33 mm central edge notch were tested in the three-point bending configuration; load versus displacement diagrams were recorded, corrected and evaluated. Each set contained 4 specimens, and a total of 20 specimens were processed. The following basic mechanical fracture parameters were assessed: modulus of elasticity, effective fracture toughness and specific fracture energy. The fracture surfaces (ligaments) of all tested specimens were analyzed in detail after the above-mentioned three-point bending tests. The ligaments were scanned via a 2D laser profilometer and the fractal dimension of selected sections of these surfaces was measured. The fractal dimension of the fracture surface sections was estimated using the walking divider method. Finally, the chapter presents the correlation among the fractal dimensions, the temperatures in the concrete at different distances from the heated side and the previously obtained and above-mentioned mechanical fracture parameters.

Keywords: concrete, high-temperature, testing, material properties, fractals

1.1. Introduction

Cement-based composites, with concrete as their main representative, rank among the most widely used building materials. Although concrete is traditionally considered to be fire-resistant, thermal loading affects the whole range of its mechanical, transport and other properties – see e.g. (Aïtcin and Mindess, 2011), (Nevile, 2011). Consequently, the monitoring of many aspects of fire-resistance – especially that of load-bearing reinforced and pre-stressed concrete structures – has long been a topical issue for research, recommendations, and codes – see e.g. (Purkiss and Li, 2011), (Wang *et al.*, 2013), (RILEM TC 129-MHT, 1997), (Eurocode EN 1991-1-2:2002/AC, 2013). This chapter is focused on a specific investigation regarding this issue: selected specimens were sawn from thermally loaded experimental plain concrete panels and submitted to fracture tests, after which the fractal dimensions of the selected fracture surface sections were evaluated. The results of this research also include observed correlations between fractal dimension values and selected (previously determined) mechanical fracture parameters of thermally loaded concrete.

1.2. Background: fracture complexity

Concrete, mortar, rock, ceramics, masonry and other building materials exhibit quasi-brittle behaviour; see (Shah *et al.*, 1995), (Bažant and Planas, 1998), etc. Advanced fracture tests performed on these materials are typically focused on the determination of mechanical fracture properties and basic relationships such as fracture toughness, fracture energy, cohesive law, tensile strength, etc. These are usually determined from specimens loaded by controlled increasing displacement at very low velocities. This loading with almost negligible global dynamic effects is known as quasi-static. However, fracture in a quasi-brittle material is a dynamic process and a naturally transient phenomenon with nonlinear characteristics. These characteristics are commonly overlooked or unknown, though their study can have a deep impact on the understanding of fracture processes and can have an effect on the definition and determination of fracture properties.

During the loading of tested specimens, a complex acoustic signal is generated containing information about changes in the inner structure of the stressed material. Nonlinear signal analysis allows, for example, metric entropy not only to estimate the dominant state variables in a loaded system but also to quantify microstructural changes in a material (Carpinteri and Lacidogna, 2008), (Edelman *et al.*, 2017). Material response to dynamic loading can be influenced by low energy periodic excitation. The influence of the generator on the propagation of microcracks or dislocations during loading has not yet been sufficiently investigated, but it is believed that provoked energy release can have a measurable impact on the entire fracture process. Methods of measuring this

nature are being developed together with the search for correlation between the structural characteristics of material and the spectrum of the excitation signal.

Today, the fracture properties of building materials are playing an increasingly important role in their application. Higher quality natural materials and especially artificial composites are now being employed in the construction industry to build structures that are required to be durable and reliable under often unknown critical loads. Thanks to this advance, properties that were previously neglected have come to the foreground.

Classical Fracture Mechanics works in the case of the quantification of parameters characterizing a fracture process with a geometrically simple fracture surface created by the projection of a fracture surface into a plane. However, in reality it is always a more or less rough surface whose properties are lost after projection. That is why Fractal Fracture Mechanics is being developed. It takes the more natural approach of looking at the fracture surface as a fractal set whose generalized dimension forms a new generic attribute of the fracture surface: see (Carpinteri *et al.*, 1999), (Carpinteri *et al.*, 2002), (Carpinteri and Puzzi, 2006), (Alves and Alkimin de Lacerda, 2012) and (Ficker, 2007). The change to viewing the fracture surface in terms of fractal geometry means that it is no longer possible to speak reliably about the fracture area of the fracture surface since its determination is linked to the scale. With increasing detail, the measured approximated area, which is not limited in mathematical terms, grows. The fracture area can then be viewed rather as a projection of the fracture surface into a plane along the propagating crack.

Thanks to the pioneering work of Benoit Mandelbrot (Mandelbrot, 1982), (Mandelbrot *et al.*, 1984), the search for relationships between the geometric properties of fracture surfaces and the mechanical properties of fractured material has begun. The fractal approach has been successfully applied to the brittle fracture of ceramics (Passoja and Amborski, 1978), (Mecholsky *et al.*, 1989), the fracture of metals (Mandelbrot *et al.*, 1984), the fracture of quasi-brittle materials (Carpinteri *et al.*, 1999), (Borodich, 1999), (Mourot *et al.*, 2005), polymers (Kozlov *et al.*, 2004), porous gel (Ficker, 2008), and rocks (Badabagli and Develi, 2003). In this chapter, fracture surface fractality is determined on a set of selected thermally loaded concrete specimens obtained from experimental concrete panels after fire tests.

1.3. Material, concrete panels, and fire tests

A total of 5 large-format concrete slabs (panels) with a nominal size of 2300 × 1300 × 150 mm were produced for extensive fire testing. The formwork was specially constructed from waterproof plywood boards and covered with plastic film to facilitate subsequent unmoulding.

To ensure safety during panel testing and handling, it was necessary to reinforce the panels with a welded wire mesh (wire diameter 6 mm, square grid 100 × 100 mm) placed 15 mm from the bottom side of the experimental panels.

Subsequently, K-type thermocouples (capable of measuring temperatures ranging from −200 °C to 1250 °C) were installed in order to record the temperatures reached during the fire tests. Each panel was provided with a total of 10 thermocouples located along the longitudinal axis of the panel. Three sensors were installed 10 mm from the bottom side of the panel, three sensors were at the upper side of the panel (here, installation took place after casting), three sensors were in the middle of the panel's thickness (i.e. 75 mm from the bottom side), and additionally one sensor was located at one fourth of the panel's thickness (i.e. 37.5 mm from the bottom side). In the direction of the panel's length, these thermocouples were positioned at the centre (cross-section with four thermocouples) and edges of the considered heated area, i.e. 350 mm from the edges of the panel (cross-sections with three sensors). A detailed scheme of the positions of the thermocouples placed in the experimental panels is shown in Fig. 1.1.
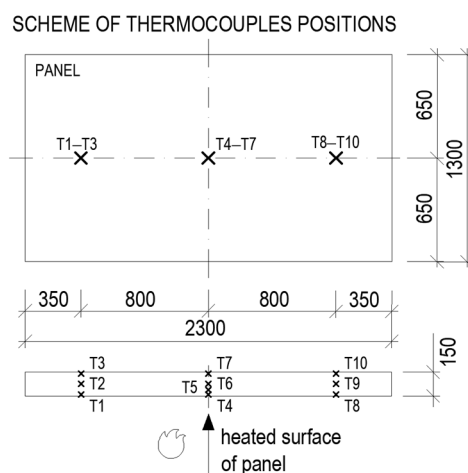
Fig. 1.1. Scheme showing the positions of thermocouples T1–T10 in the experimental panels

Standard structural concrete was selected for the concrete mixture used to produce the experimental panels. No modifications were performed to achieve better fire-resistance properties. The panels were made of C30/37 strength class concrete with quartz aggregate (maximum grain size 16 mm). The composition of the fresh concrete mixture is shown in Table. 1.1. After casting, the surface of the specimens was covered with plastic film to prevent water evaporation. When

seven days had passed, the formwork and foil were removed. Then, the panels were unmoulded and kept under standard laboratory conditions for another 5 to 6 months, after which the fire tests were carried out.

Table. 1.1. Fresh concrete composition

Component	Amount per 1 m³ [kg]
Cement CEM I 42.5 R	335
Water	170
Sand 0–4	840
Aggregate 8–16	880
Fly ash	50
CX Isoflex 833 Superplasticizer	2.67

The concrete experimental panels were subjected to high temperatures from a gas furnace designed for the testing of building components and structures. The furnace is installed at the AdMaS Science Centre, which belongs to the Faculty of Civil Engineering, Brno University of Technology, Czech Republic. The panels were positioned on the top of the furnace (see Fig. 1.2.), thereby heating them on one side. The unheated sides of the panel were left to cool spontaneously.
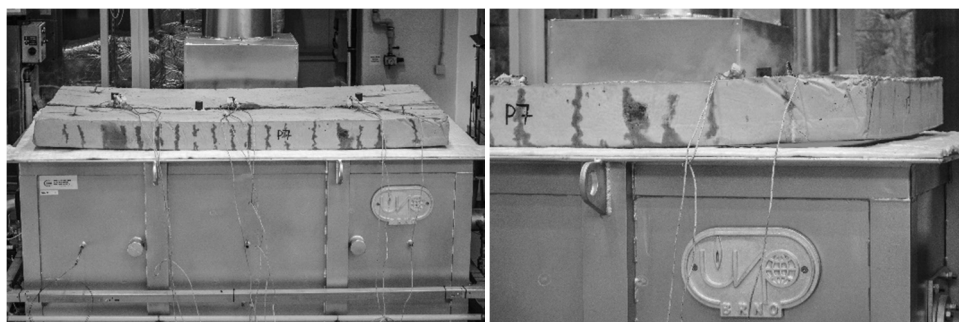
Fig. 1.2. The gas furnace designed for studying the behaviour of materials exposed to high temperatures at the AdMaS Science Centre during the fire testing of panel P7, which was heated up to a maximum nominal temperature of 1000 °C; detail on the right

The exposure of panels to high temperatures can be divided into two phases. First, the panels were loaded by a rapid rise in temperature from the furnace, where the individual nominal maximum temperatures were 550, 600, 800, and 1000 °C (corresponding panel designations P1, P2, P3, and P7, respectively; P4 was a reference panel without thermal loading). The temperature increase in the furnace was controlled according to the ISO 834 standardized curve specified in EN 1992-1-2 until the desired temperature level was reached. In the second phase, the temperature in the furnace was maintained at the maximum nominal

temperature for 60 minutes. After the second phase had finished, the furnace was turned off and the panels were left on the top of the furnace to cool spontaneously to room temperature. Records of the temperatures measured in the gas furnace during each fire test are shown in Fig. 1.3. Part of the evaluation of these fire experiments can be found in, for example, (Rozsypalová *et al.*, 2018).
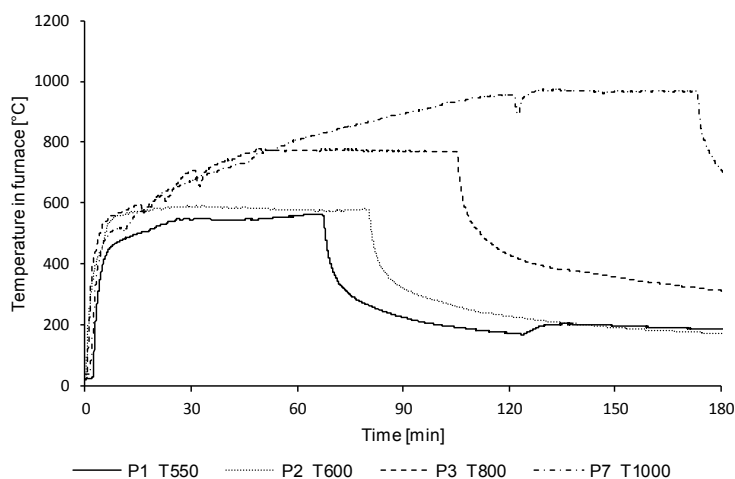

Fig. 1.3. Graph of the temperatures measured in the furnace during the fire testing of experimental panels P1, P2, P3, and P7

1.4. The specimens sawn from panels for fracture testing, and their basic mechanical fracture parameters

The four specimens intended for the fracture experiments (Rozsypalová *et al.*, 2017) were cut from the central (most thermally loaded) part of each of the above-mentioned experimental panels – see the scheme in Fig. 1.4. These specimens were labelled A, B, C and D (with nominal dimensions of 100 × 100 × 400 mm). The specimens were subsequently provided with an initial central edge notch cut to a depth of approximately 1/3 of the specimen height and then tested in the three-point bending configuration – see the selected photos in Fig. 1.5. for illustration. Details regarding the evaluation of the fracture tests from various points of view can be found in, for example, (Šimonová *et al.*, 2017a) and (Šimonová *et al.*, 2017b). After the fracture tests had been performed, the fracture surface of each specimen was scanned via a 2D laser profilometer – Fig. 1.4. (right) schematically shows the surface area of the ligament (A_{lig}) under investigation. The maximum temperatures within the concrete specimens at different distances from the heated side of the panels are presented in Table. 1.2. These data were obtained via the nonlinear approximation of the temperatures measured by the

thermocouples – see (Rozsypalová *et al.*, 2018) for details. The mean values obtained for several basic mechanical fracture parameters of the concrete specimens presented in (Rozsypalová *et al.*, 2017) are introduced in Table. 1.3.
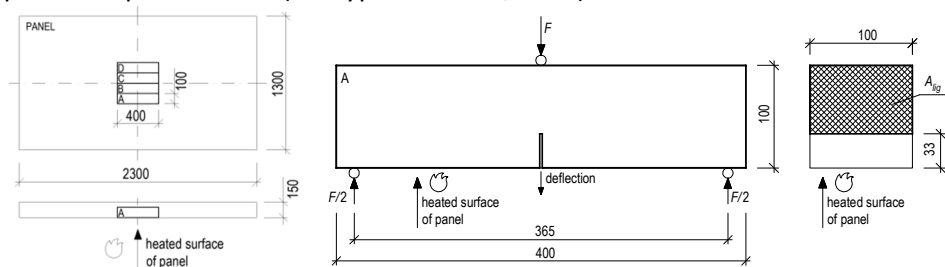
Fig. 1.4. Panel diagram and positions of specimens sawn off for fracture experiments (left), configuration of the fracture test in three-point bending and designation of the investigated ligament area
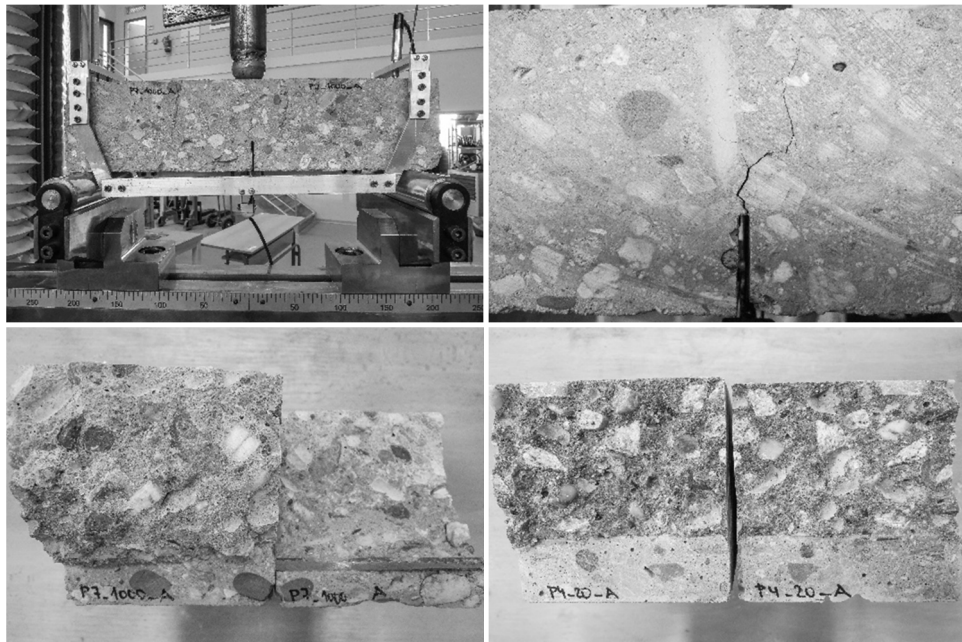

Fig. 1.5. Illustration of a fracture test in the three-point bending configuration and detail of the crack path; examples of selected specimens after testing – the ligament of P7_1000_A (maximum furnace temperature 1000 °C) and P4_20_A (reference specimen)

Table. 1.2. Maximum temperature [°C] in specimens at different distances from the heated side of the panel/specimen

Distance [mm]	P4_20	P1_550	P2_600	P3_800	P7_1000
0 (heated side of panel)	20	565	591	777	974
33 (depth of specimen notch)	20	251	293	388	501
100 (upper side of specimen)	20	113	137	168	248

Table. 1.3. Mean values obtained for basic mechanical fracture parameters of the concrete specimens

Parameter	Unit	P4_20	P1_550	P2_600	P3_800	P7_1000
Elasticity modulus	GPa	38.0	13.7	9.87	3.91	2.48
Fracture toughness	MPa·m$^{-1/2}$	1.181	0.922	0.938	0.774	0.449
Fracture energy	J·m^{-2}	138.1	191.2	198.1	321.8	442.0

1.5. Ligament scanning procedure

Optical profilometry is widely used to determine surface roughness and topography in a variety of industrial applications. A number of different target surfaces can be measured and evaluated via this contactless and non-destructive method. Several principal methods, such as triangulation and interference, provide two-dimensional data (line scans) or three-dimensional surface images. A commercially available laser profilometer was used to precisely scan the topography of the concrete specimens in our experiments.

2D laser profilometers generally operate with a semiconductor laser of a defined wavelength and use the laser triangulation principle for two-dimensional profile detection on different target surfaces. The laser beam is enlarged using special lenses to form a static laser line and is projected onto the target surface. The diffusely reflected light from the laser line is replicated on a sensitive sensor matrix by a high-quality optical system and evaluated in two dimensions. In addition to distance information (z-axis), the exact position of each point on the laser line (x-axis) is also acquired by an integrated controller. The obtained values are finally output in a two-dimensional coordinate system that is fixed with respect to the sensor (Micro-Epsilon: Instruction manual, 2D/3D laser scanner). The basic design of a typical 2D laser profilometer is shown in Fig. 1.6.

A mobile laser profilometer (a *scanCONTROL 2750-100* made by Micro-Epsilon) was used in this measurement system. It employs a semiconductor laser with a wavelength of 660 nm (visible red line). The declared minimum resolution is 25 μm and it achieves scanning speeds of up to 4000 profiles per second (with 640 points per profile) (Micro-Epsilon: Instruction manual). It is possible to obtain the surface topography in 3D by moving either the target samples or the laser scanner

itself. In our experimental set-up, the laser scanner is mounted on a tripod and specimen motion under the fixed 2D profilometer is realized by a precise linear motion sliding table with a stepper motor. The designed system is capable of smooth and adjustable specimen motion (smallest step 2.5 µm) and supports a maximum specimen weight of 10 kg. Sliding table motion is controlled by a developed microprocessor driver that is linked to the master control PC. The issue of distance selection between the acquired line profiles should be solved with respect to achieving a compromise between the expected measurement accuracy and the amount of processed and evaluated data. In the case of our evaluated surfaces, a distance of 50 µm between the scanned lines/profiles (shift on the *y*-axis) was selected, and the spacing between neighbouring points within one line/profile (*x*-axis) was also 50 µm. Illustrative photos of the experimental set-up in the laboratory are shown in Fig. 1.7.
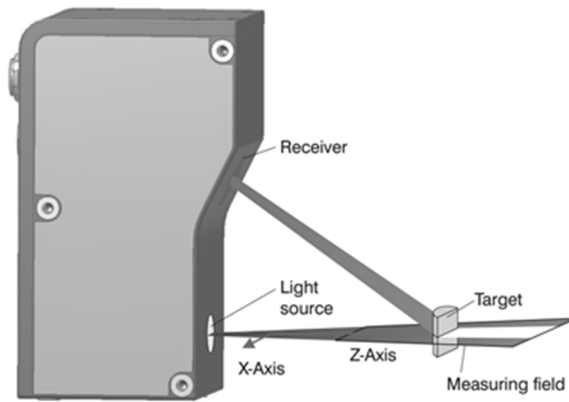
Fig. 1.6. The basic design of a typical 2D laser profilometer, taken from (Micro-Epsilon: Instruction manual)
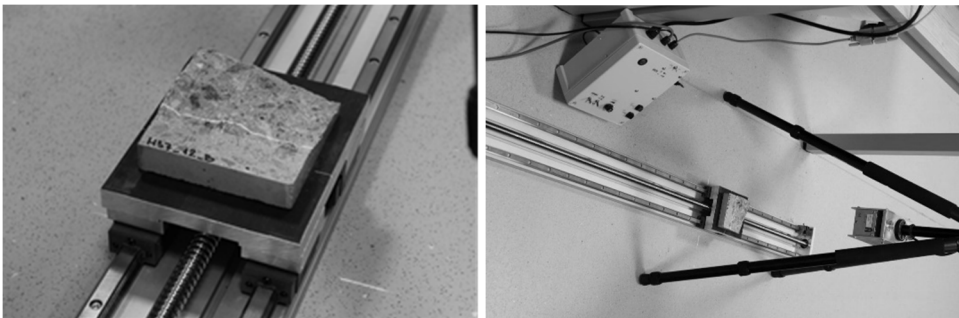
Fig. 1.7. Photos from the experimental set-up

The whole experimental set-up is fully automated and the measuring process is controlled by software developed in the MATLAB environment. It allows the control of movements defined specifically for each specimen via the microprocessor driver and continuous profile measurement by the 2D profilometer. The integrated FireWire interface enables complete control of the laser scanner via the computer, as well as high-speed data acquisition. The software also provides pre-processing (profile averaging and basic filtration) of the obtained data, including their storage in the resulting data matrix. After the surface scanning, the final 3D specimen topography can also be displayed using this software (see Fig. 1.8. and Fig. 1.9. for illustration) and some additional operations can be performed (cropping the monitored area, rendering 2D and 3D surfaces, saving results in different data formats, etc.).
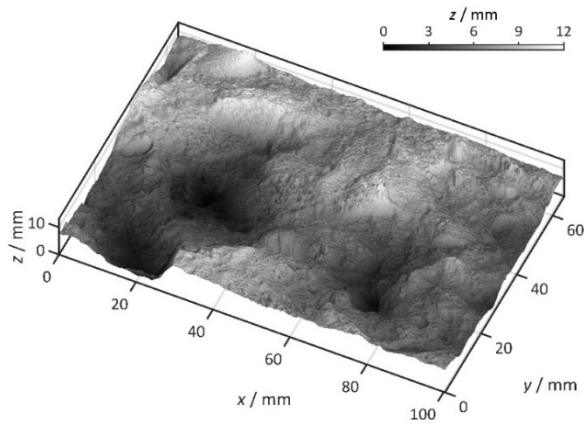
Fig. 1.8. 3D topography – specimen P4_20_C_2
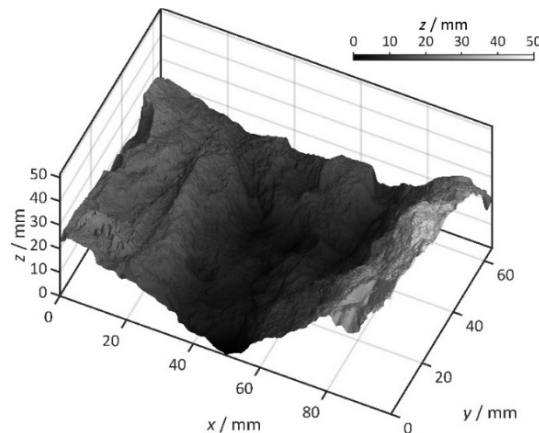
Fig. 1.9. 3D topography – specimen P7_1000_C_2

A complex and modular software package was also developed for the post-processing of the measured data. The basic module allows the calculation of some basic surface roughness parameters inspired by technical standards such as ISO 25178, ISO 4287:1997 (Geometrical Product Specifications (GPS) – Surface texture: Profile method – Terms, definitions, and surface texture parameters), etc. The proposed roughness parameters can be evaluated from individual 2D profiles or whole 3D surfaces. Another separate module is focused on the determination of the total fracture area in a selected region of the scanned surfaces. It is solved by a simple algorithm that allows the approximate surface area between the four neighbouring points of the data matrix (z-axis) to be quantified by dividing the resulting pattern in a 3D coordinate system into two triangles. The area of these triangles can be calculated on the basis of Heron's formula or suitably selected vector products. The total fracture area is therefore determined by the sum of the areas of all triangles in the region of interest.

1.6. Fractal dimension calculations

The estimation of the fractal dimension of each selected fracture surface section was performed using the walking divider method – see e.g. (Annadhason, 2012). The procedure for calculating the dimension estimate is to determine how many lines of a given length l (scale) are required to cover the measured curve. Changing this scale determines how the number of covering lines $N(l)$ is changed, while for the measured length $L(l)$ the following applies: $L(l) = N(l) \cdot l$. Ideally, the dependence of the number of covering segments given by the expression $N(l) = a \cdot l^{-D}$ is linear in a logarithmic representation (see Fig. 1.10. for the ligament of specimen P7_1000_A2 and a selected section at a distance of 5 mm from the initiation notch), where a is an unknown constant and a D is an estimate of the fractal dimension. The result is an expression for the length, $L(l) = a \cdot l^{1-D}$. The constants can be obtained by approximating the measured lengths of the curve for the selected scales. The calculated dimension D estimate for the curves (sections) at different distances d from the notch for the selected fracture surface P7_1000_A2 is illustrated in Fig. 1.11. In this case, the dimensionless value of the fractal dimension is $D = 1 - (-0.0135) = 1.0135$.
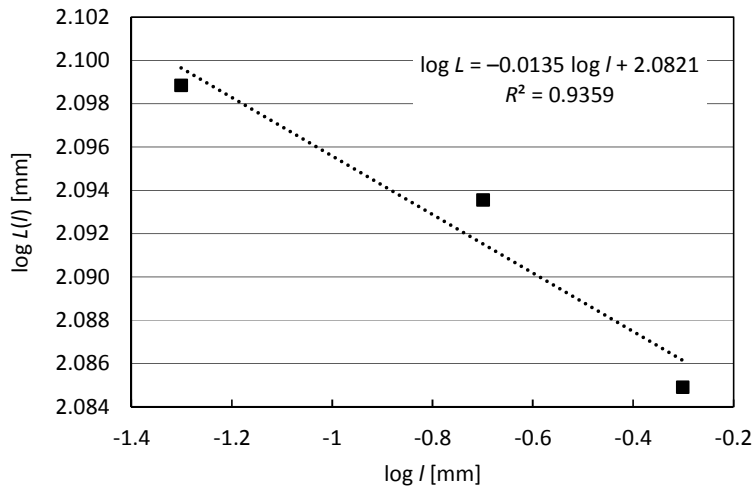
Fig. 1.10. Regression line (including coefficient of determination) approximating the points of the logarithm of the length of the curve *L(l)* to the logarithm of the length of scale *l*, which is the source for determining the fractal dimension of the selected section of the ligament
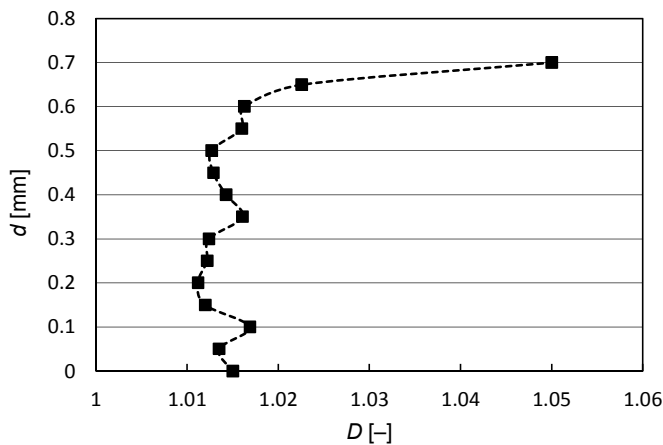
Fig. 1.11. Estimated fractal dimension *D* along the height *d* of the ligament (at different distances from the notch) of specimen P7_1000_A2 for 15 selected sections

1.7. Results and discussion

1.7.1. Primary characterization of ligament roughness

For the primary evaluation of the roughness of the obtained fracture surfaces a procedure was programmed which calculates the roughness parameter *r* defined as $r = L/L_p$ [–], where *L* means the length of the curve representing a section of the fracture surface and L_p is the length of its projection onto axis *x*. The graphs in Fig. 1.12. to Fig. 1.16. show the results of the calculation of ratio *r* for the studied specimens (a selected surface for each specimen: A, B, C, and D), while only a carefully selected area of the complete scanned surface was included in the calculation (trimming the edges of the specimen and focusing on the ligament fracture area A_{lig} only). Basic statistics for all roughness parameters *r* are shown in Table. 1.4. This statistical evaluation was based on eight mean values obtained for the parameters *r* of each ligament of four specimens after the fracture tests.

Table. 1.4. Basic statistics for roughness parameters *r* for all tested specimens/panels

Parameter	Unit	P4_20	P1_550	P2_600	P3_800	P7_1000
Mean value	–	1.127	1.173	1.185	1.258	1.265
Standard deviation	–	0.008	0.023	0.029	0.055	0.118
Coefficient of variation	%	0.7	1.9	2.4	4.4	9.4

Fig. 1.12. The roughness parameter along the height of the ligament after the fracture test (section number) for specimens from the reference panel for 20 °C, i.e. without thermal load
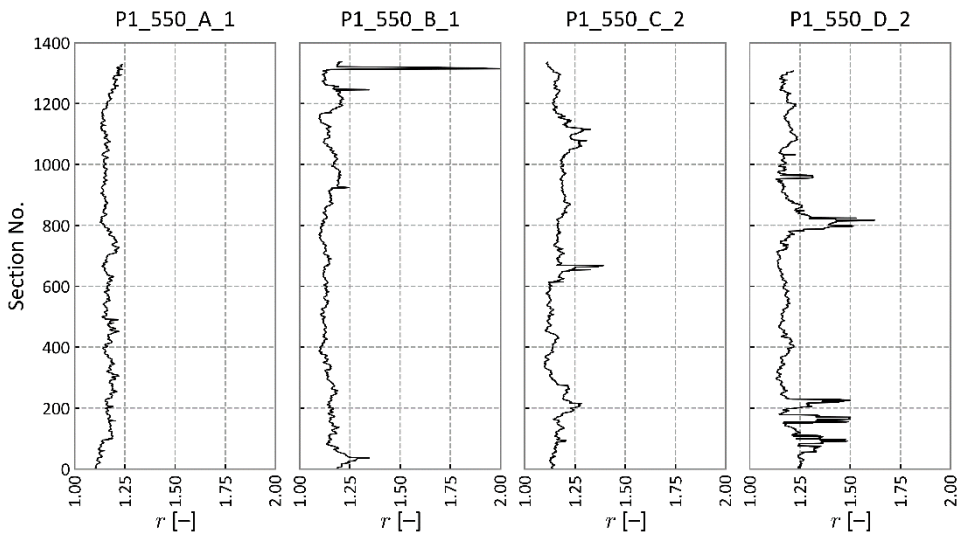
Fig. 1.13. The roughness parameter along the height of the ligament after the fracture test (section number) for specimens from the panel thermally-loaded with a nominal maximum furnace gas temperature of 550 °C
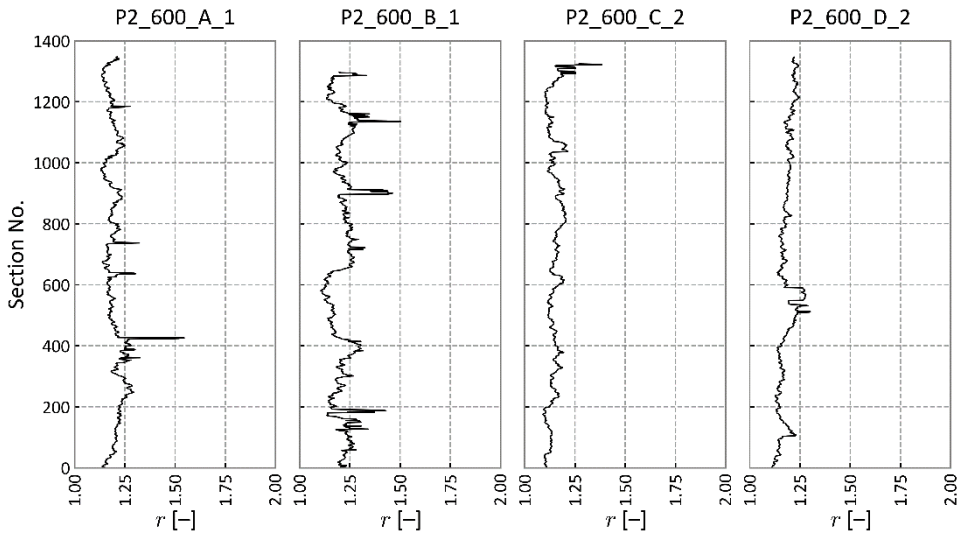
Fig. 1.14. The roughness parameter along the height of the ligament after the fracture test (section number) for specimens from the panel thermally-loaded with a nominal maximum furnace gas temperature of 600 °C
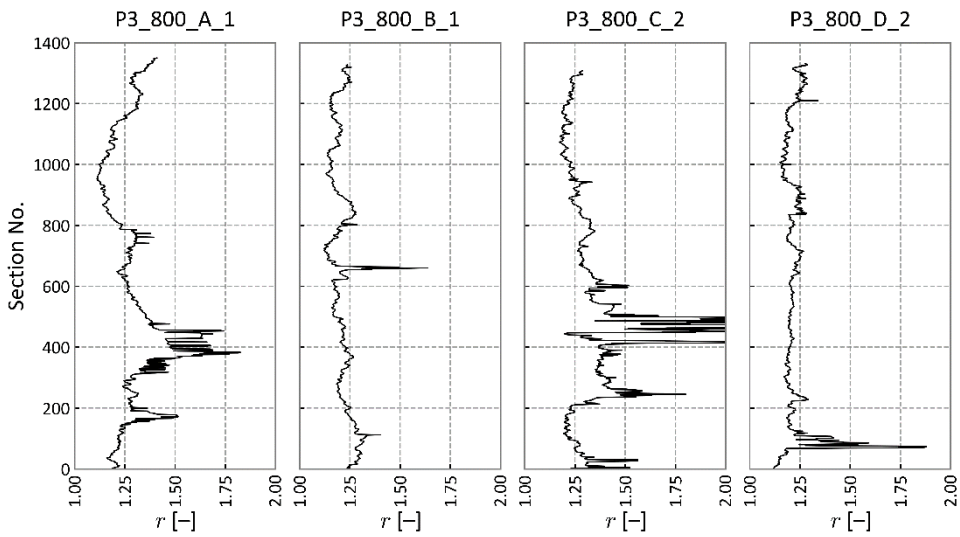
Fig. 1.15. The roughness parameter along the height of the ligament after the fracture test (section number) for specimens from the thermally-loaded panel with a nominal maximum furnace gas temperature of 800 °C

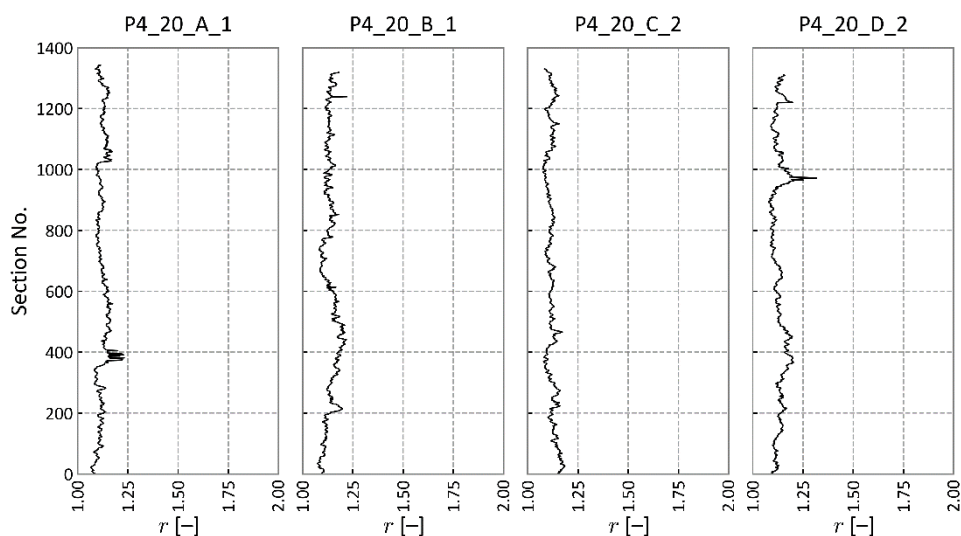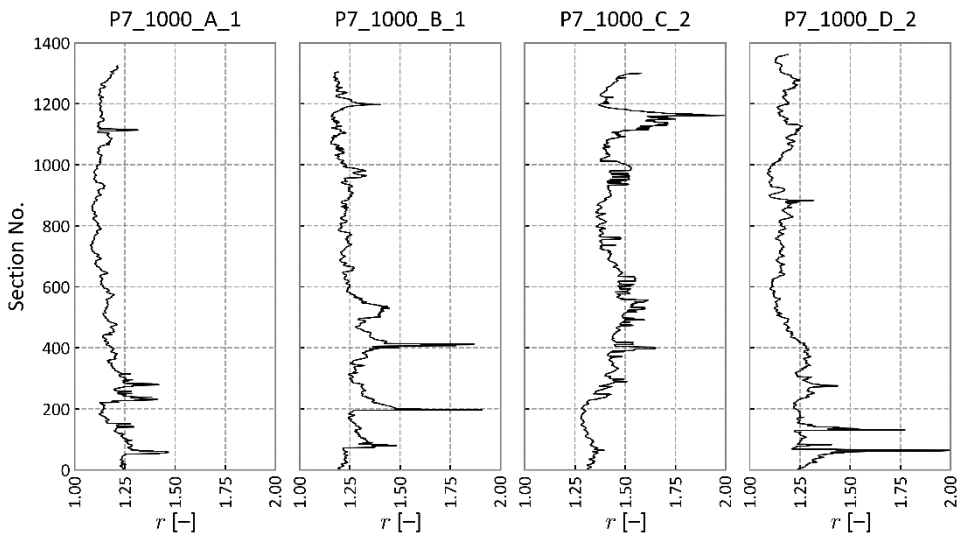**Fig. 1.16.** The roughness parameter along the height of the ligament after the fracture test (section number) for specimens from the thermally-loaded panel with a nominal maximum furnace gas temperature of 1000 °C

1.7.2. Fractal dimensions of ligaments

The procedure for the estimation of the fractal dimension D of selected fracture surface sections was introduced in the pertinent previous subchapter. Results for all studied fracture surfaces and 14 selected sections of these surfaces at increasing distances from the end of the initial notch are depicted in the following figures. In each figure it is possible to see four particular values for the fractal dimension D of the section of the fracture surface and a mean value with the range of standard deviation: Fig. 1.17. shows results for specimens from panel P4 (reference panel), while Fig. 1.18. to Fig. 1.21. show results for specimens from panels P1 (nominal maximum gas temperature 550 °C), P2 (600 °C), P3 (800 °C), and P7 (1000 °C), respectively. Global statistics for all the fractal dimension D measurements (mean values of individual mean values, etc.) are shown in Table. 1.5.
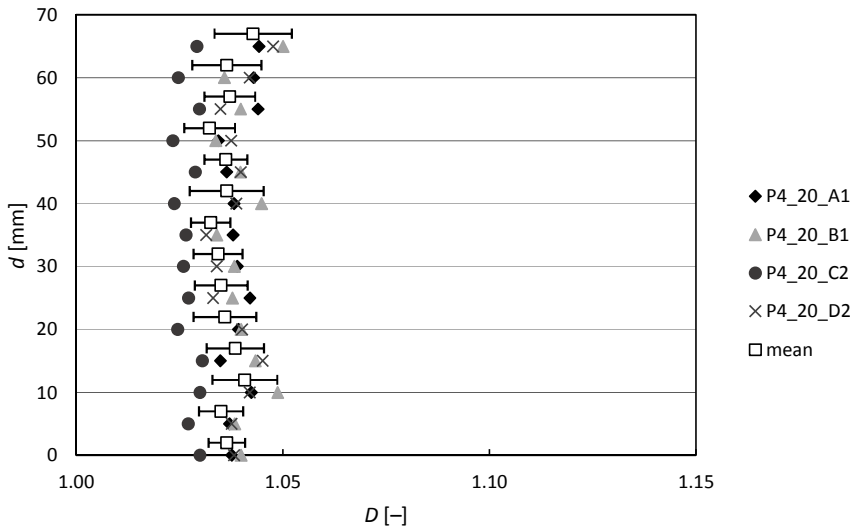
Fig. 1.17. Fractal dimension along the height of 4 ligaments P4_20 for selected line profiles; estimated temperature range between the lower and upper edge of the ligament: 20–20 °C (reference panel)
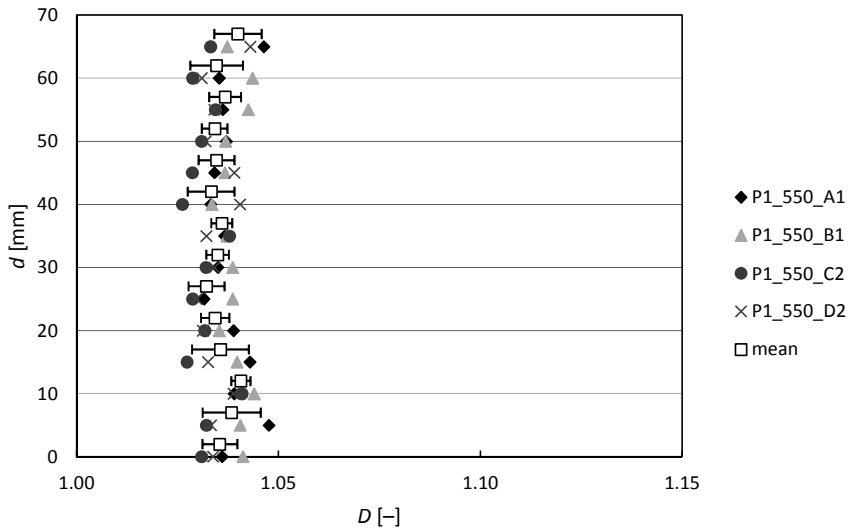
Fig. 1.18. Fractal dimension along the height of 4 ligaments P1_550 for selected line profiles; estimated temperature range between the lower and upper edge of the ligament: 250–115 °C
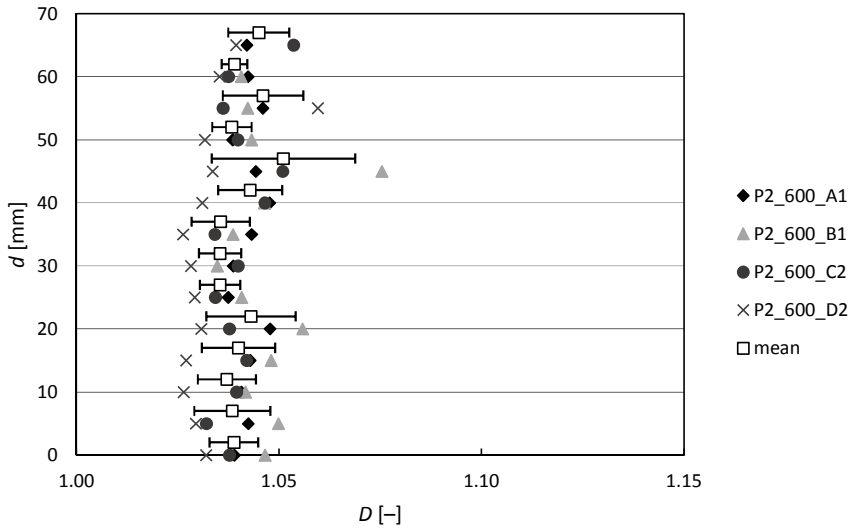
Fig. 1.19. Fractal dimension along the height of 4 ligaments P2_600 for selected line profiles; estimated temperature range between the lower and upper edge of the ligament: 300–140 °C
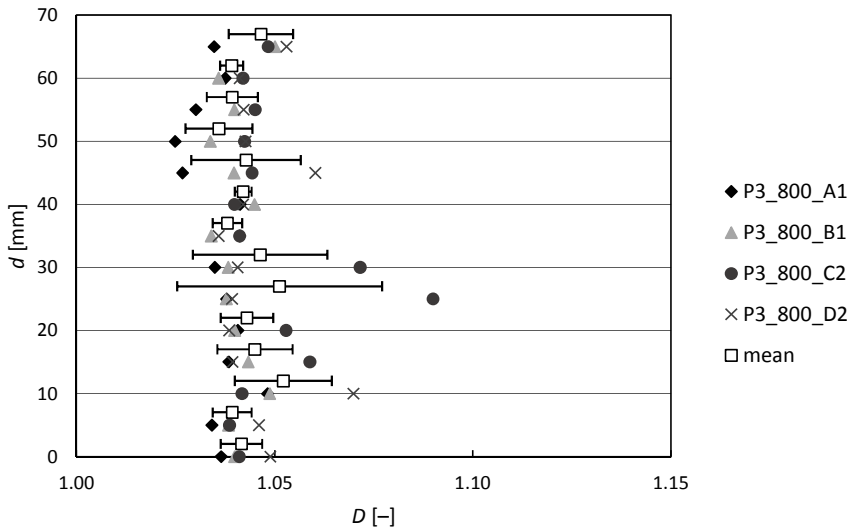
Fig. 1.20. Fractal dimension along the height of 4 ligaments P3_800 for selected line profiles; estimated temperature range between the lower and upper edge of the ligament: 390–170 °C
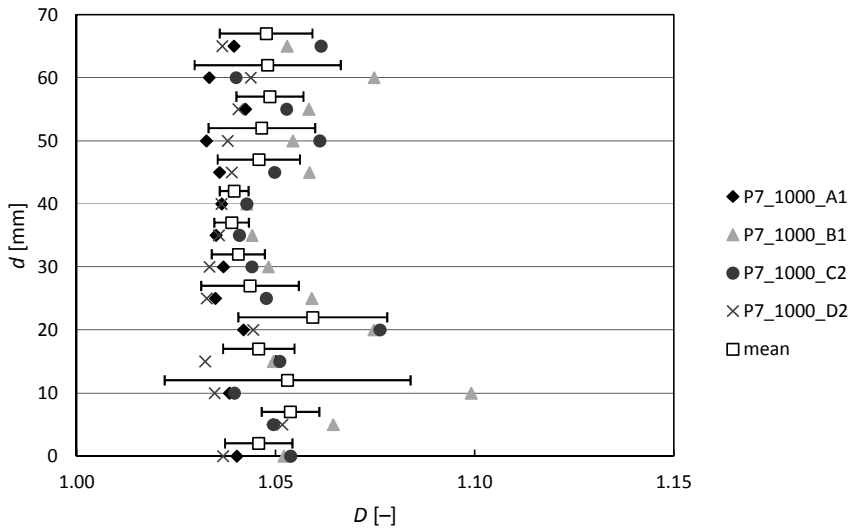
Fig. 1.21. Fractal dimension along the height of 4 ligaments P7_1000 for selected line profiles; estimated temperature range between the lower and upper edge of the ligament: 500–250 °C

Table. 1.5. Basic statistical parameters of fractal dimension *D* for all tested specimens/panels

Parameter	Unit	P4_20	P1_550	P2_600	P3_800	P7_1000
Mean value	–	1.0364	1.0358	1.0405	1.0431	1.0469
Standard deviation	–	0.00284	0.00242	0.00461	0.00480	0.00564
Coefficient of variation	%	0.27	0.23	0.44	0.46	0.54

1.7.3. Correlation among temperature, fracture properties and fractal dimensions

Correlation coefficients among the maximum temperatures, the mean values of selected, previously obtained, mechanical fracture parameters, and the values determined for roughness characteristics are shown in Table. 1.6. – the lower part of the symmetrical correlation matrix. The maximum temperatures correspond to three distances from the heated surface of the concrete specimens during fracture tests in three-point bending. In Table. 1.6. below the following notation is used to refer to parameters:

$T_{max, d0}$ – the maximum temperature at the heated side of the concrete panel ($d = 0$ mm), i.e. at the bottom side of the specimens,

$T_{max, d33}$ – approximation of the maximum temperature at distance $d = 33$ mm, equal to the depth of the specimen notch,

$T_{max, d100}$ – approximation of the maximum temperature at distance $d = 100$ mm, i.e. at the upper side of the specimen,

E – modulus of elasticity,

K_{Ice} – effective fracture toughness,

G_F – specific fracture energy,

r – roughness parameter,

D – fractal dimension.

Table. 1.6. Correlation coefficients [–] among the maximum temperatures, mechanical fracture parameters, and roughness characteristics

	$T_{max, d0}$	$T_{max, d33}$	$T_{max, d100}$	E	K_{Ice}	G_F	r	D
$T_{max, d0}$	1							
$T_{max, d33}$	1.00	1						
$T_{max, d100}$	0.98	0.99	1					
E	−0.97	−0.96	−0.92	1				
K_{Ice}	−0.94	−0.95	−0.98	0.84	1			
G_F	0.87	0.91	0.93	−0.76	−0.97	1		
r	0.93	0.95	0.93	−0.89	−0.92	0.94	1	
D	0.81	0.87	0.90	-0.74	-0.89	0.94	0.91	1.00

1.7.4. Discussion of the achieved results

The achieved results allow a number of conclusions to be drawn. These are conclusions about the influence of thermal loading on the roughness of fracture surfaces, the direction of one-side heating and distance from the heated surface, and on the values of mechanical fracture parameters. The possibility of characterizing fracture surface roughness also appears to be an important result.

The dependency of the roughness parameter *r* and also fractal dimension *D* of the fracture surface section on exposure to high temperatures and section position (distance *d* from the heated surface) was presented. It has been shown that exposure to high temperatures causes increased variability in the roughness parameter as well as the fractal dimension values and a slight increase in their mean values; an exception to this tendency can be seen in the case of the fractal dimensions of sections of the fracture surfaces of specimens after thermal loading at a nominal maximum temperature of 550 °C, which clearly shows the lowest mean values and variability of fractal dimensions. In some cases, a more significant change in the fractal dimension *D* was visible near the upper part of the specimen (the section at the highest distance from the notch), which may be related to the fact that the material was under higher compressive stress in this part.

Among all the results (mean values of parameters) a high degree of correlation was shown – the lowest absolute correlation coefficient was approximately 0.74 [–], which means that the correlation indicates a strong to (almost) perfect linear relationship between pairs of parameters in all cases, whether positive or negative.

The modulus of elasticity *E* shows an almost perfect negative correlation with maximum temperature, the correlation in absolute value slightly decreasing with distance from the heated surface. This corresponds well to the fact that the value of the elastic modulus is calculated from the linear initial branch of the diagram of load versus midspan deflection.

A similar almost perfect negative correlation at maximum temperature was shown by effective fracture toughness K_{Ice}. Its value expresses a degree of non-linearity before reaching the maximum load in the load versus midspan deflection diagram, thus reflecting some initiation of concrete damage in front of the notch – the initiation of the fracture process zone. From this perspective, it is adequate that the absolute value of the correlation coefficient increases slightly with the distance from the notch.

Specific fracture energy G_F is calculated from the work of fracture in relation to the originated concrete test specimen surfaces and showed a very strong positive correlation with the maximum applied temperature. As in the case of fracture toughness K_{Ice}, it is again satisfactory that the value of the correlation coefficient increases slightly with the distance from the notch.

Fractal dimension *D* shows a very strong correlation with maximum temperature and at the same time with both concrete fracture parameters – negative in the case of effective fracture toughness and positive in case of specific fracture energy. With higher maximum temperatures, the concrete becomes brittle in relation to the response around the top of the load versus midspan deflection diagram, but becomes more tough (ductile) due to the formation of a larger and more complicated fracture process zone – thus increasing resistance against the principal crack propagation of the concrete and correspondingly forming a more complicated fracture surface with a higher fractal dimension.

It has also been shown that, in the absence of a fractal dimension *D*, the fracture surface can be characterized very well in a similar (and easier) way by the roughness parameter *r* – the correlation coefficient between these parameters was 0.91 [–].

1.8. Conclusions

In the chapter, the possibilities of characterizing the roughness of the ligament of a concrete specimen after fracture testing by the fractal dimension were shown. The fracture surfaces of specimens taken from thermally-loaded experimental panels were analysed. It was shown that fracture surface roughness significantly depends on the thermal load, and also that the estimated fractal dimension shows dependence on the distance of the selected section of ligament from the notch, i.e. from the heated side of the specimens.

All of the above-presented analyses allow the following conclusions to be drawn:
• concrete surfaces after fracture tests have a fractal nature;
• the fractal dimension most suitably describes fracture surface roughness;
• the application of thermal loading to concrete causes changes in basic mechanical fracture parameters;
• fractal dimension highly correlates with all investigated mechanical fracture parameters;
• the roughness parameter is a perfect approximation of fractal dimension;
• the spatial temperature gradient significantly affects fracture parameters;
• the temperature gradient very slightly influences the fractal dimension of a fracture surface, and its variability;
• it is open to discussion as to whether and how different maximum temperatures should be distinguished along a ligament according to its measured fractal dimension.

Acknowledgement

References

AdMaS Science Centre (no date). Available at: http://www.admas.eu/.

Aïtcin Pierre-Claude, M. S. (2011) *Sustainability of Concrete*. 1st edn. London: CRC Press. doi: https://doi.org/10.1201/9781482266696.

Annadhason, A. (2012) 'Methods of Fractal Dimension Computation', *IRACST - International Journal of Computer Science and Information Technology & Security*.

Bazant, Z. P. and Planas., J. (1998) *Fracture and size effect in concrete and other quasibrittle structures*. Boca Raton and London: CRC Press.

Babadagli, T. and Develi, K. (2003) 'Fractal characteristics of rocks fractured under tension', *Theoretical and Applied Fracture Mechanics*. doi: 10.1016/S0167-8442(02)00139-8.

Borodich, F. M. (1999) 'Fractals and fractal scaling in fracture mechanics', *International Journal of Fracture*.

Carpinteri, A., Chiaia, B. and Invernizzi, S. (1999) 'Three-dimensional fractal analysis of concrete fracture at the meso-level', *Theoretical and Applied Fracture Mechanics*. doi: 10.1016/S0167-8442(99)00011-7.

Carpinteri, A., Chiaia, B. and Cornetti, P. (2001) 'A scale-invariant cohesive crack model for quasi-brittle materials', *Engineering Fracture Mechanics*. doi: 10.1016/S0013-7944(01)00085-6.

Carpinteri, A. and Puzzi, S. (2006) 'A fractal approach to indentation size effect', *Engineering Fracture Mechanics*. doi: 10.1016/j.engfracmech.2006.04.020.

Carpinteri, A. and Lacidogna, G. (2008) *Acoustic Emission and Critical Phenomena From Structural Mechanics to Geophysics*. 1st edn. London: CRC Press. doi: https://doi.org/10.1201/9780203892220.

Edelman, M., Macau, E. E. N. and Sanjuan, M. A. F. (2018) *Chaotic, Fractional, and Complex Dynamics: New Insights and Perspectives*. Springer International Publishing AG. doi: 10.1007/978-3-319-68109-2_1.

EN 1991-1-2:2002/AC (2013) *Eurocode 1: Actions on structures – Part 1-2: General actions – Actions on structures exposed to fire*. Brussels: CEN.

Ficker, T. (2007) 'Dimension of Fracture Surfaces', *Acta Polytechnica*, 46(6), pp. 27–30.

Ficker, T. (2008) 'Fractal strength of cement gels and universal dimension of fracture surfaces', *Theoretical and Applied Fracture Mechanics*, 50(2), pp. 167–171. doi: 10.1016/j.tafmec.2008.07.004.

John, A. P. and Li, L.-Y. (2011) *Fire Safety Engineering Design of Structures*. Boca Raton: CRC Press.

Kozlov, H. V., Burya, O. I. and Aloev, V. Z. (2004a) 'Application of fractal fracture mechanics to polymers and polymeric composites', *Materials Science*. doi: 10.1007/s11003-005-0066-1.

Kozlov, H. V., Burya, O. I. and Aloev, V. Z. (2004b) 'Application of fractal fracture mechanics to polymers and polymeric composites', *Materials Science*, 40(4), pp. 491–496. doi: 10.1007/s11003-005-0066-1.

Mandelbrot, B. B. (1982) *The fractal geometry of nature*, *New Scientist*. New York: Freeman.

Mandelbrot, B. B., Passoja, D. E. and Paullay, A. J. (1984) 'Fractal character of fracture surfaces of metals', *Nature*, 308, pp. 721–722. doi: 10.1038/308721a0.

Mecholsky, J. J., Passoja, D. E. and Feinberg-Ringel, K. S. (1989) 'Quantitative Analysis of Brittle Fracture Surfaces Using Fractal Geometry', *Journal of the American Ceramic Society*, 72(1), pp. 60–65. doi: 10.1111/j.1151-2916.1989.tb05954.x.

Micro-Epsilon: 2D/3D laser scanner (laser profile sensors) (no date). Available at: https://www.micro-epsilon.com/download/products/cat--scanCONTROL--en-us.pdf.

Mourot, G. *et al.* (2005) 'Anomalous scaling of mortar fracture surfaces', *Physical Review E - Statistical, Nonlinear, and Soft Matter Physics*, 71(1), pp. 1–7. doi: 10.1103/PhysRevE.71.016136.

Nevile, A. M. (2011) *Properties of Concrete*. Harlow: Pearson Education Limited.

Passoja. D. E. and Amborski, D. J. (1978) 'Fractal profile analysis by Fourier transform methods', *Microstructural Science*, 6, pp. 143–148.

RILEM TC 129-MHT (1997) 'TC 129 MHT: Test methods for mechanical properties of concrete at high temperatures: Part 6: Thermal strain', *Materials and Structures*, 33, pp. 17–21.

Rozsypalová, I. *et al.* (2017) 'Mechanical Fracture Parameters of Concrete Specimens from One-Side-Heated Panel', in *SP Report 2017:43 Proceedings from the 5th International Workshop on Concrete Spalling*. Boras: RISE Research Institutes of Sweden AB, p. 105–111.

Rozsypalová, I. *et al.* (2018) 'Mechanical fracture parameters of concrete exposed to high temperatures related to approximation of temperature fields in experimental panels', in *Proceedings for the 2018 fib Congress held in Melbourne*. Lausanne: Fédération internationale du béton (fib), p. 670–671.

Shah, S. P., Swartz, S. E. and Ouyang, C. (1995) *Fracture mechanics of structural concrete: applications of fracture mechanics to concrete, rock, and other*

quasi-brittle materials. New York: John Wil. and Sons.

Šimonová, H., Trčka, T., *et al.* (2018) 'Detailed Determination of Mechanical Fracture Parameters of Concrete after Fire Experiments', in *Solid State Phenomena: 24th Concrete Days*. Switzerland: Trans Tech Publications, p. 220–225.

Šimonová, H., Rozsypalová, I., *et al.* (2018) 'Thermal Analysis of Concrete from Panels Subjected to Fire Experiments', in *Solid State Phenomena: 24th Concrete Days 2017*. Switzerland: Trans Tech Publications, p. 47–52.

Wang, Y. *et al.* (2017) *Performance-Based Fire Engineering of Structures*. Boca Raton: CRC Press.

2. Contribution to comparison of methods for the investigation of chloride ingress related resistance

Petr Lehner [1,a], Petr Konečný[1,b], Tuan Duc Le[1,2,c] and Vlastimil Bílek[1,d]

[1]*VSB-Technical University of Ostrava, Faculty of Civil Engineering, Ostrava, Czech Republic,*

[2]*Saigon Technology University, Faculty of Civil Engineering, HoChiMinh City 73018, Vietnam,*

[a]*petr.lehner@vsb.cz, orcid.org/0000-0002-1478-5027*

[b]*petr.konecny@vsb.cz, orcid.org/0000-0001-6667-7522*

[c]*tuan.leduc@stu.edu.vn, orcid.org/0000-0003-3188-6759*

[d]*vlastimil.bilek@vsb.cz, orcid.org/0000-0001-6433-4892*

Abstract: The quality of the resistance of concrete structures to chloride penetration may be determined via the diffusion coefficient. This parameter can be derived from several laboratory based tests through long-term penetration testing approaches or accelerated experiments using electrochemical methods, such as NT Build 443 on which sample surface is exposure to NaCl solution and AASHTO TP-95 where correlation of different physical mechanism with chloride profiling is investigated. Two sample mixtures made of cement type I 42.5 R of which strength are classified as C50/60 and C90/105, representing for ordinary Portland cement (OPC) and high-performance concrete mixtures, respectively. Both samples are intended for prestressed concrete structures. Estimated time-dependent diffusion coefficient were analysed with respect to resistance of prestressed concrete structures against chloride ingress. Results of this work could be used for the current research of prestressed concrete structures and also for studies on potential corrosion risk of reinforcement.

Keywords: chloride ingress, diffusion coefficient, chloride penetration tests, prestressed concrete structures, resistance.

2.1. Introduction

The concept of prestressed concrete structures originated from the need for concentric or eccentric forces acting in the longitudinal direction of the structural member to prevent early cracking cracks (Nawy, 2009). Also the current trend is to improve the performance of concrete and reduce the use of cement by utilizing advanced high performance materials (Aïtcin, 2010; Ghosh *et al.*, 2017; Konečný *et al.*, 2017). In practice, prestressed concrete design methods has been significantly developed in recent decades (Nawy, 2009) and the current trend is driven to the evaluation of advanced nonlinear modelling capabilities (Sucharda *et al.*, 2017).

Prestressed concrete structures, e.g. beams in Fig. 2.1, must be studied in point of view of the static behaviour (Le, Konečný and Matečková, 2018), however, chemical and physical properties of concrete mixtures are very important too. One of the serious problems of the prestressed concrete structures is the corrosion of the reinforcement. Since this kind of structure is oftenly used as the bridge parts, salt encounter must be considered during the processes of durability design and assessment. This calls for the knowledge of the diffusion of chloride into concrete structures.

It is worth mentioning that diffusion coefficient is an important parameter since it represents the material characteristics of concrete. The coefficient is usually integrated in diffusive based models in respect to Fick's law. It can be either constant (time independent) in simple models of steady state systems or time dependent in rather complicated models of non-steady-state processes (Crank, 1975; Basheer, Chidiac and Long, 1996; Costa and Appleton, 1999). However, this parameter can be derived through laboratory based tests (Andrade, 1993; Morris, Moreno and Sagüés, 1996; Andrade and Sanjuán, 2012; Layssi *et al.*, 2015). Although many robust tests were available, their testing scheme can be classified as: (i) chloride profile analysis via long-term exposure to NaCl solution, and (ii) chloride profiling based on the correlation of various physical mechanism of diffusive processes. The former is often exploited with NT Build 443 (Nordtest NTBuild 443, 1995) while the latter is usually conducted with rapid chloride penetration ASTM C1202 or electrical resistivity based test AASHTO TP-95 (ASTM C1202, 2012; AASHTO TP95, 2014). Diffusion coefficient of concrete estimated from electrochemical testing methods is then used to predict the behaviour of experimental samples.

This research is aimed at the comparison of the two testing approaches on chloride ingress into prestressed reinforced concrete structures. Two concrete mixture samples made of cement type I 42.5 R are used and they are classified based on Eurocode as C50/60 (ordinary Portland cement concrete) and C90/105 (high performance concrete), respectively. Both mixtures will be examined

through NT Build 443 and AASHTO TP-95. Aging effect is considered. Derived time-dependent diffusion coefficient will be comparatively calculated and by which resistance of the prestressed concrete structure is investigated.

Fig. 2.1. Prestressed reinforced concrete beams.

2.2. Material and mechanical properties

The composition of mixtures is under patent protection, but at least basic knowledge of composition can help evaluate the results. The incomplete composition of the mixtures is shown in Table 2.1.

Table. 2.1. Characteristics of mixtures

Mixture No.	C50/60	C90/105
Cement type I 42.5 R	450 kg	650 kg
Water	180 kg	165 kg
Slag	0 kg	60 kg
Natural crushed aggregate 0/4	690 kg	400 kg
Natural crushed aggregate 4/8	215 kg	600 kg
Natural crushed aggregate 8/16	845 kg	0
Superplastificator	0	17 kg
Pucolanically curing additive	0	75 kg
Polycarboxylate plastificator	4.5 kg	
Water/cement ratio (W/C)	0.40	0.25

Cylindrical samples of standard dimensions were prepared for the diffusion tests presented herein (diameter 150 mm, height 300 mm). For NordTest NT Build 443,

three samples were prepared for each mixture. The markings were C50/60-A, C50/60-B, C50/60-C and C90/109-A, C90/109-B, C90/109-C, respectively. Furthermore, to measure the electrical resistance using the AASHTO TP-95, the same sized cylinders were prepared in two pieces for each mixture. The electrical resistance results below are average values.

It should be noted that laboratory experiments were also composed of several mechanical tests related to other requirements of the entire research. Some results are shown in the Table 2.2.

Table. 2.2. Mechanical properties

Mixture No.	C50/60	C90/105
Compressive Strength (Cube test) 28 days	85 MPa	106 MPa
Compressive Strength (Cylindrical test) 28 days	54 MPa	99 MPa
Modulus of elasticity – statically, 28 days	35 GPa	41 GPa
Modulus of elasticity – dynamic, 28 days	38 GPa	49 GPa

2.3. Chloride profile by NT Build 443

A modified NordTest NT Build 443 (Nordtest NTBuild 443, 1995) is selected for diffusion coefficient analysis. Concrete samples were immersed in NaCl solution for 90 days (see Fig. 2.2). This natural diffusion test gives enough data to produce a curve for the measured chloride profile. It is then approximated by the least squares method (Lehner, Turicová and Konečnỳ, 2017). Because there was no tool available for grinding the surface with the collection of concrete dust according to NT Build 443, the procedure was modified based on removing the chloride profile by drilling according to AASHTO T95 (AASHTO TP95, 2014).
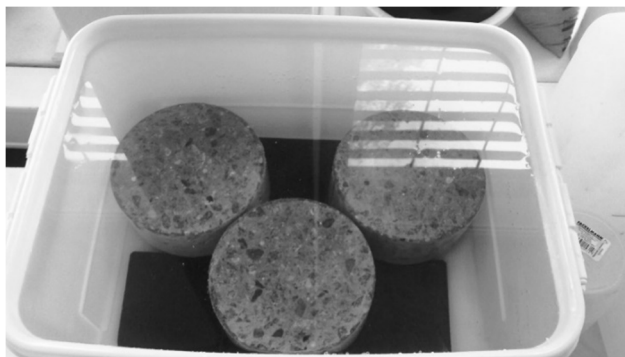
Fig. 2.2. Probes in the NaCl solution for test according NT Build 443.

After subsequent laboratory chemical evaluation of the collected dust, a chloride profile was prepared for each sample. The amount of chloride in the concrete powder obtained can be determined by potentiometric titration. These profiles for the mixture C50 / 60 can be seen in Fig. 2.3, the results for the mixture C90 / 105 are shown in Fig. 2.4. We can observe that the C50 / 60 mixture has a much greater slope of the curves than the C90 / 105 one. This factor, among other things, influences the subsequent calculation through the diffusion coefficient.

When the concentration of chlorides in given depths known, then the measured chloride profile is approximated. For best fit calculation, the method of least squares is used. The whole process is described in great detail in the article (Lehner, Turicová and Konečnỳ, 2017).

It should be noted that the unknown parameters are both diffusion coefficient and surface chloride concentration. Both parameters serve as inputs for modelling of chloride diffusion and subsequent using for estimating the life of concrete structures.

Since one diffusion coefficient value for each mixture from the selected method is needed for the evaluation, the average values of the diffusion coefficients from the mixture of C50 / 60 and C90 / 105 are presented below.
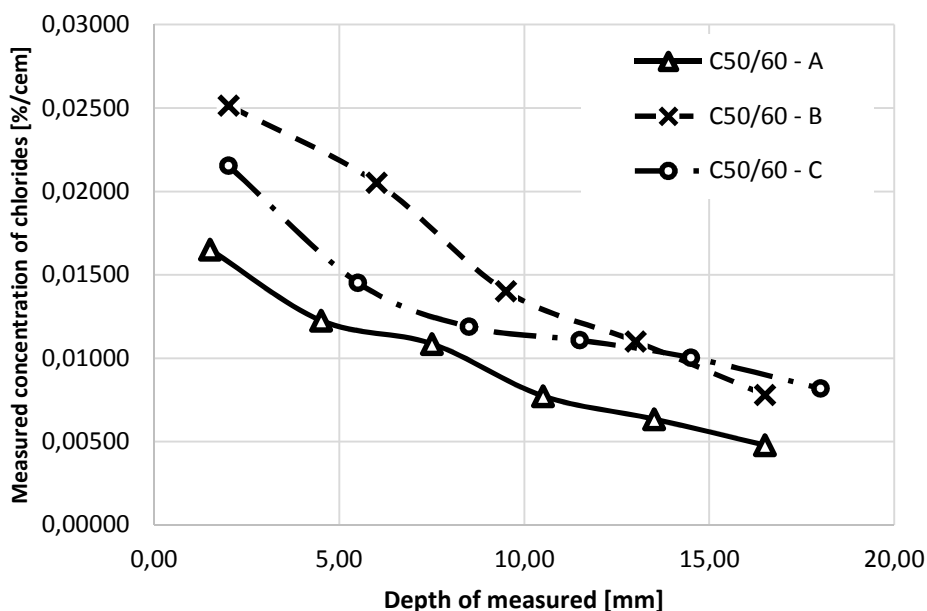
Fig. 2.3. The measured chloride profile of mixture C50/60 from NT Build 443 test.
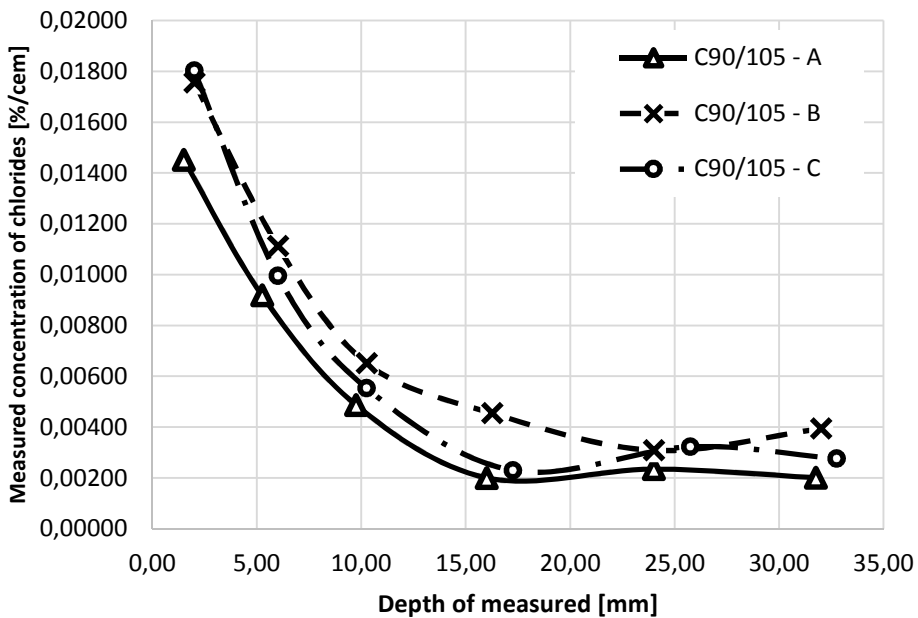
Fig. 2.4. The measured chloride profile of mixture C90/105 from NT Build 443 test.

2.4. Electrical resistivity and aging effect

For the electrical resistance measurement, the Wenner's probe was also selected (see Fig. 2.5). This measurement is based on the AASHTO T95. The basic information are provided in the articles (AASHTO TP95, 2014).
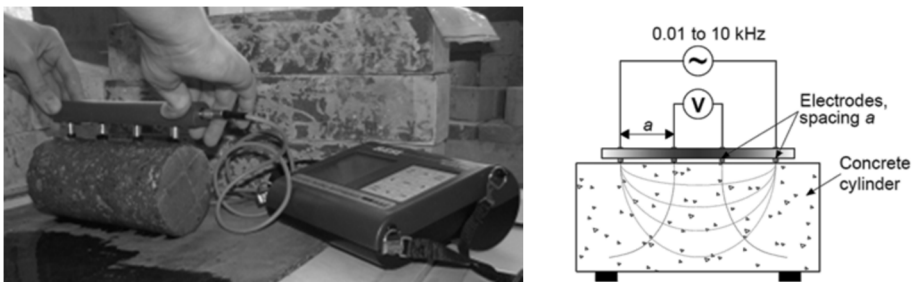
Fig. 2.5. Photo and scheme of surface resistivity measuring by the AASHTO T259.

The method is non-destructive, so the repeated measurement is possible to be able to determine the time depending of diffusion. On the other hand, this measurement method may have a relatively large variation, partly due to the

heterogeneity of the test material and the usage of rather uncontrollable contact conditions. These findings should be considered in the evaluation. As mentioned, this is a non-destructive test. It is, therefore, possible to measure electrical properties during maturing of concrete. In this case, it was tested at 7, 14, 28, 56, 91 and 161 days after concreting. The initial results of these tests for both mixtures are shown in Fig. 2.6.
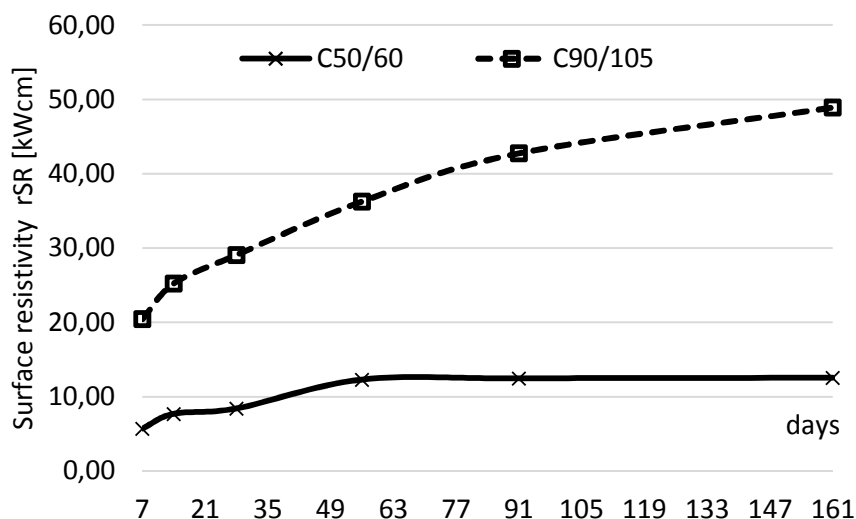
Fig. 2.6. The measured surface resistivity of mixture C50/60 and C90/105 by the AASHTO T259.

After measuring, the results of surface resistivity can be converted to volume resistance using geometric correlation relationships (Morris, Moreno and Sagüés, 1996). From these values, a diffusion coefficient can be determined by the Nernst-Einstein equation (Lu, 1997; Ghosh, 2011; Lehner, Ghosh and Konečný, 2018).

2.5. Results and discussion

A diffusion coefficient is a suitable parameter to determine the resistance of concrete to chloride ions contained in road salt. If this parameter is smaller, resistance is higher. In Fig. 2.7, we can see the results of the diffusion coefficients in the logarithmic scale from both mixtures and both presented methods.
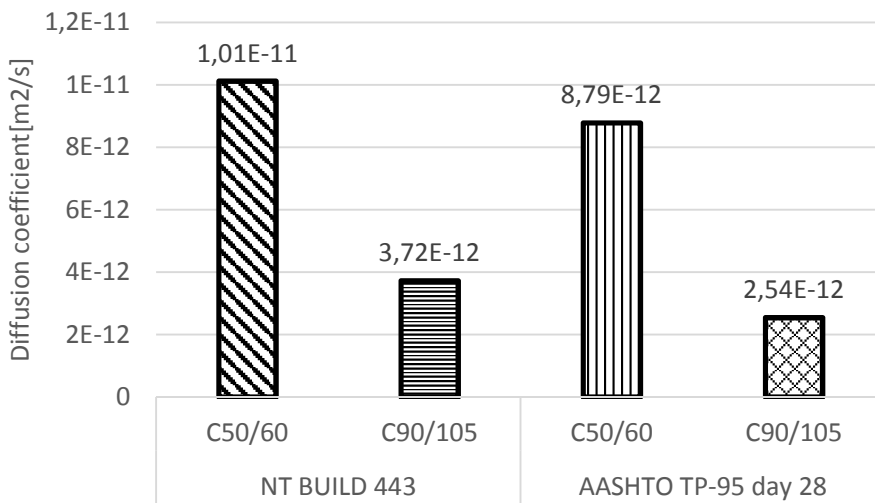
Fig. 2.7. Comparison of the diffusion coefficient calculate from the NT BUILD 443 and AASHTO T259.

At the first sight, there are quite large differences in diffusion coefficients of both mixtures. On the other hand, the comparing of mixtures using two methods is quite satisfactory. The value of the diffusion coefficient must be considered better if its value is close to zero. Thus, in Figure 7, these are the lower columns. The mixture C90/105 have better values than the C50/60 one in both methods. If we look at Figure 6, we can observe that the behaviour of both concrete mixtures meets expectations. Concrete C50/60 shows a light increase in resistance until 50 days from concreting before keeping at almost constant value. Conversely, C90/105 concrete shows a gradual increase over the entire measurement period.

2.6. Conclusions

The resistance of concrete structures to chloride penetration can be expressed through the diffusion coefficient. This parameter was derived from two electrochemical methods: NT Build 443 on which sample surface is exposures to NaCl solution and AASHTO TP-95 where correlation of electrical resistivity and diffusion of ions is investigated. Two sample mixtures made of cement type I 42.5 R of which strength are classified as C50/60 and C90/105 were presented. Both mixtures are intended for prestressed concrete structures and the research focuses on improving properties in different areas.

The study shows expected differences in the results from both used methods. Concrete with higher strength class, i.e. C90/105, is more resistant. The difference between the diffusion coefficient of NT BUILD 443 and AASHTO TP-95 is visible in both mixtures. But due to the same order, the difference is almost negligible. Results should be taken with caution, but they are good enough to use for comparing mixtures. The results of this work could be used for current research of prestressed concrete structures and for studies of possible corrosion risk of reinforcement.

References

AASHTO TP95 (2014) 'Standard Test Method for Surface Resistivity of Concretes Ability to Resist Chloride Ion Penetration', p. 10.

Aïtcin, P. C. (2010) 'Materials selection', in *High-Performance Concrete*. doi: 10.4324/9780203475034_chapter_7.

Andrade, C. (1993) 'Calculation of chloride diffusion coefficients in concrete from ionic migration measurements', *Cement and Concrete Research*, 23(3), pp. 724–742. doi: 10.1016/0008-8846(93)90023-3.

Andrade, C. and Sanjuán, M. A. (2012) 'Experimental procedure for the calculation of chloride diffusion coefficients in concrete from migration tests', *Advances in Cement Research*. doi: 10.1680/adcr.1994.6.23.127.

ASTM C1202 (2012) 'Standard Test Method for Electrical Indication of Concrete's Ability to Resist Chloride Ion Penetration', *American Society for Testing and Materials.*, (C), pp. 1–8. doi: 10.1520/C1202-12.2.

Basheer, P. A. M., Chidiac, S. E. and Long, A. E. (1996) 'Predictive models for

deterioration of concrete structures', *Construction and Building Materials*. doi: 10.1016/0950-0618(95)00092-5.

Costa, A. and Appleton, J. (1999) 'Chloride penetration into concrete in marine environment-Part II: Prediction of long term chloride penetration', *Materials and Structures*, 32(5), pp. 354–359. doi: 10.1007/BF02479627.

Crank, J. (1975) 'Methods of Solution when the Diffusion Coefficient is Constant', in *The mathematics of diffusion*, p. 414. doi: 10.1016/0306-4549(77)90072-X.

Ghosh, P. (2011) *Computation of Diffusion Coefficients and Prediction of Corrosion Initiation in Concrete Structures*.

Ghosh, P. *et al.* (2017) 'Probabilistic time-dependent sensitivity analysis of HPC bridge deck exposed to chlorides', *Computers and Concrete*, 19(3), pp. 305–313. doi: 10.12989/cac.2017.19.3.305.

Konečný, P. *et al.* (2017) 'Comparison of Chloride Diffusion Coefficient Evaluation Based on Electrochemical Methods', in *Procedia Engineering*, pp. 193–198. doi: 10.1016/j.proeng.2017.05.326.

Layssi, H. *et al.* (2015) 'Electrical Resistivity of Concrete', *Concrete International*, 37, pp. 41–46.

Le, T. D., Konečný, P. and Matečková, P. (2018) 'Time dependent variation of carrying capacity of prestressed precast beam', in *IOP Conference Series: Earth and Environmental Science*. doi: 10.1088/1755-1315/143/1/012013.

Lehner, P., Ghosh, P. and Konečný, P. (2018) 'Statistical analysis of time dependent variation of diffusion coefficient for various binary and ternary based concrete mixtures', *Construction and Building Materials*, 183, pp. 75–87. doi: 10.1016/j.conbuildmat.2018.06.048.

Lehner, P., Turicová, M. and Konečnỳ, P. (2017) 'Comparison of selected methods for measurement of the concrete electrical resistance to chloride penetration', *ARPN Journal of Engineering and Applied Sciences*, 12(4).

Lu, X. (1997) 'Application of the Nernst-Einstein equation to concrete', *Cement and Concrete Research*, 27(2), pp. 293–302. doi: 10.1016/S0008-8846(96)00200-1.

Morris, W., Moreno, E. I. and Sagüés, A. A. (1996) 'Practical evaluation of resistivity of concrete in test cylinders using a Wenner array probe', *Cement and Concrete Research*, 26(12), pp. 1779–1787. doi: 10.1016/S0008-8846(96)00175-5.

Nawy, E. G. (2009) 'Prestressed concrete: A fundamental approach', p. 915.

Nordtest NTBuild 443 (1995) *Nordtest Method: Accelerated Chloride Penetration into Hardened Concrete*, *Nordtest method*. Esbo, Finland: Nordtest.

Sucharda, O. *et al.* (2017) 'Comparative Evaluation of Mechanical Properties of Fibre-Reinforced Concrete and Approach to Modelling of Bearing Capacity Ground Slab', *Periodica Polytechnica Civil Engineering*. doi: 10.3311/ppci.10688.

3. Requirements for BIM model

Maciej Major[1], Jacek Nawrot[2], Izabela Major[3]

[1] *Czestochowa University of Technology, Faculty of Civil Engineering, Częstochowa, Poland,*
mmajor@bud.pcz.pl, orcid.org/ 0000-0001-5114-7932

[2] *Czestochowa University of Technology, Faculty of Civil Engineering, Częstochowa, Poland,*
jaceknawrot@o2.pl, orcid.org/0000-0002-9581-1388

[3] *Czestochowa University of Technology, Faculty of Civil Engineering, Częstochowa, Poland,*
imajor@bud.pcz.pl, orcid.org/ 0000-0003-1234-9317

Abstract: The paper discusses the requirements that should be met by a properly designed BIM model of a building structure in the phases of design, construction and use. The scope of potential information contained in the model in the context of its multidimensional character was presented. The knowledge of BIM modelling was reviewed, with particular emphasis on barriers and problems related to the use of this technology in different areas of the investment process. The factors that should be taken into account to create a BIM model that can be effectively used at all stages of the life cycle of a building were discussed.

Keywords: BIM model, interoperability, IFC standard

3.1. Introduction

The building information modelling (BIM) technology is increasingly being used in the implementation of construction projects, also in Poland. Its application allows for a reduction of costs associated with the construction and use of the building and effective management of its entire life cycle, from design through construction to the phase of use. In order to make it possible, a virtual model of a building (the BIM model) should be a perfect reflection of the actual building at every stage of the investment process and use, the so-called detailed model. The digital model should be updated on an ongoing basis and take into account all possible corrections in relation to the design and changes resulting from repairs and modernizations made after the facility has been put into service.

An important issue related to the model quality and the way it is created is the so-called BIM maturity levels (Fig. 3.1).
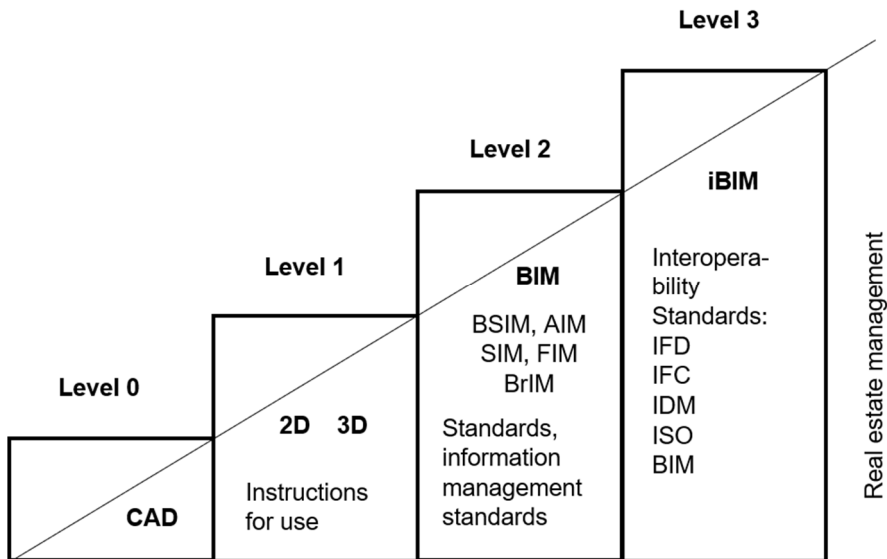
Fig. 3.1. BIM maturity levels: author's own elaboration based on "A report for the Government Construction Client Group", 2019; acronyms used in the figure: CAD - computer-aided design, 2D - two-dimensional modelling, 3D - three-dimensional modelling, BIM - building information modelling, BSIM - building services information model, AIM - architecture information model, SIM - structural information model, FIM - facilities information model, BrIM - bridge information model, IFD - international framework for dictionaries, IFC - recording and exchange format for virtual building models, IDM - documentation guidelines for information exchange

Level 0 is the stage preceding the application of BIM. The primary carrier of information is the paper design documentation (2D), which is prepared with the use of CAD programs. Level 1 BIM is characterized by the creation of spatial models for individual disciplines (architecture, structures, installations), but there is no exchange of information between individual participants of the design process, the design documentation (2D drawings) is also in paper form. Level 2 BIM means the creation of an integrated 3D building model that contains information on architecture, construction, installation and building management, without the need for this information to be contained in a single file. Based on the resulting model, it is possible to detect possible collisions between individual disciplines and automatically create 2D documentation. BIM Level 3 is characterised by the generation of a model containing all required information about the building in one file, linked (if necessary) to external databases, while two-way communication between the model and external data is ensured. All participants of the investment process (within the framework of their authorization) have continuous access to the model, which allows for obtaining information, updating data and cooperation, termed model interoperability. At the moment, due to the high requirements of the appropriate IT infrastructure, data transmission speed, database security, etc., level 3 is the objective currently being pursued by BIM.

The requirements for BIM models can be classified according to the two general concepts, LOD (Level Of Detail or Development) and LOI (Level Of Information). However, there are also many other additional requirements related to the prepared model and the objectives of its development. It should be stressed that, depending on the needs, the BIM model may be the basis for coordination and verification of solutions adopted during the design process. Furthermore, it may be used during the construction process, as well as serve other purposes, such as those related to the development of visualization critical at the stages of planning and implementation of the investments serving marketing purposes.

Due to the nature of the information contained in the BIM model, its multidimensionality can also be highlighted (Fig. 3.2). The acronym 3D refers to data concerning spatial geometry of the building (architecture, structure, installations). By adding another dimension i.e. time, a 4D model is obtained, which can be used to create schedules for the progress of works and deliveries. Supplementing such a model with construction costs yields the 5D model, which allows for preparation of cost estimates and construction budget. By adding information about the environmental impact of the investment (noise level, amount of waste generated) one can move on to the 6D model, which, supplemented with information on the use (utility consumption, data on repairs and maintenance) becomes the 7D model.
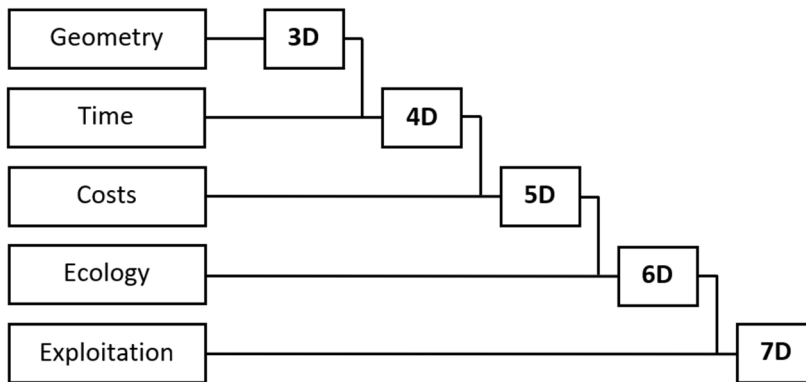
Fig. 3.2. Individual dimensions of the BIM model depending on the scope of information: author's own elaboration

Effective implementation of BIM technology in Poland requires the development and implementation of regulations that would regulate underlying issues such as the creation and management of BIM documentation, the scope of responsibility of the parties in the investment process, exchange of information, etc. Despite attempts being currently made by various institutions (e.g. PZITB and Polish Association of Construction Employers), no such regulations have been developed and implemented yet. Consequently, BIM users are to some extent based on Western standards (e.g. British standards covering PAS 1192-2) and the details of the complexity of the model (the scope of the information contained in the model) are governed by contractual agreements. Apart from formal and legal problems, a critical issue is to determine the requirements that should be met by an adequately construed model of BIM building in order to be effectively used by all participants of the investment process. In this paper, an attempt has been made to specify such requirements for particular stages of the life cycle of a building.

3.2. Literature review on BIM

BIM modelling can be used for different purposes by different participants in the investment process, but it is essential to define the principles of communication and cooperation between all stakeholders of the process (Papadonikolaki *et al*., 2019). The benefits of using this technology in the design, construction or management of a building are well known (Ghaffarianhoseini *et al*., 2017). An interesting proposal is to use the BIM model in building sustainability assessment (BSA). Carvalho *et al*., 2019, proposed the SBToolPT-H (Sustainable Building Tool) method to assess the sustainability of new and renovated buildings. The process takes into account the assessed 25 criteria (e.g. use of recycled materials, water

demand, thermal comfort, etc.), of which as many as 24 criteria can be obtained directly or indirectly from the BIM model itself. The actions taken at this level aim to develop an automated BSA method in order to identify and compare different sustainability design scenarios as early as at the concept choice stage. It is worth emphasizing here that in certain situations the BIM model created in the design phase and used in the implementation phase requires the necessary modifications in order to be further used for various analyses (e.g. energy performance analysis of a building). This is the case, for example, if a more complex building geometry is used, when the problem may occur with the transformation of the IFC (Industry Foundation Classes) file containing information about the BIM model to the building energy model (BEM). This situation occurs, among others, in objects with curved surfaces. Ying and Lee, (2019), proposed an algorithm for the automatic transformation of curved wall geometry into polyhedrons, which can be further processed by available transformational approaches. With this algorithm, arched surfaces are converted into multi-walled geometries while maintaining correct geometric proportions and a new IFC file is generated, which can be imported into the BIM model of the designed building using the available transformation tools. The use of the BIM model to assess the energy consumption of buildings was also discussed in the paper of by Andriamamonjy *et al.*, 2019, where a set of tools needed to obtain information from the BIM model to the so-called grey box model used to optimise the energy performance of a building is presented. Since the highest cost component in the entire life cycle of a building is its operating costs (accounting for ca. 80% of total costs), (Kasznia *et al.*, 2019), BIM models should be developed in such a way that they can be effectively utilized in facility management (FM) (Pishdad-Bozorgi *et al.*, 2019). Nowadays, this becomes a necessity and should be developed during the preparation of the BIM model. In addition to economic aspects, the BIM modelling used in FM improves the quality of life (QOL) by ensuring a higher level of functionality of the environment built through integration of people, place, processes and technologies (Aziz *et al.*, 2016). Another issue related to building management is the integration of BIM and the Internet of Things (IoT). Tang *et al.*, (2019) indicated the objectives of research that should be undertaken in order to establish BIM-IoT integration standards, solve problems with interoperability and cloud computing. Barriers related to the adoption of the BIM model for the needs of building management by large organizations of owners were presented in the paper of Cavka *et al.*, 2017. A method of identification and characterization of owners' expectations was developed in order to adjust the information contained in the BIM model to their individual needs, which sometimes constitute the essence of things to the extent that it unequivocally forces the final solutions. In some cases, the solution preferred by large contractors is to outsource the implementation of the BIM

model to external entities, i.e. specialized IT companies with experience and competencies enabling them to obtain target solutions that guarantee their high level. This approach helps avoid potential model errors or imperfections due to the insufficient experience of the contracting entities in BIM modelling. However, the results of research conducted for the US market showed that outsourcing of such services is less efficient than internal BIM (Fountain and Langar, 2018), because a common phenomenon during BIM modelling is making further adjustments to the model, and these should be preferably implemented in an internal team directly involved in the construction process. Furthermore, Juszczyk *et al.*, 2016 discussed problems related to change management in the BIM model and presented tools dedicated to this process since BIM in the phase of building construction (realization of the investment process) can be used not only at the construction site but also in the structure prefabrication plant. The issue of applying BIM modelling in manufacturing of prefabricated building components was discussed in the paper of Tan *et al.*, (2019), which indicated the major barriers to the implementation of this technology and proposed a three-level strategy for its implementation in order to achieve the intended final results. The BIM modelling, which is focused on the digital representation of buildings (construction objects) at the micro level, is complemented by the geographical information systems (GIS) system, which ensures representation of the external environment of buildings at the macro level (Wang *et al*. 2019). Correct BIM-GIS integration is the key to the next stage of building digitalization, enabling the creation of a virtual model of not only individual buildings but also the entire urban space covering both the housing estate and the entire city in the future.

3.3. Requirements for BIM models

A problem that concerns all phases of the life cycle of a building is the adaptation of the scope of information contained in the model to the needs of individual users, while an important issue is a certain unification of the complexity of the models due to the set of information assigned to them. This issue was resolved by the American Institute of Architects developing a classification of the levels of development (Level of Development - LOD) of BIM models, as already mentioned in the introduction. This classification implies that each level of LOD is assigned an appropriate level of detail of the information contained in the BIM model (Table 3.1).

Table 3.1. LOD classification for different degrees of detail of information in the BIM model; author's own elaboration based on Level of Development (LOD) Specyfication, Part I & Commentary, For Building Information Models and Data 2019

LOD	Data content
100	A model element is represented by a symbol and does not need to have a real shape, size or precise location. All information contained in the LOD is approximate. It does not meet the requirements of LOD 200 (without geometric data).
200	An element of a BIM model is graphically represented in the model as a general system, object, or assembly with approximate size, shape, position, and orientation.
300	A model element is graphically represented in a model as a specific system, object, or assembly in terms of quantity, size, shape, location, and orientation. Its quantities can be directly measurable from the BIM model, from which project documentation can be generated.
350	A model element is graphically represented in a model as a specific system, object or assembly in terms of quantity, size, shape, location, orientation and connections with other building systems (supports, connectors).
400	A model element is graphically represented in a model as a specific system, object or assembly in terms of size, shape, location, quantity and orientation along with details, and information about manufacturing and assembly. The quantity, size, shape, position and orientation of the designed element can be measured directly from the model.
500	A model element is a representation verified in a real object in terms of size, shape, location, quantity and orientation (e.g. through a 3D geodetic inventory). This level does not involve a higher level of detail of the model geometry, whereas LOD 500 does not have to be a detailed upgrade of the LOD 400.

As a general rule, the higher the level of detail of the model, the higher the LOD level. Of course, this classification was prepared by taking into account the realities of the US market, but in the absence of similar regulations in force in Poland, it is used by national operators using BIM technology to carry out the construction process, even though, as mentioned above, there is currently no internal standardization in this respect.

3.3.1. Design in BIM technology

Since the BIM model is mainly developed at the design stage, it is essential that it is properly developed from the very beginning. Any mistakes made in this phase of the investment project will have consequences on further stages of working with the model. The first and most important issue is to ensure interoperability, i.e. the possibility of exchanging data contained in the model between the individual participants in the design process. Designers of individual areas and disciplines (architecture, construction, installations) work using different

programs and save information in native files. In order to integrate this information into a single, multi-discipline project, a standard is needed to enable communication between native files of programs used in individual disciplines. The most popular standard for exchanging this data is the IFC (Industry Foundation Classes) format. A program for a given discipline working in a BIM environment has the capability to convert native files to IFC format so that the information contained in them can be read by programs from other disciplines, which translates into the effectiveness of the project process (Fig. 3.3).
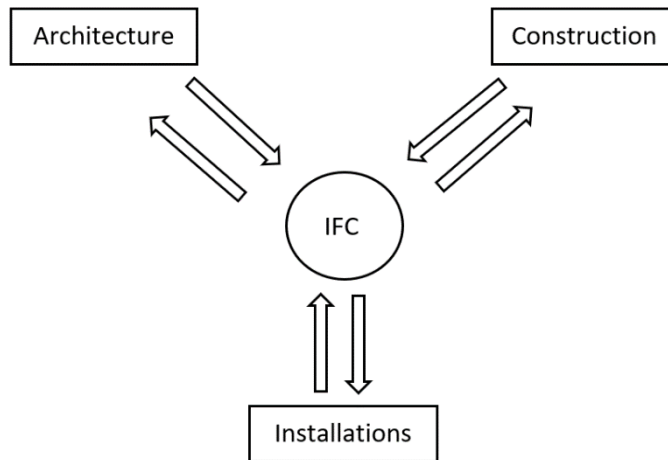
Fig. 3.3. Diagram of data exchange between individual areas and disciplines using IFC format (author's own elaboration)

Another factor equally important for the correctness of the design process which significantly determines the correctness of the model is the lack of design collisions between individual areas and disciplines. Overlapping the area and discipline projects yields a complete model of the building, so it is possible to capture all potential incompatibilities at the interface between architecture/construction/installations. An example diagram of this process is illustrated in Fig. 3.4.

Designers from a given area of the project implementation as well as discipline designers save their projects in source files of programs they use and then export them to IFC format. Based on the information contained in IFC files, a target model is created for all participants of the design process, commonly known as a multi-discipline project, allowing for the detection of possible collisions. After discussing how to solve (eliminate) the collision, feedback is provided to the designers who make the respective corrections in the source files, and the design process is continued. In the case of further collisions, the entire operation is repeated in the same way.
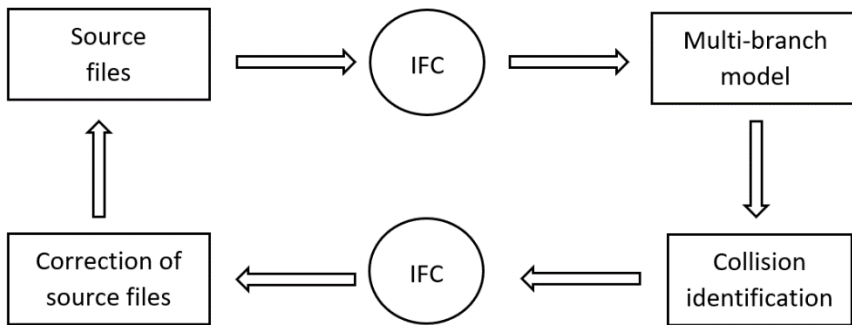
Fig. 3.4. Diagram of the process of identification and elimination of design collisions based on the area and multi-sector BIM model: author's own elaboration

Another issue to be considered when developing the BIM model is the definition of the types of individual elements in accordance with the IFC standard. If, for example, the thermal insulation layer of the ceiling is incorrectly defined as a floor slab, then during the cost estimation based on the IFC file with such data, errors in the cost estimation may occur. Another problem that should also be addressed is the correct determination of the geometry of individual elements - cutting off walls at the floor level, a proper definition of ceiling/wall and wall/wall contacts, verification of beam and column cross-sections after performing static calculations in relation to the initially accepted sections, etc. All errors resulting from incorrect modelling of individual elements (according to both type and geometry) do not allow for effective use of the model during the implementation of the investment and may lead to making unintended mistakes by its subsequent users. Such a situation is not only undesirable but should be eliminated at the level of project creation.

Furthermore, the model should be made in such a way that it can automatically "refresh" itself after changing its properties in terms of geometry, materials, etc. Such parameterization of the model allows for its immediate modification at low labour intensity, which is extremely efficient and therefore necessary for implementation in the design process.

3.3.2. Construction based on the BIM model

The factor necessary to maintain consistency between the actual status and the design is the ongoing updating of the BIM model as discussed above. During the implementation of an investment (due to factors that could not have been predicted during the design phase), a situation often arises that requires changes to be made during the construction process. Therefore, continuous verification of the digital model of the building is necessary. It should be carried out at strictly defined intervals and cover all introduced changes, whether in terms of the

geometry of the building, the materials used, the equipment installed, changes of location, etc. This will ensure that the model remains entirely usable throughout the construction period and during the final use of the building.

Another equally important requirement from the standpoint of the contractor is a properly constructed BIM model, which will allow for proper development of schedules, bills of quantities or cost estimates. This is extremely important for the implementation of the entire investment process and should be taken into account by all participants in the implementation of the project with due diligence. If the BIM model being implemented (or already implemented) is prepared in accordance with the principles described in 3.3.1, it will be possible to fully utilize the opportunities offered by BIM technology, e.g. automated bills of quantities, scheduling and cost estimation. Any mistakes made at the stage of design and creation of the model will potentially imply executive errors. One should avoid such situations because they are or can be very expensive and often also time-consuming. The importance of this aspect of the implementation of future investment and the consequences of mistakes made at the stage of the project implementation should be emphasized. The BIM project prepared for implementation must guarantee the correctness of the construction process - the implementation of the investment project. Figure 3.5 shows an erroneously defined wall corner, which results in the common part of the wall being included in both elements at the stage of the bill of quantities, which leads to overestimating the quantity of material and the resulting inflated material costs.
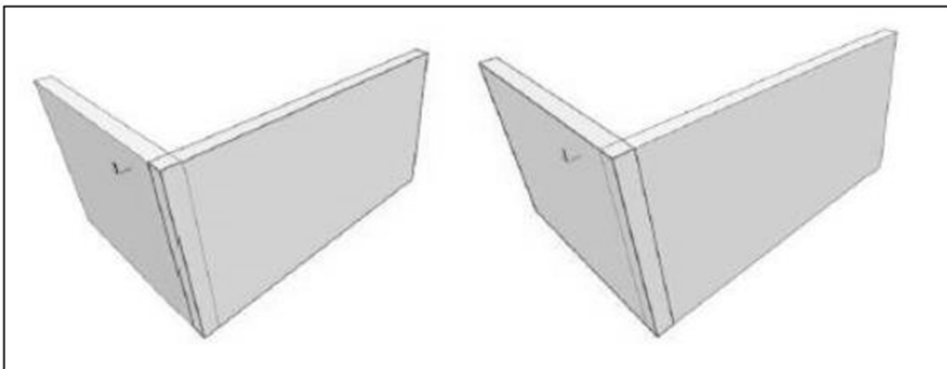
Fig. 3.5. Erroneous definition of the wall contact resulting in an incorrect bill of quantities: author's own elaboration

3.3.3. Operation and management of the building

Due to the fact that the costs of building use in a certain time perspective are many times higher than the costs of its construction, all the tools that contribute to their reduction are extremely desirable for owners and managers of real estate. One of the main reasons for the excessive increase in operating costs is insufficient knowledge about the building, especially in the case of large-size buildings, where the amount of data generated during their use is enormous. Efficient and fast access to all necessary information is critical for effective property management. The answer to these needs can be a properly construed BIM model, which, updated with operating data, becomes digital documentation of the building operation (Building Owner Operations Model - BOOM). This effective way of working of the owner or manager of the building translates into financial and time dimension related to the implementation of operation-related tasks.

Moreover, while construing such a model, the specificity of the building and the resulting needs of the owner/manager should be taken into account. The scope of the data should include:

- technical information (data about the building, equipment, systems, installations, etc.),
- financial data (receipts, expenses),
- information about the employees employed in the facility (personal data, courses, training),
- information on tenants,
- data concerning repairs, breakdowns and maintenance,
- other information resulting from the nature of the facility.

In a correctly made model, the individual elements of the 3D model should be associated with relevant documents (e.g. devices - warranty cards) and external databases (e.g. temperature sensors - temperature readings). This is necessary to maintain the effectiveness of the implementation of maintenance tasks because the availability of a record of the operation of equipment included in the individual systems and installations allows for rapid detection of possible irregularities, immediate corrective actions and actions to prevent potential negative effects of failure. Thanks to the knowledge of the current condition of the property, it will be possible to prepare energy and economic analyses, etc., which will allow effective management of the facility and will eliminate to a large extent the risks resulting from the lack of sufficient technical condition of individual systems and elements.

3.4. Conclusions

In order to take full advantage of the possibilities offered by BIM technology in the entire life cycle of a building, from concept implementation through design to final operation, special attention should be paid to the correctness of the digital model of the building. Such a model should be free from any errors. It is unacceptable for the element to be improperly modelled so that geometric inconsistencies, poorly defined contacts and collisions etc. might occur. Only then will the BIM model be fully useful for all participants in the investment process and guarantee the correct implementation of the construction projects at every stage. Otherwise, the errors contained in the model will lead to collecting false information, and thus any actions taken based on this information will lead to duplication of erroneous results having a negative effect on the process of investment implementation.

Constant ongoing updating of the aggregated data in the model is necessary so that the digital image of the object reflects its real state at any time. This is a prerequisite for making the right decisions at every stage of the investment as well as during the operation of the completed construction project.

The level of detail of the model should be adjusted to the needs of stakeholders and precisely defined, e.g. by using the LOD classification. This will help avoid possible discrepancies in the expectations of individual users of the developed BIM model regarding the scope of information contained in the model.

Unfortunately, a certain barrier in the development of BIM technology in Poland is the lack of standards regulating the basic issues related to the use of this technology. This encourages entities using BIM in their activity to follow the standards used in other countries (e.g. in the UK or the USA) or to develop their own guidelines. Such internal guidelines are implemented at the level of the enterprise, which may lead to some interpretation problems concerning the obligations of particular parties in the investment process concerning the principles of creating and managing BIM documentation. This also applies to the type and content of BIM data contained in the model.

References

'A report for the Government Construction Client Group: Building Information Modelling (BIM) Working Party Strategy Paper', https://www.cdbb.cam.ac.uk/Resources/ResoucePublications/BISBIMstrategyReport.pdf [access 2019, May].

Andriamamonjy, A. *et al.* (2019) 'Automated grey box model implementation using BIM and Modelica', *Energy & Buildings*, 188-189, pp. 209-225, https://doi.org/10.1016/j.enbuild.2019.01.046.

Aziz, N. D. *et al.* (2016) 'Building Information Modelling (BIM) in Facilities Management: Opportunities to be considered by Facility Managers', *Procedia - Social and Behavioral Sciences*, 234, pp. 353 – 362, https://doi.org/10.1016/j.sbspro.2016.10.252.

Carvalho, J.P. *et al.* (2019) 'Optimising building sustainability assessment using BIM', *Automation in Construction,* 102, pp. 170-182, https://doi.org/10.1016/j.autcon.2019.02.021.

Cavka, H.B. *et al.* (2017) 'Developing owner information requirements for BIM-enabled project delivery and asset management', *Automation in Construction*, 83, pp. 169-183, https://doi.org/10.1016/j.autcon.2017. 08.006.

Fountain, J. and Langar, S. (2018) 'Building Information Modeling (BIM) outsourcing among general contractors', *Automation in Construction*, 95, pp. 107-117, https://doi.org/10.1016/j.autcon.2018.06.009.

Ghaffarianhoseini, A. *et al.* (2017) 'Building Information Modelling (BIM) uptake: Clear benefits, understanding its implementation, risks and challenges', *Renewable and Sustainable Energy Reviews*, 75, pp. 1046–1053, https://doi.org/10.1016/j.rser.2016.11.083.

Juszczyk, M. *et al.* (2016) 'Current issues of BIM-based design change management, analysis and visualization', *Procedia Engineering*, 164, pp. 518 – 525, https://doi.org/10.1016/j.proeng.2016.11.653.

Kasznia, D. *et al.* (2019) 'BIM w praktyce. Standardy, wdrożenie, case study', Wydawnictwo Naukowe PWN SA, Warszawa.

'Level of Develompent (LOD) Specyfication, Part I & Commentary, For Building Information Models and Data', April 2019, https://bimforum.org/lod/ [access 2019, May].

Papadonikolaki, E. *et al.* (2019) 'Organising and Managing boundaries: A structurational view of collaboration with Building Information Modelling (BIM)', *International Journal of Project Management*, 37, pp. 378– 394, https://doi.org/10.1016/j.ijproman.2019.01.010.

Pishdad-Bozorgi, P. *et al*. (2019) 'Planning and developing facility management-enabled building information model (FM-enabled BIM)', *Automation in Construction*, 87, pp. 22-38, https://doi.org/10.1016/j.autcon.2017.12.004.

Tan, T. *et al.* (2019) 'Barriers to Building Information Modeling (BIM) implementation in China's prefabricated construction: An interpretive

structural modeling (ISM) approach', *Journal of Cleaner Production*, 219 pp. 949-959, https://doi.org/10.1016/j.jclepro.2019.02.141.

Tang, S. et al. (2019) 'A review of building information modeling (BIM) and the internet of things (IoT) devices integration: Present status and future trends', *Automation   in   Construction*,   101,   pp.   127-139,   https:// doi.org/10.1016/j.autcon.2019.01.020.

Wang, H. *et al.* (2019) 'Integration of BIM and GIS in sustainable built environment: A review and bibliometric analysis', *Automation in Construction*, 103, pp. 41-52, https://doi.org/10.1016/j.autcon.2019. 03.005.

Ying, H. and Lee, S. (2019) 'An algorithm to facet curved walls in IFC BIM for building   Energy',   *Automation   in   Construction*,   103,   pp.   80-103, https://doi.org/10.1016/j.autcon.2019.03.004.

4. Comparative study of Building Law in Poland and Russian Federation

Seweryn Malazdrewicz

Wroclaw University of Science and Technology, Faculty of Civil Engineering, Wroclaw, Poland

Abstract: The comparison between legal requirements (building law) compulsory in Poland and Russian Federation has been presented in the paper. Relations between national requirements in Poland and European Union are described and discussed. The similar comparison has been carried out for relations binding in Russian Federation and Eurasian Economic Unit. Final conclusions concern the similarities and differences for both legal systems applied in building industry an Poland and Russian Federation.

Keywords: Building law, comparative study, Poland, Russian Federation

4.1. Introduction

Building acts, codes or regulations (name specific for each country) can be defined as an administrative law department, which regulates issues related to all stages of the construction of facilities, such as buildings and structures. Buildings must comply with building regulations in order to obtain a building permission, usually from the local council. The main objective of these acts is to protect public health, safety and general well-being, as they concern the construction and use of buildings and structures. Construction law becomes the law of a particular jurisdiction when it is formally adopted by an appropriate government or private authority (F. Ching, S. Winkel 2015).

The early building laws appeared in ancient times. The oldest known written collection of building regulations is contained in the Hammurabi Code from about 1772 B.C. It is worth mentioning the punishment for collapsing the house and killing the owner by it- the death penalty. The protection of the health, safety and welfare of the public is the main reasons that building regulations exist (F. Ching, S. Winkel 2015).

There are many different approaches worldwide depending on a country, region or state. The most known are shown in the figure 4.1.
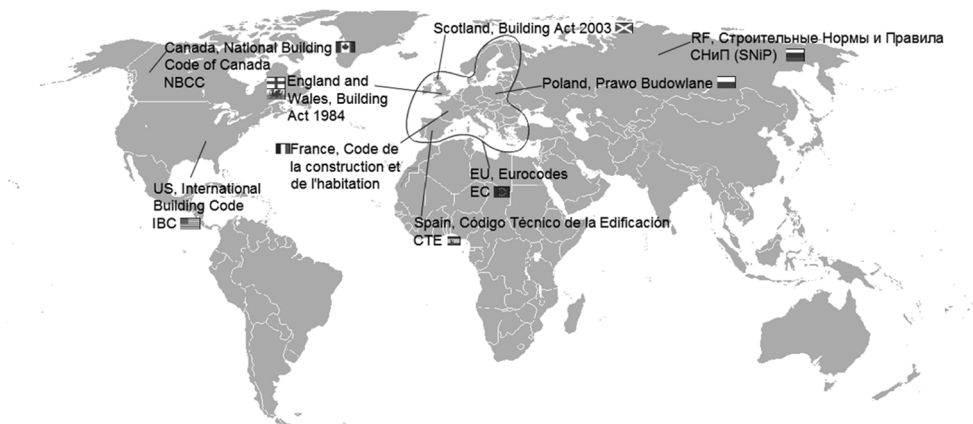

Fig. 4.1. Building Law in selected countries around the world

As we can see even within The Great Britain the law varies among nations.

There are basically two ways of implementing building law: national and local. The national one is being initiated by the government or standard organization connected to it and applied to the whole country territory and therefore called national building codes. The local one as we may suspect lies in the fact that local administration choose to start own rules valid for their jurisdiction. An example of such solution can be system of model building codes. It is maintained by an independent from the local administration standard organization and can be chosen by the authorities to use, then it becomes law. There are examples like in India where each regional unit develops its own variants, additions of National Building Code. Similar in Europe each country using Eurocodes has their own national annexes.

Every regulation no matter the country generally includes standards for structure, placement, size, usage, wall assemblies, location; rules regarding parking and traffic impact; case of fire and unusual events like earthquake, flood, hurricane etc.; energy provisions and consumption; qualification of individuals or corporations doing the work; requirements for specific building uses.

4.2. Approach in Poland

In 2004 Poland has joined the European Union. This means Poland started to use the Eurocodes, which are ten European standards for the European Union countries. Eurocodes define the rules of designing and execution of construction structures, ways of verifying the characteristics of building products of constructional significance, valid on the basis of the Harmonization Document (Polish Committee for Standardization).

Before that Poland was using its national Polish Standards. The Regulation of the Minister of Infrastructure of 12 March 2009 (Rozporządzenie Ministra Infrastruktury) changing the Regulation on the technical conditions to be met by buildings and their location granted the status of withdrawn for some parts of Polish Standards for building structures, gradually replacing them with Eurocodes as they started being approved and published in Polish language. Any changes approved by the European Committee for Standardisation are being translated by the Polish Committee for Standardisation up to date. By 2020 it is also planned to develop a completely new version of the Eurocodes, which will have to be retranslated and implemented in Poland.

The Eurocodes are divided into packages for specific issues and types of construction.

EN 1990 Basis of structural design	Safety, serviceability, durability of structures
EN 1991 Actions on structures	Loads,actions
EN 1992 Design of concrete structures	Design of structures from different materials
EN 1993 Design of steel structures	
EN 1994 Design of composite steel and concrete structures	
EN 1995 Design of timber structures	
EN 1996 Design of masonry structures	
EN 1997 Geotechnical design	Geotechnical and seismic design
EN 1998 Design of structures for earthquake resistance	
EN1999 Design of aluminium structures	

Fig. 4.2. The system of Eurocodes showing the approach in Poland

Each of the codes (except EN 1990) is divided into a number of Parts covering specific aspects of the subject. In total there are 58 EN Eurocode parts distributed in the ten Eurocodes (EN 1990 – 1999). The purpose of the Eurocodes is to provide compliance with the requirements for mechanical strength, stability and safety in case of fire within EU, a basis for construction and engineering contract specifications and a framework for creating harmonized technical specifications for building products (CE mark).

By March 2010 the Eurocodes are mandatory for the specification of European public works and are intended to become the de facto standard for the private sector. Although the Eurocodes replaced the existing national building each country is expected to issue a National Annex to the Eurocodes which will need referencing for a particular country (A. Lukianenko 2012).

It is worth adding that using Polish versions of Eurocodes is voluntary. However, Polish Standards are closely related to other technical construction regulations. According to the official position of the Polish Committee for Standardization, the use of old, withdrawn standards is possible, but this fact should be agreed between cooperating parties.

Apart from using European standards which define the designing process Poland has its own regulations. The most important document is Building Law (ustawa

Prawo Budowlane 1994), an act in the field of design, construction, supervision, maintenance and demolition of buildings and the principles of public administration authorities in this field.

The Act also regulates matters related to:

-environmental protection during activities related to demolition, building new facilities and their maintenance

-the place of investment execution and the manner of obtaining a building permission and demolition one, as well as the definition of types of construction works and constructions which do not require a building permission

-putting construction into use

-professional activities of people related to the construction industry (rights to perform independent functions in the construction industry, the so-called building licenses) and their criminal and professional responsibility

-the rights and obligations of participants in the construction process

-management when a construction disaster occurs

The act was released in 1994 but was many times changed. The last change was made in October 2018.

The act also mentions other documents- the regulation on technical conditions of the buildings and their location (Rozporządzenie Ministra Infrastruktury 2012). This Regulation establishes the technical conditions to be met by buildings and associated equipment, its location on a building plot and plot's management. The rules of the Regulation shall apply to design and construction, including restoration, extension, reconstruction and change in the use of buildings and structures aboveground and underground buildings fulfilling the functional functions of buildings and related construction equipment.

4.3. Approach in Russian Federation

Russian Federation is a part of Eurasian Economic Union and so some regulations are valid not only in the country but for the whole union. The Russian legislation, in particular, the act "About Technical Regulation" («О техническом регулировании» 2002) establishes that the main documents in the field of technical rules are technical regulations (технические регламенты). Technical regulations have a form of federal laws or acts within the Eurasian Economic Union.

The main technical regulations in the field of construction are:

-The federal law from 30th December 2009 No. 384-FZ "Technical regulations about safety of buildings and constructions" («Технический регламент о безопасности зданий и сооружений»)

-The federal law from 22th July 2008 No. 123-FZ "Technical regulations about requirements of fire safety" («Технический регламент о требованиях пожарной безопасности»)

-Technical regulations of the Eurasian Customs union of TR TS November 2011 "Safety of elevators" («Безопасность лифтов»)

From the state point of view standard technical acts (national standards and sets of rules) have to be applied in order that the construction could correspond to technical regulations.

The part of national standards and sets of rules is obligatory to use —they are approved by the resolution of the Government of the Russian Federation. For instance the list of national standards and sets of rules (or parts of such standards and sets of rules) which application provides an obligatory compatibility with requirements of the Federal Law "Technical regulations about safety of buildings and constructions". The others are applied as voluntary. At the same time the executive authorities develop and approve lists of the regulations recommended for implementing to meet the requirements of technical regulations, for example:

-the list of documents in the field of standardization as a result of which met the voluntary compatibility with requirements of "Technical regulations about safety of buildings and constructions"

- the list of documents in the field of standardization as a result of which met the voluntary compatibility with requirements of "Technical regulations about requirements of fire safety"

Federal norms are divided into three parts as we can see in figure 4.3. Moreover, republics of the Russian Federation prepare their own regulatory documents called territorial construction norms (TSN) for issues not regulated federally. The State Construction Committee approves and registers these territorial norms. The whole system of construction norms is gradually being updated (https://ru.wikipedia.org).
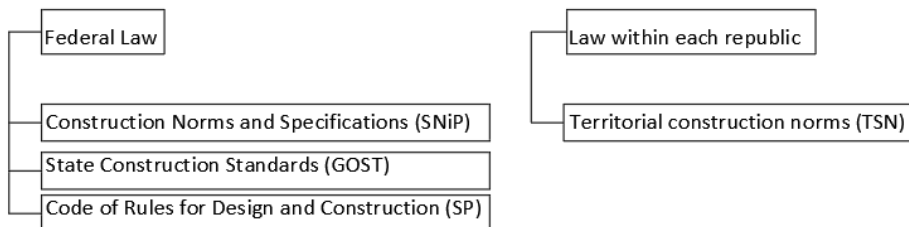
Fig. 4.3. Types of regulatory documents in Russian Federation

The most important voluntary documents, similar in meaning to Eurocodes are SNiPs- Construction Standards and Rules (Строительные нормы и правила); set of the regulations of technical, economic and legal character regulating implementation of urban planning activities, and also engineering researches, architectural and construction design and construction adopted by executive authorities.

Part 1	—— Organization, management and economics
Part 2	—— Norms of structural design
Part 3	—— Organization, production and acceptance of work
Part 4	—— Estimeted norms
Part 5	—— Rates of material and labour resources
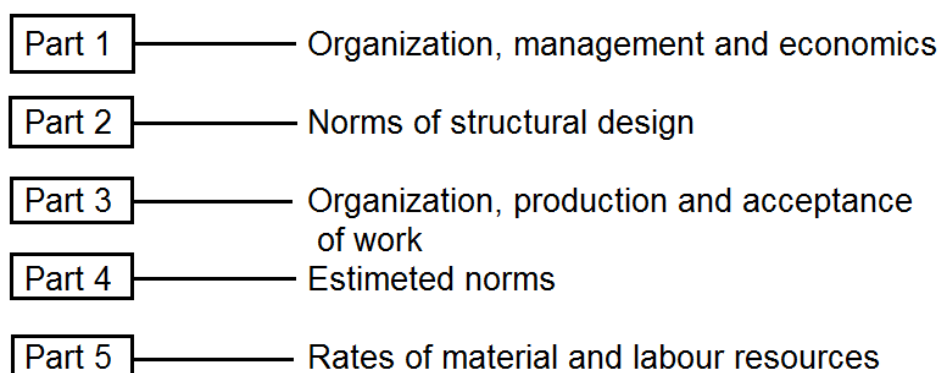
Fig. 4.4. Construction Norms and Specifications (SNiPs)

The system of normative documents in construction in the USSR worked along with system of the standardization in construction which was part of the State System of Standardization and also with system of standardization within CMEA (The Council for Mutual Economic Assistance , economic organization from 1949 to 1991 under the leadership of the Soviet Union that comprised the countries of the Eastern Bloc along with a number of communist states elsewhere). Since 1995 SNiPs were a special case of technical regulations. In 2010 the existing SNiPs were recognized by sets as codes of procedures.

The total list of SNiPs includes rules within the Eurasian Economic Union and those specific for Russian Federation (General department of standardization 1994).
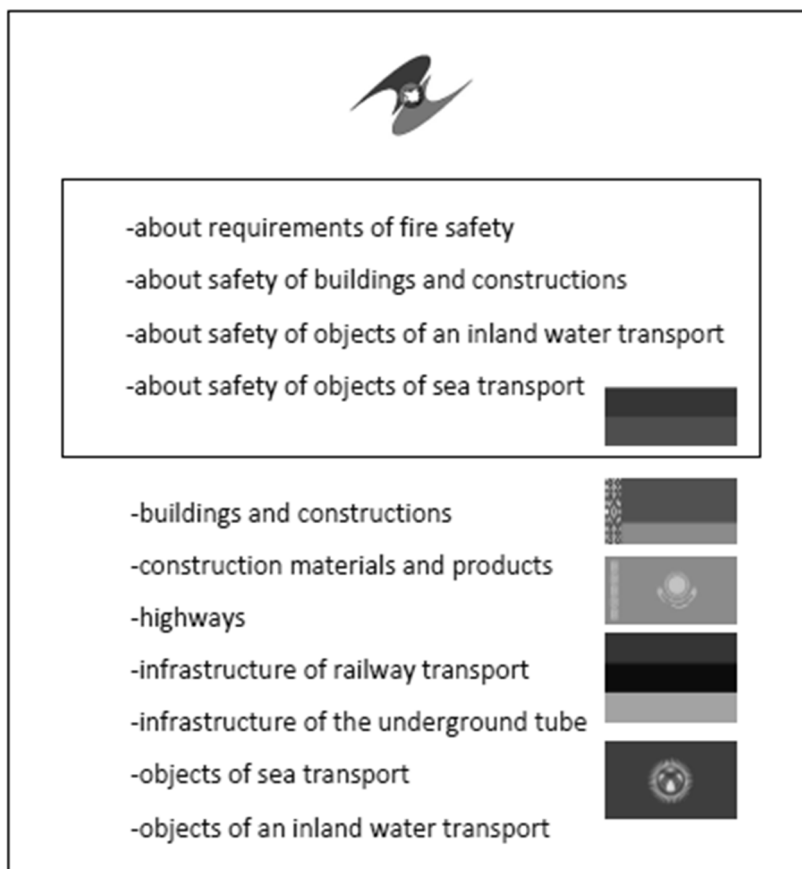
Fig. 4.5. Construction Norms and Specifications valid in Eurasian Economic Union and only in Russia

To meet obligatory requirements of technical regulations of the EAEU international standards (in case of their absence — national) are used as voluntary. In case of non-use of these standards the compliance assessment of risk analysis is carried out. In the meantime also the technical regulations of the EAEU "About safety of buildings and constructions, construction materials and products" are being developed (The federal law 2008).

Another important set of documents are GOSTs (Межгосударственный стандарт)- interstate standards. These are the regional standard accepted by the EAEU and used in this territory as voluntary. In 1992 members of the EAEU concluded the agreement in which they recognized the existing state of specification standards "GOST USRR" although removing the USSR part. GOSTs are necessary for quality control of the production made and sold in the territory of

the Russian Federation. It includes the construction branch but also many other categories like food.

Speaking about construction industry in RF you have to also mention "Town Planning Code of Russian Federation" (Градостроительный кодекс Российской Федерации 2004) - the codified regulatory legal act governing urban-planning and some relations connected to them in the territory of the Russian Federation. Although it consists of matters like territorial planning, planning zoning etc. in this code you can find architectural and construction design including survey researches, renovation which affect reliability and safety of construction, reconstruction, usage of buildings, constructions. The act was accepted in 2004.

4.4. Comparision

In this section you can find an example of approach in Poland and RF about everything before the construction stage of a single-family house and an industrial hall- all necessary documents, regulations that need to be taken into account and general procedures. The second part is a brief comparison between the codes-Eurocodes and SNiPs.

4.4.1. Detached, single-family house

4.4.1.1. General assumptions

The house consists of three floors- basement, ground floor and attic. The total area and cubature of the building are: usable area 315,12m^2, total area 350,20m^2, building area 289,00m^2, cubature 865,00m^2. The plot is not located in nature protected area. The impact of the construction does not exceed the plot. The investment is dedicated for five people to live in. The basic structure of the building is the system of external supporting walls together with internal ones.

4.4.1.2. Approach

Table. 4.1. Single family house

Procedure in Poland (https://muratordom.pl)	**Procedure in Russian Federation** (http://muravel.ru) (https://www.superdoms.ru)
I. Purchase of a plot for the construction of a house	
The basic conditions, limitations or possibilities concerning the plot and possible construction are specified in two documents. The first one, the local zoning plan (Miejscowy plan zagospodarowania przestrzennego) is passed by the Commune Council and specifies whether single-family development is allowed in an area, what is the allowed area of development, lines of development, dimensions of objects etc. The second one is the decision determining the conditions of development (decyzja ustalająca warunki zabudowy) it does not give any rights to the land, does not infringe the interests of third parties, and may be issued to several interested parties. What is important, the decision is valid indefinitely.	If it is a single-family house, procedure will be quite easy. It is necessary to fill in the relevant documents in local administration office. The fragment from the local zoning plan can be received on hands within several days. If your ground is in the area which has no plan of zoning, you have to contact the local administration for zoning.
II. Architectural and construction project	
When we already have the above decision or we know the provisions of the zoning plan, we can proceed to the selection of the project. We can delegate an authorised person, i. e. an architect, to prepare an individual project for us or we can choose a catalogue design. Each project consists of: -actual house project, called architectural and construction project, -parcel or land development project	It is the main document which is the basis for issuing the construction license. It is necessary to have prepared project or to ask the architect to design the individual project (usually such solution is a little more expensive). It should be noted that decision-making for the individual project takes a little more than time for the approval of the prepared project. Each project should consists of map noting property borders, sewage map,

	communication system and land development plan, arrangement and outline of the planned constructions, project of land management. Lack of any of the above documents causes the project being incomplete and therefore that the construction cannot begin.
III. Application of the construction	
The basic legal act regulating the whole procedure is the Budiling Law Act. The Act allows the construction of buildings only on the basis of a notification, without obtaining a final decision on the building permit. Having all the required documents we need to go to the district office and report there the intention to start building the house. The notification shall specify the type, extent and manner of execution of the works and the date of their commencement. The notification shall be made before the beginning of the construction works and the administration may object within 21 days. If there is no objection, we can proceed with the construction.	When applying you have to have the project of real estate. Thus you have to specify type of an investment, characteristics of construction, the expected access to real estate or ground, the need of water supply, estimated quantity of parking spaces, the ground free from a building. In RF it is required to have a building permission with the documents above. The license is given by executive authority of the Russian Federation or local government according to their competence. The nowadays legislation in the construction field constantly changes. Is it even recommended to ask special companies for help because procedure of paperwork demands serious legal knowledge. Obtaining technical documentation is equivalent to permission to connect the electricity, water, gas and the sewerage. You have to apply the demand for terms of delivery to the energy, water, sewerage.
IV. The beginning of the construction	
This stage takes place at the moment of commencement of preparatory works on the construction site such as: geodetic delineation, levelling of the area, development of the construction site, realizations of connections to the technical infrastructure network.	Similar in meaning to Polish approach.

4.4.2. Industrial hall

4.4.2.1. General assumptions

Industrial one-storey hall intended for warehouse purposes and made of steel. The construction consists of repeatable transverse systems with a truss and columns. Its designed length is 160,60m and width 26,00m with the total cubature 45514,04m^2. The structure will be insulated.

4.4.2.2. Approach

Table. 4.2. Industrial hall

Procedure in Poland (https://www.mcmproject.com.pl)	Procedure in Russian Federation (http://stroy-trading.ru) (https://maistro.ru)
I. Architectural plan	
Development of the architectural concept, prepared by the architect specifying the planned size of the building, the use of production technology and the number of employees . The role of such a document is significant, as it allows to check whether the planned investment size will fit in a given area.	Analogical; concept should define the purpose of investment, exact production, parameters of the investment, energy consumption, etc.
II. The administrative documentation	
Obtaining a decision on land development and development conditions. Anyone can get a permit without having ownership of the property. You must complete the application for issuing the decision in which you have to specify planned function of the facilities, the building area, the height of the buildings, the biologically active area, method of water supply, sewage disposal and rainwater, possibilities of heating and power supply. It is advisable to attach 2 copies of the map to the so-called location purposes and a statement on ensuring the supply of the required amount of electricity, heat, water, gas, etc. The document prepared in this way must be	Documents are given by the local government, the organizations operating engineering systems, the controlling structures and so when the applicant has property rights to the land plot. The initial documentation includes: documents confirming the ownership of the land; town planning documentation confirming the possibility of placing the object planned for construction on the selected site; decisions of the city administration; conclusions and approvals from the controlling; sanitary-epidemiological service,

submitted to the Urban Planning Department of the relevant local administration. When the investment area is covered by the so-called local zoning plan there is no need to apply for a decision, the local zoning plan contains a sufficient description of all the required parameters. All you have to do is apply to the Urban Planning Department for an extract and an outline from the local plan.	technical conditions of fire supervision, conclusion of natural resources management and environmental protection.
III. Construction project	
The project should include: the concept of land development, architecture, sanitary and electrical installations, both external and internal, propositions for the deployment of roads and exits. During the work on the construction project, every solution should be consulted with the owners of technical infrastructure, road management, restorer, Food Safety and Inspection Service, experts for fire protection and an investor.	The project should include: scheme of planning organization of the plot; architectural solutions; constructive and space-planning solutions; information about engineering equipment, engineering and technical support; organization of construction; impact on the environment; fire safety; agreements with experts, restorer etc.
IV. Application of the construction	
Having all documents above time to apply for this document. It can do only a person or company that proves the so-called the right to use the property for construction purposes. The document should be submitted to the Department of Architecture of the County Office which, by conducting the administrative proceedings, informs about the planned investment owners or managers of neighbouring real estates. The entire procedure takes about 65 days.	"Working documentation" is developed on the basis of technical solutions defined in the project. The document regulating the composition, form and content of materials at this stage is the National Standard GOST R21.1101-2013 "Requirements for design and working documentation". Similar to house construction you have to have a building permission. The license is given by executive authority or local government according to their competence. If the main technical solutions have already been agreed between the construction participants, the construction can begin immediately after receiving a positive expert opinion and a construction permit.

4.4.3. Eurocodes and SNiPs

In the 70s "the construction boom in the USSR" (http://muravel.ru) pushed also Europe to create of similar system of standards which basis had the same principles, as in SNiPs. However distinction in economic formations — market and planned ones — introduced the amendments. In Europe they didn't specify actual processing methods and decisions and gave only the unified models and lists of the normalized parameters determined at the national level. They both are based on the limit state design system, present regulations to define the principal objectives, affect the design issues with almost all the major construction materials but Eurocodes are divided into different parts by the material issue and SNiPs by the structural design issues.

Unlike SNiPs the system of Eurocodes doesn't include norm of design of buildings and constructions of a different functional purpose (industrial and civil, inhabited, multipurpose, hotels, etc.), and also question of town planning, engineering systems, architectural supervision, etc. (A. Lukianenko 2012).

In some of the formal soviet republics Eurocodes became or are planning to be national standards like in Ukraine, Kazakhstan. This means also in RF there is growing interest of using Eurocodes. Acceptance of eurocodes involves big changes. These are changes in regulations of technical regulation and standardization, but also to pricing in construction, budget documentation, to create new specialized software.

More than a half of the lands in Russia are karst zones. Essential differences of standards are observed in question of high constructions. It is necessary to perform installation and construction works on the fast-built technologies in such places accurately, without any deviations from design calculations. It is impossible to implement the European standards in zones where there are various slope processes: flooding, landslides, mudflows, avalanches, etc. All these differences of standards because of national, social and climatic features don't allow to carry out prefabricated constructions usage of only Eurocodes. It concerns also those regions of Russia which territorially are considered as seismically dangerous zones. But as said before Eurocodes are becoming more and more popular. One of their advantage is a significant metal saving, and the other is a reduction of the cost of design and construction installations. It is believed that the Eurocodes are developed taking into account the analytics of the latest catastrophes and accidents that occur in different countries in the world (https://www.superdoms.ru).

Nowadays economic and production prerequisites appeared according to which Eurocodes and SNiPs should exist in parallel. For the domestic producer and the contractor of installation and construction works so he or she could regulate prices for products and services, it is necessary to harmonize Eurocodes and

SNiPs. And for this purpose the optimal decisions answering to the general rules of construction and design both in Europe, and in Russia will be necessary.

4.4. Conclusion

As described Poland and Russian Federation are parts of different Unions- EU and EAEU. This means their national rules have to comply with the union law. In a few words although Poland is part of the EU using Eurocodes isn't obligatory, but it is rather a standard connected to other national regulations. It is also possible to use old Polish codes, but only with the agreement of both sides. Eurocodes establish technical uniform norms for all member countries of the European Union and uniform approach to design with national annexes. However the most important regulation is Building Law regarding matters of design, construction, supervision, maintenance and demolition of buildings and the principles of public administration authorities.

The RF law is more complicated. There are three levels of legislation in the Russian Federation: federal, regional and local. The major laws regulating construction and that were described in the article are established at a federal level, and may be made more specific at the regional or local levels.

The systems of Eurocodes and SNiPs are similar but have also many differences. They both are based on the limit state design system, present regulations to define the principal objectives, affect the design issues with almost all the major construction materials but Eurocodes are divided into different parts by the material issue and SNiPs by the structural design issues. SNiPs and Eurocodes differ on structure and the contents in a format and the status. And at the same time the purposes and tasks which are implemented as a result of application of these documents are similar. Their basic purpose is safety of construction from various materials on two key aspects: their mechanical durability and fire resistance.

References

(1994) The act *Building Law*

(2002) *Regulation of the Minister of Infrastructure on technical conditions of the buildings and their location*

Polish Comitee for Standarization *Designing building structures using Eurocodes*

A. Lukianenko (2012) *Comparison of Russian norms (SNiPs) and European norms (Eurocodes) for road and railway bridges*

(2004) The act *Town Planning Code of Russian Federation*

(2002) Federal law *About Technical Regulation*

(2009) The federal law No. 384-FZ *Technical regulations about safety of buildings and constructions*

(2011) Technical regulations of the Eurasian Customs union of TR TS *Safety of elevators*

General department of standardization, technical regulations and certifications, (1994) *System of normative documents in construction. Basic principles, Moscow*

F. Ching, S. Winkel (2015) *Building Codes Illustrated: A Guide to Understanding the 2015 International Building Code*

(2008) The federal law No. 123-FZ *Technical regulations about requirements of fire safety*

СП 56.13330.2011 SNiP 31-03-2001 Production Buildings

Websites accessed since 7th to 23rd November 2018

https://ru.wikipedia.org

https://muratordom.pl

http://muravel.ru

https://www.superdoms.ru

http://stroy-trading.ru

https://maistro.ru

https://www.mcmproject.com

5. Numerical analysis of a semi-circular disc with an angled crack loaded in mixed-mode

Lucie Malíková[1], Petr Miarka[2], Hana Šimonová[3], Barbara Kucharczyková[4]

[1] *Brno University of Technology, Faculty of Civil Engineering, Institute of Structural Mechanics, Brno and Czech Republic and Institute of Physics of Materials, Brno, Czech Republic, malikova.l@fce.vutbr.cz, orcid.org/0000-0001-5868-5717*

[2] *Academy of Sciences of the Czech Republic, Institute of Physics of Materials, Brno, Czech Republic and Brno University of Technology, Faculty of Civil Engineering, Institute of Structural Mechanics, Brno, Czech Republic, petr.miarka@vut.cz, orcid.org/0000-0002-4953-4324*

[3] *Brno University of Technology, Faculty of Civil Engineering, Institute of Structural Mechanics, Brno, Czech Republic, simonova.h@vutbr.cz, orcid.org/0000-0003-1537-6388*

[4] *Brno University of Technology, Faculty of Civil Engineering, Institute of Building Testing, Brno, Czech Republic, barbara.kucharczykova@vutbr.cz, orcid.org/0000-0002-7123-5099*

Abstract: A semi-circular disc with an angled crack loaded in mixed-mode (mode I + II) was chosen for a numerical analysis of crack deflection angles. Although the mode I of loading is often dominant in engineering praxis, lots of structures are subjected at least at the beginning of the crack propagation to a mixed-mode loading. Therefore, it is necessary to study the crack behaviour under such conditions and it has been shown that the multi-parameter fracture mechanics approach can be useful in this case of loading. Thus, various cracked configurations of the semi-circular disc were simulated numerically under three-point bending and a generalized form of selected fracture criteria is applied to calculate the crack deflection angle. It is discussed, which configurations can be safely described by means of the classical single-parameter fracture mechanics (i.e. only the stress intensity factors K_I and K_{II} controls the crack propagation), and which ones shall be analysed via multi-parameter fracture mechanics based on the Williams expansion. As the result, several configurations of the semi-circular disc with an angled crack under three-point bending are recommended to be tested experimentally in order to prove the results of the numerical simulations based on the finite elements.

Keywords: Surface cracks, Finite element analysis, stress

5.1. Introduction

Fracture mechanics appeared in order to be able to assess the reliability and lifetime of structures with defects and cracks (Anderson, 1995) that are presented everywhere because of structures production as well as because of their handling and using.

In 1920, Griffith found a quantitative connection between fracture stress and flaw size (Griffith, 1920). He took advantage of the work of stress analysis of an elliptical hole (made by Inglis in 1913 (Inglis, 1913)) applying it to the unstable crack propagation. The progress in the fracture mechanics concepts takes place up to now. There exist still lots of problems in assessment of fracture response in various novel as well old materials. One of the directions, where the fracture mechanics is oriented, is the multi-parameter concept, what represents using of more than only one controlling parameter for the crack behavior description.

The stress tensor components were firstly expressed as a series expansion by Williams (Williams, 1957) assuming its coefficients dependent on the loading conditions. In the last years, lots of studies have proved that not only the first term of the Williams expansion (corresponding to the stress intensity factor), but also the second one (corresponding to *T*-stress) is important when the crack-tip stress states shall be properly described (Chen, 2002; Ayatollahi and Zakeri, 2007; Christopher *et al.*, 2007; Aliha, Ayatollahi and Kharazi, 2009). The necessity of considering also the higher-order terms in some practical cases has been published for instance in (Ramesh, Gupta and Kelkar, 1997).

Another example, how the multi-parameter approach can be applied, is its utilization in fracture criteria derived for estimation of the further crack propagation angle (Smith, Ayatollahi and Pavier, 2001; Malíková, 2015; Hou *et al.*, 2016). Again, the referred works show that taking into account more than only single parameter for approximation of the crack-tip stress field can be very useful for some specific geometric configuration, materials etc.

In this work, a crack deflection angle in a semi-circular disc loaded under 3-point bending is investigated. The various initial inclination angles of the crack ensure various levels of mixed-mode (I+II) conditions. A numerical parametric analysis is performed in order to study the influence of several parameters on the crack deflection angles and in order to prove the importance of the higher-order terms of the Williams expansion. Conclusions are made based on the results obtained and several particular cracked SCB configurations are recommended for future experiments on a novel quasi-brittle composite material to establish the significance of the multi-parameter fracture mechanics concept via comparison of the numerical analysis with experimental results.

5.2. Williams-expansion-based crack-tip stress field

As stated above, the stress tensor components were firstly expressed as a series expansion by Williams (Williams, 1957). The relations were derived for a homogeneous elastic isotropic cracked body subjected to an arbitrary remote loading and can be written as follows:

$$\sigma_{ij} = \sum_{n=1}^{\infty} \frac{n}{2} r^{\frac{n}{2}-1} f_{ij}(n,\theta) A_n + \sum_{m=1}^{\infty} \frac{m}{2} r^{\frac{m}{2}-1} g_{ij}(m,\theta) B_m \ . \quad (5.1)$$

Where:

l, j	–	stress tensor components indexes: $i, j \in \{x, y\}$,
r,θ	–	polar coordinates considering the centre of the system at the crack tip,
f_{ij}, g_{ij}	–	known stress functions corresponding to the loading mode I and II, respectively,
A_n, B_m	–	unknown coefficients of the higher-order terms of the Williams expansion (WE).

A similar series can be derived for displacement vector components and it is directly applied when the over-deterministic method is used for calculation of the unknown coefficients A_n and B_m.

5.3. Estimation of the WE coefficients

There have been presented several methods for estimation of the WE coefficients. Each of them is based on a different principle. The most known methods can be the boundary collocation method, hybrid crack element method, as well as over-deterministic method etc. (Tong, Pian and Lasry, 1973; Karihaloo and Xiao, 2001; Xiao, Karihaloo and Liu, 2004; Su and Fok, 2007; Ayatollahi and Nejati, 2011). Each from the methods mentioned has its advantages and disadvantages. For purposes of this paper, the over-deterministic method (ODM) was chosen because of its simplicity. The ODM requires neither utilization of special crack elements nor special mathematical theories. Its principle consists in direct application of the WE series derived for the displacement vector components.

Practically, a common finite element analysis on the cracked specimen under study is performed and displacements of a selected set of nodes around the crack tip are obtained together with their polar coordinates during post-processing. Thus, quite a large system of equation is built and its solution is represented by the coefficients of the higher-order terms. An arbitrary number of the WE coefficients can be chosen until the following condition is fulfilled:

$$2k > N + M + 2 \ . \quad (5.2)$$

Where:

   N –   number of mode I WE terms,
   M –   number of mode II WE terms,
   k –   number of nodes selected around the crack tip.

Several more recommendations on the use of the over-deterministic method, its accuracy etc. can be found in literature (Šestáková, 2013; Růžička, Malíková and Seitl, 2017).

5.4. Multi-parameter fracture criteria

When the WE coefficients are known an arbitrary stress component can be expressed via multi-parameter power series. This idea is used within the fracture criteria that were suggested for estimation of the further crack propagation angle. In this work, two very common criteria are mentioned. The former one is the maximum tangential stress (MTS) criterion and the latter one is the minimum strain energy density (SED) criterion. Both criteria are applied in their generalized form, which is connected to assuming more than only one parameter (i.e. the stress intensity factor) for assessment of the crack behaviour. The multi-parameter form of the fracture criteria is related to one more phenomenon and it is their dependence on a length parameter that is often called the *critical distance* (Sih and Ho, 1991; Seweryn and Lukaszewicz, 2002; Susmel and Taylor, 2008). Note that classical MTS as well as SED criteria can be expressed only via the stress intensity factors and there is not any dependence on a length parameter.

The idea of the MTS criterion (Erdogan and Sih, 1963) consists in the assumption that a crack propagates in a material in the direction where the tangential stress reaches its maximum. This condition can be mathematically written by means of derivatives:

$$\frac{\partial \sigma_{\theta\theta}}{\partial \theta} = 0 \ \text{ and } \ \frac{\partial^2 \sigma_{\theta\theta}}{\partial \theta^2} < 0 \ . \tag{5.3}$$

Where:

   $\sigma_{\theta\theta}$ –   tangential stress,
   θ –   angle of the polar coordinate system defined with its origin at the crack tip.

The multi-parameter approach consists in the approximation of the tangential stress via the WE expansion considering various numbers of the WE terms.

Similarly, the energy-based SED criterion (Sih, 1973, 1974) assumes that a crack will propagate in a material in the direction where the strain energy density reaches its minimum. Again, mathematically written:

$$\frac{\partial S}{\partial \theta} = 0 \ \text{ and } \ \frac{\partial^2 S}{\partial \theta^2} > 0 \ , \text{ where } S = \frac{1}{2\mu}\left[\frac{\kappa+1}{8}(\sigma_{rr} + \sigma_{\theta\theta})^2 - \sigma_{rr}\sigma_{\theta\theta} + \sigma_{r\theta}^2\right]. \tag{5.4}$$

Where:

S – strain energy density factor,

θ – angle of the polar coordinate system defined with its origin at the crack tip.

$\sigma_{\theta\theta}$ – tangential stress,

σ_{rr} – radial stress,

$\sigma_{r\theta}$ – shear stress in the polar coordinate system,

μ – shear modulus,

κ – Kolosov's constant.

The tangential, radial and shear stress in the expression for the strain energy density factor are approximated via WE considering various number of its initial terms.

The procedure of searching for maximum (MTS criterion) or minimum (SED criterion) is programmed in Wolfram Mathematica software ('Wolfram Mathematica Documentation Center', 2018) and the values of the further crack propagation angles of the crack in SCB specimen are presented in the section devoted to presenting of obtained results.

5.5. Semi-circular disc with and angled crack under three-point bending

The schema of the specimen selected for the analysis of investigation of the further crack deflection with impact to the importance of the higher-order terms of the WE can be seen in Fig. 5.1. In the referred figure, the P represents the loading force, S is the span between the supports, R is the radius of the disc, β is the initial crack inclination angle and a represents the crack length. Because the analysis presented in this work should be parametric and should involve more various mixed-mode levels, several parameters were not constant but varied within the analysis. The following values of the individual parameters were considered: $P = 1$ kN, $R = 50$ mm, $S = 60 \div 80$ mm, $a = 10 \div 25$ mm, $\beta = 10° \div 50°$. Combination of these values of the parameters ensures the mixed-mode level varying between $K_I/K_{II} = 0.2 \div 8.2$. Material properties of the numerical model were set up with accordance to the properties of concrete, because an experimental campaign on a novel fine-grained composite based on the alkali-activated slag is prepared: Young's modulus $E = 35$ MPa, Poisson's ratio $\nu = 0.23$.
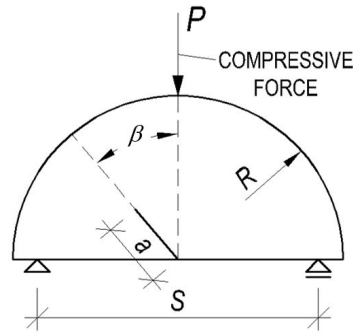
Fig. 5.1. Schema of the Semi-Circular disc under 3-point Bending (SCB) with an angled crack

A two-dimensional numerical model of the cracked SCB disc was created in a commercial finite element software ANSYS ('ANSYS Program Documentation', 2019). Plane strain boundary conditions were set up and a quadrilateral element type PLANE183 were used for meshing the cracked specimen. The crack-tip singularity was modelled through special crack elements that are implemented in the software. For evaluation of the ODM, the displacements of nodes at the radial distance of 4 mm were used and 10 coefficients of the WE were calculated from the system of equations. Then, the fracture criteria introduced above were applied at various critical distances r_c = 0.1, 0.5 and 1.0 mm in order to estimate the angle of the further crack propagation direction, see the obtained results in the following section.

5.6. Achieved results and their discussion

The dependences of the crack deflection angle are displayed as functions of the mixity parameter as has been used in several works of other authors (Aliha and Ayatollahi, 2012; Li *et al.*, 2018):

$$M^e = \frac{2}{\pi} arctg \frac{K_I}{K_{II}} \ . \tag{5.5}$$

Where:

K_I –   mode I stress intensity factor,

K_{II} –   mode II stress intensity factor.

The mixity parameter can achieve the values between 0 (pure mode II) and 1 (pure mode I). Note that the positive crack deflection angles represent the crack propagation towards the loading force. Only selected results are presented in order to point to the most important conclusions. The basic set of result is in Figs. 5.2 and 5.3, where the dependences of the crack deflection angle γ obtained via MTS and SED criterion, respectively, on the mixity parameter M^e for the span

S = 80 mm, relative crack lengths a/R = 0.2 and 0.5, critical distances r_c = 0.1, 0.5 and 1.0 mm and 1, 2, 3, 6 and 10 initial WE terms considered for stress approximation are presented.
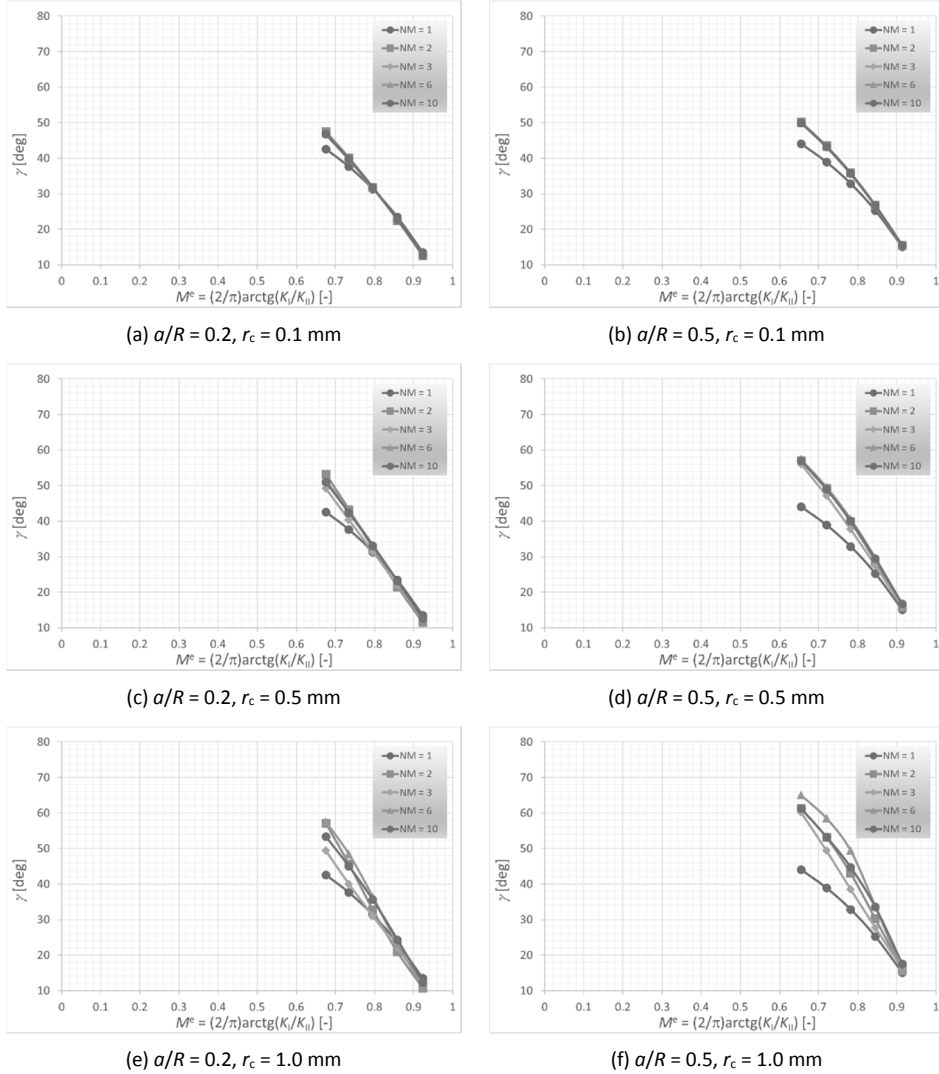

(a) a/R = 0.2, r_c = 0.1 mm

(b) a/R = 0.5, r_c = 0.1 mm

(c) a/R = 0.2, r_c = 0.5 mm

(d) a/R = 0.5, r_c = 0.5 mm

(e) a/R = 0.2, r_c = 1.0 mm

(f) a/R = 0.5, r_c = 1.0 mm

Fig. 5.2. Dependence of the crack deflection angle γ obtained via MTS criterion on the mixity parameter M^e for the span S = 80 mm, relative crack lengths a/R = 0.2 and 0.5, critical distances r_c = 0.1, 0.5 and 1.0 mm and 1, 2, 3, 6 and 10 initial WE terms considered for stress approximation.
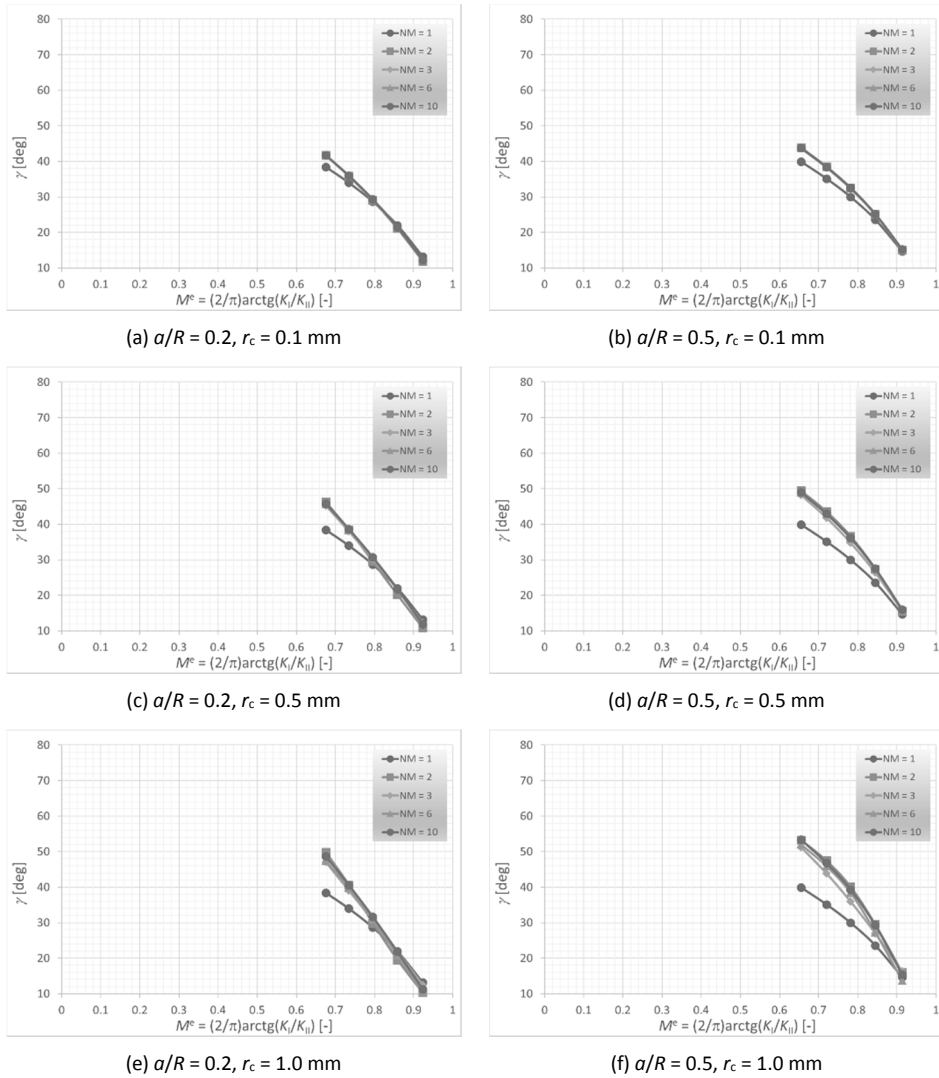
(a) $a/R = 0.2$, $r_c = 0.1$ mm

(b) $a/R = 0.5$, $r_c = 0.1$ mm

(c) $a/R = 0.2$, $r_c = 0.5$ mm

(d) $a/R = 0.5$, $r_c = 0.5$ mm

(e) $a/R = 0.2$, $r_c = 1.0$ mm

(f) $a/R = 0.5$, $r_c = 1.0$ mm

Fig. 5.3. Dependence of the crack deflection angle γ obtained via SED criterion on the mixity parameter M^e for the span $S = 80$ mm, relative crack lengths $a/R = 0.2$ and 0.5, critical distances $r_c = 0.1$, 0.5 and 1.0 mm and 1, 2, 3, 6 and 10 initial WE terms considered for stress approximation.

The results in Figs. 5.2 and 5.3 enables to summarize several conclusions:

- The classical single-parameter fracture mechanics concept differs from the multi-parameter one even at small critical distances from the crack tip

(r_c = 0.1 mm). Nevertheless, if the mode I of loading prevails, the classical form of the fracture criteria can be used safely.

- Generalized fracture criteria become more significant for cracked configuration, with increasing effect of loading mode II.
- The differences between the results, when more WE terms are considered, increase with larger distances from the crack tip, where the generalized fracture criteria are used.
- The SED criterion seems to be less sensitive to the choice of the number of the WE higher-order terms than the MTS criterion; but it surely proves the difference between the single-parameter and multi-parameter concept.
- The differences between the crack deflection angles obtained via single-parameter and multi-parameter fracture criteria are more evident in cases of the longer crack a/R = 0.5.

With respect to the dependences plotted in Figs. 5.2 and 5.3, further results are presented only for MTS criterion applied at larger distances for the SCB configuration with a longer crack (a/R = 0.5). Now, the effect of the various span between the supports of the SCB specimen is analysed, see Fig. 5.4, where the dependences of the crack deflection angle γ on the mixity parameter M^e for the supports span S = 60, 70 and 80 mm, critical distances r_c = 0.5 and 1.0 mm and 1, 2, 3, 6 and 10 initial WE terms considered for stress approximation are displayed.

Based on the results in Fig. 5.4, the following summary can be stated:

- When the distance between the supports decrease, loading mode II becomes more dominant (as show the values of the mixity parameter M^e approaching the zero value) and the crack deflection angles are generally higher.
- At larger distances from the crack tip, the multi-parameter MTS criterion gives more different values of the crack deflection angle than the single-parameter one.
- When the results obtained via the single-parameter and multi-parameter form of the MTS criterion are compared, the values of the crack deflection angle can differ by up to 20°, which is the case of the longer span between the supports (S = 70 or 80 mm) considering the larger critical distance value r_c = 1.0 mm.
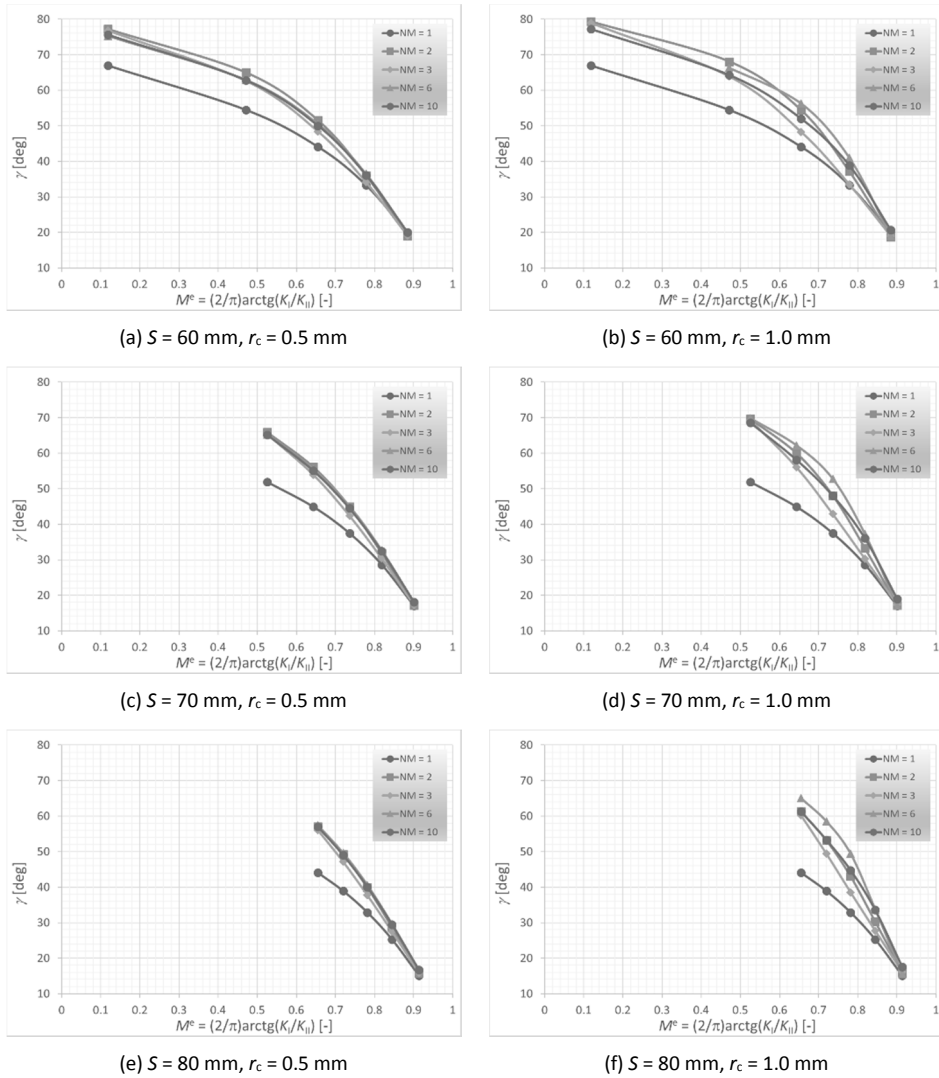
(a) S = 60 mm, r_c = 0.5 mm

(b) S = 60 mm, r_c = 1.0 mm

(c) S = 70 mm, r_c = 0.5 mm

(d) S = 70 mm, r_c = 1.0 mm

(e) S = 80 mm, r_c = 0.5 mm

(f) S = 80 mm, r_c = 1.0 mm

Fig. 5.4. Dependence of the crack deflection angle γ obtained via MTS criterion on the mixity parameter M^e for the span S = 60, 70 and 80 mm, relative crack length a/R = 0.5, critical distances r_c = 0.5 and 1.0 mm and 1, 2, 3, 6 and 10 initial WE terms considered for stress approximation.

5.7. Conclusions

A semi-circular disc with an angled crack under three-point bending was investigated via the multi-parameter fracture mechanics concept. Particularly, the crack deflection angle was studied and results obtained by means of the generalized form of the MTS and SED criteria taking into account various numbers of the initial WE terms were compared. It was found out that the largest differences in comparison to the classical single-parameter fracture criteria concept occur when:

- the length of the crack is larger,
- the fracture criterion is applied at larger distance from the crack tip
- the MTS criterion instead of SED criterion is applied,
- loading mode II becomes significant,
- the span between the supports of the SCB configuration is higher.

Based on the results presented in this work, a particular geometry can be chosen in order to verify the conclusions stated above and prove the significance of the higher-order terms of the WE.

Acknowledgment

References

Aliha, M. R., Ayatollahi, M. R. and Kharazi, B. (2009) 'Mode II fracture assessment using ASFPB specimen', *International Journal of Fracture*, 159, pp. 241–246.

Aliha, M. R. M. and Ayatollahi, M. R. (2012) 'Analysis of fracture initiation angle in some cracked ceramics using the generalized maximum tangential stress criterion', *International Journal of Solids and Structures*. Elsevier Ltd, 49(13), pp. 1877–1883. doi: 10.1016/j.ijsolstr.2012.03.029.

Anderson, T. L. (1995) *Fracture mechanics: fundamentals and applications*. Florida: CRC Press LLC.

'ANSYS Program Documentation' (2019). Houston: Swanson Analysis System, Inc.

Ayatollahi, M. R. and Nejati, M. (2011) 'An over-deterministic method for calculation of coefficients of crack tip asymptotic field from finite element analysis', *Fatigue and Fracture of Engineering Materials and Structures*, 34(3), pp. 159–176. doi: 10.1111/j.1460-2695.2010.01504.x.

Ayatollahi, M. R. and Zakeri, M. (2007) 'T-stress effects on isochromatic fringe patterns in mode II', *International Journal of Fracture*, 143, pp. 189–194.

Chen, Y. Z. (2002) 'Closed form solution of T-stress in plane elasticity crack problems', *International Journal of Solids and Structures*, 37, pp. 1629–1637.

Christopher, C. J. *et al.* (2007) 'Towards a new model of crack tip stress fields', *International Journal of Fracture*, 148, pp. 361–371.

Erdogan, F. and Sih, G. C. (1963) 'On the crack extension in plates under plane loading and transverse shear', *Journal of Basic Engineering*, 55(6), pp. 519–525.

Griffith, A. A. (1920) 'The phenomena of rupture and flow in solids', *Philosophical Transactions, Series A*, 221, pp. 163–198.

Hou, C. *et al.* (2016) 'Determination of fracture parameters in center cracked circular discs of concrete under diametral loading: A numerical analysis and experimental results', *Theoretical and Applied Fracture Mechanics*, 85, pp. 355–366.

Inglis, C. E. (1913) 'Stresses in a plate due to the presence of cracks and sharp corners', *Transactions of the Institute of Naval Architects*, 55, pp. 219–241.

Karihaloo, B. L. and Xiao, Q. Z. (2001) 'Accurate determination of the coefficients of elastic crack tip asymptotic field by a hybrid crack element with p-adaptivity', *Engineering Fracture Mechanics*, 68(15), pp. 1609–1630. doi: 10.1016/S0013-7944(01)00063-7.

Li, X. H. *et al.* (2018) 'Instability of cracks initiation from a mixed-mode crack tip with iso-stress intensity factors K I and K II', 96(May), pp. 262–271. doi: 10.1016/j.tafmec.2018.05.004.

Malíková, L. (2015) 'Multi-parameter fracture criteria for the estimation of crack propagation direction applied to a mixed-mode geometry', *Engineering Fracture Mechanics*, 143. doi: 10.1016/j.engfracmech.2015.06.029.

Ramesh, K., Gupta, S. and Kelkar, A. A. (1997) 'Evaluation of stress field parameters in fracture mechanics by photoelasticity-revisited', *Engineering Fracture Mechanics*, 56, pp. 25–45.

Růžička, V., Malíková, L. and Seitl, S. (2017) 'Over-deterministic method: The influence of rounding numbers on the accuracy of the values of williams' expansion terms', *Frattura ed Integrita Strutturale*, 11(42). doi: 10.3221/IGF-ESIS.42.14.

Šestáková, L. (2013) *How to enhance efficiency and accuracy of the over-deterministic method used for determination of the coefficients of the higher-order terms in williams expansion*, *Applied Mechanics and Materials*. doi: 10.4028/www.scientific.net/AMM.245.120.

Seweryn, A. and Lukaszewicz, A. (2002) 'Verification of brittle fracture criteria for elements with V-shaped notches', *Engineering Fracture Mechanics*, 69, pp. 1487–1510.

Sih, G. C. (1973) 'Some basic problems in fracture mechanics and new concepts', *Engineering Fracture Mechanics*, 5, pp. 365–377.

Sih, G. C. (1974) 'Strain energy density factor applied to mixed mode crack problems', *International Journal of Fracture Mechanics*, 10, pp. 305–321.

Sih, G. C. and Ho, J. W. (1991) 'Sharp notch fracture strength characterized by critical energy density', *Journal of Theoretical and Applied Fracture Mechanics*, 16, pp. 179–214.

Smith, D. J., Ayatollahi, M. R. and Pavier, M. J. (2001) 'The role of T-stress in brittle fracture for linear elastic materials under mixed-mode loading', *Fatigue and Fracture of Engineering Materials and Structures*, 24(2), pp. 137–150.

Su, R. K. L. and Fok, S. L. (2007) 'Determination of coefficients of the crack tip asymptotic field by fractal hybrid finite elements', 74, pp. 1649–1664. doi: 10.1016/j.engfracmech.2006.09.009.

Susmel, L. and Taylor, D. (2008) 'The theory of critical distances to predict static strength of notched brittle components subjected to mixed-mode loading', *Engineering Fracture Mechanics*, 75, pp. 534–550.

Tong, P., Pian, T. H. and Lasry, S. J. (1973) 'A hybrid-element approach to crack problems in plane elasticity', *International Journal of Numerical Methods in Engineering*, 7, pp. 297–308.

Williams, M. L. (1957) 'On the stress distribution at the base of a stationary crack', *Journal of Applied Mechanics*, 24, pp. 109–114.

'Wolfram Mathematica Documentation Center' (2018). Champaign: Wolfram Research.

Xiao, Q. Z., Karihaloo, B. L. and Liu, X. Y. (2004) 'Direct determination of SIF and higher order terms of mixed', *International Journal of Fracture*, 2(3), pp. 207–225.

6. Methodology for static analysis of pre-stressed plane cable systems

Dimitar Mitashev[1], Svetlana Lilkova-Markova[2]

[1]*University of Architecture, Civil Engineering and Geodesy, Faculty of Hydraulic Engineering, Department of Technical Mechanics, Sofia, Bulgaria, mitashev@abv.bg, orcid.org/0000-0001-6494-1879*

[2]*University of Architecture, Civil Engineering and Geodesy, Faculty of Hydraulic Engineering, Department of Technical Mechanics, Sofia, Bulgaria, lilkovasvetlana@gmail.com, orcid.org/0000-0003-0582-8176*

Abstract: Cable systems are an important structural type of systems. They are elegant, vivid and competitive and they always lead structures „towards the limit". The article presents the theoretical model, asumptions and the main elements' static analysis of one of the major types of cable systems – the "two-cables" plane systems. The article presents a description of the geometry and the elements of these systems, their static analysis and a somewhat simplified methodology for analysis with the use of conventional and not that complex softwares. The use of "main unknowns" in the methodology allows for an analytical derivation and expression of all system's state parameters - geometry, axial force in the main cables, tie forces etc. Some general conclusions about the influence of the pre-stress magnitude on displacements are made, also. The definition of the governing equations goes along with an analysis for unique solution for the systems. The commonly complex non-linear static analysis goes smoothly and is hidden behind a single governing equations system.

Keywords: cable, static, pre-stressed, non-linear

6.1. Theoretical model – general description and assumptions

Two-cable plane truss systems are composed from two types of elements: main cables and ties. The cases presented here follow the main ideas in (Mitashev, D., 2016) and account strictly for vertical ties. If the ties are inclined, the system gets more rigid, but at the end the inclination presents some difficulties only from mathematical point of view (for correct description of the system's geometry).

The main cables limit the system from above and below and the vertical ties are the connection between these main cables.

The main cables are two, one of them is convex down and the other one – up. They are usually called "bearing" and "prestressed". The structural function of the main cables depends on load position, pre-stress method etc.

The down-convex cable is assumed to be called "top cable", and the up-convex cable – "bottom cable".

The vertical ties connect the main cables. They can be designed as rods or/and cables. Of course, they can be designed as rods in any cases. Whether they can be designed as cables depends on the system configuration with account for all possible load cases.

The basic configuration of the system for which the theoretical study is made is as shown on Fig.6.1. From the obtained expressions, with accepting some variables as algebraic, the expressions for the other possible system configurations can be easily obtained. As an example, the distances l_i and h in (6.3) and (6.4) can get negative values.

There are three major system configurations, shown on Fig.6.1., Fig.6.2. and Fig.6.3.
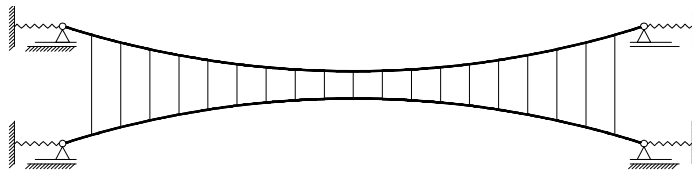

Fig. 6.1. System with vertical ties under tension

The system configuration shown on Fig.6.1. allows all vertical ties to be designed as cables.
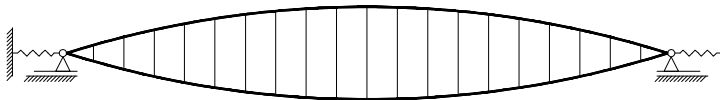

Fig. 6.2. System with vertical ties under compression

The system configuration shown on Fig.6.2. demands all vertical ties to be designed as rods because the inner system is under compression.
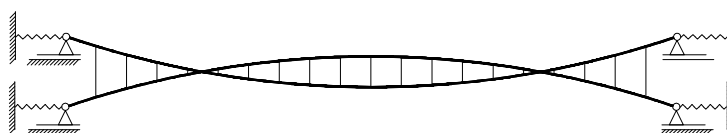

Fig. 6.3. System with vertical ties under tension & compression

The system configuration shown on Fig.6.3., allows the verticals between the supports and the inflection points of the main cables to be designed as cables, and demands for the rest of the ties to be designed as rods. That system is somewhat a mixed case of the other two and combines both their advantages and disadvantages.

General assumptions:

1. The main cables have constant cross section. The cross sections may be different for each of them independently.
2. The supports for each main cable are on the same level.
3. Vertical ties are accepted to be not-deformable. That is a common acceptance. It is assumed that vertical deformability has an insignificant influence on forces and displacements of the main cables. Some clarification on that issue is given in paragraph 6.3.
4. Forces are acting only in nodes. They are concentrated and vertical.
5. Main cables are with small sag (in the spirit of technical cable theory).
6. The structural material used behaves in accordance with Hooke's law. Strains are as for common structural materials i.e. small.
7. Due to the small sag of the main cables and their small deformability the loads are assumed to be acting along constant vertical lines.
8. Vertical ties of the system remain on these same vertical lines.
9. Elastic displacements of the supports do not influence the ratio between the lengths of the separate spans – that ratio remains constant while the total span of the system becomes smaller or larger.
10. When calculating the length of the main cables, because of their small sag, the square root under the integral in (6.21) is substituted with two members of the power series expansion.

11. Due to the main cables' small sag, normal forces in them are substituted with their horizontal projections for the small dimensions (variables) – elasticlengthening/shortening, temperature lengthening/shortening, support displacements. For that same reason instead of using the length of the cables the total span length is used.

It is seen from the assumptions listed above, that for the main cables the technical cable theory is accepted with two additional assumptions – that the verticals are non-deformable they remain constant on a vertical line.

6.2. Element numbering

The vertical lines that cross the supports and the verticals of the system are number from left to right with $0, 1, ..., n$. The separate spans between them have numbers $1, 2, ..., n$. That results in separate spans and boundary vertical line from their right side having the same numbers. The vertical ties have the same number as the vertical line they stand on i.e. $1, 2, ..., n-1$. All dimensions (variables) etc. corresponding to the top cable have an index of 1, and these for the bottom cable – 2.

Each of the main cables might be assumed as composed from a number of separate straight cables. They resemble the part of the main cable that is situated between two vertical lines. These separate cables and all dimensions (variables) etc. corresponding to them have a two-figure numbering: the number of the main cable and the number of the separate span they are in.

Nodes also have two-figure numbers – the number of the main cable and the number of the vertical line.

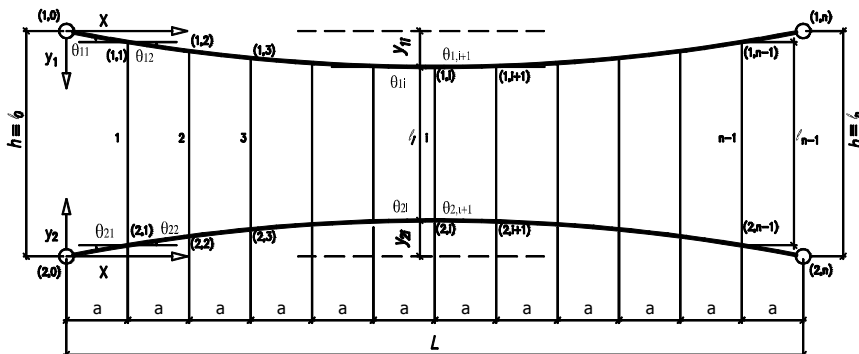All element numbering and some other designations are given on Fig.6.4.

Fig. 6.4. System scheme and element numbering

6.3. Main unknowns

It is assumed that for all load states of the system, the external loads like self-load, live-load, temperature etc. are previously known, exactly as for the geometric and physical characteristics of the cables. Unlike for the conventional truss system, knowing all these parameters here is not enough for unambiguousdefinition of the cable-truss system variables: cable forces, nodal displacements etc.

Cable-truss systems need additional variables to be defined and their type depends on specific problem solved. It is best for these variables to be defined in a way that allows a following simple definition and calculation of all other system variables, like forces, displacements etc. These additional variables are called "main unknowns". For the systems that are analyzed here, the most suitable main unknowns are the <u>thrusts</u> in the main cables $H_1 \; and \; H_2$.

The thrusts represent the horizontal projections of the normal forces in the main cables. According to the previously assumptions made, the thrusts $H_1 \; and \; H_2$ are constant in all sections of the corresponding main cable. It can be firstly assumed that these two thrusts are the horizontal projections of the reactions in the left supports.

The thrusts $H_1 \; and \; H_2$ give us the opportunity to define all other variables of the system. The expressions shown below give the ability to solve problems in which the thrusts are previously given, as well as problems where other variables are previously known. In that second case, we should use some of the expressions in order to define (calculate) the main unknowns.

6.4. System variables expressed by the main unknowns

With the assumptions previously made, each of the cables turns out to be loaded with only two kinds of nodal forces : external vertical forces applied in the nodes - $F_{\alpha i}$ and forces in the vertical ties $S_i \; (\alpha = 1, 2 \; ; \; i = 1, 2, ..., n-1)$. The forces $F_{\alpha i}$ are taken as positive when acting downwards. Forces in the vertical ties S_i are assumed to be positive if they are acting downwards for the top main cable and upwards for the bottom main cable. (Fig.6.5).
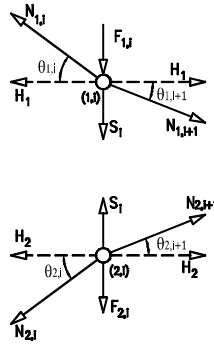
Fig. 6.5. Nodal external forces, main cable forces and forces in the vertical ties

According to the assumptions, the main cable ordinates y_{1i} and y_{2i} are calculated with the expressions

$$y_1(x) = \frac{M_1^{(SUB)}(x)}{H_1}$$

(6.1)

$$y_2(x) = \frac{M_2^{(SUB)}(x)}{H_2}$$

Positive ordinates for the top cable are measured downwards from the line, connecting the supports of the top cable.

Positive ordinates for the bottom cable are measured upwards from the line, connecting the supports of the bottom cable.

$M_1^{(SUB)}(x)$ and $M_2^{(SUB)}(x)$ are the bending moments in the so called "substituting beam".That beam is simply supported and has the same span and loading as the corresponding main cable. Bending moments are assumed to be positive when causing increase in length of the bottom fibers of the substituting beam. In the expression for y_2 is taken into account that these ordinates are taken as positive when measured upwards. The abscissas x are measured to the right from the vertical line crossing the left supports.

As long as the superposition principle is valid, the expressions (6.1) can be presented also as

$$y_1(x) = \frac{M_1(x) + M_S(x)}{H_1}$$

(6.2)

$$y_2(x) = \frac{-M_2(x) + M_S(x)}{H_2}$$

where:

$M_1(x)$ is the bending moment caused by the nodal forces F_{1i} acting on the top main cable

$M_2(x)$ is the bending moment caused by the nodal forces F_{2i} acting on the bottom main cable with $(i = 1, 2, ..., n-1)$.

$M_S(x)$ is the bending moment caused by the vertical forces S_i acting on the top main cable, again with $(i = 1, ..., n-1)$. In the expression for y_2 it is taken into account that these ordinates are taken as positive when measured upwards from the line connecting the supports. It is obvious that loads and forces acting on the bottom main cable shall have as a result bending moments with equal values and opposite signs.

Bending moments $M_1(x) \ and \ M_2(x)$ are practically known, because they are easily found by the loading given. The question about the bending moment $M_S(x)$ though is somewhat different. That bending moment is unknown because the forces S_i in the vertical ties are also unknown. In order to find the unknown forces S_i we need some additional relations.

One of the assumptions made previously was for non-deformability of the vertical ties. In all cases when the vertical ties work in compression and are designed as rods, their cross sections are usually significantly greater than needed for strength purposes – that comes as a result of their stability control check. So their linear elastic deformations become naturally small. The influence of the vertical ties is not substantial even in cases when they work in tension. That is because small elastic deformations of the vertical ties have as a result a significantly smaller change in the lengths of the main cables.

When the assumption for non-deformability of the vertical ties is taken into consideration, then between the node ordinates y_{1i} and y_{2i} of the main cables exists the following relation:

$$y_{1i} + y_{2i} + l_i = h \quad , \quad (i = 1, ..., n-1) \tag{6.3}$$

where:

-   l_i is the length of the vertical tie i. If the upper node of the vertical tie belongs to the top main cable, the length is taken as positive, and if it belongs to the bottom main cable – as negative.

-   h is the distance between the lines connecting the supports of the top and bottom main cables respectively. That variable is taken as negative in case the top

main cables supports are situated entirely under the bottom main cable supports (a modified system configuration of that shown on Fig.6.2., when the main cables are with supports on different levels).

The number of the equations (6.2) is equal to the number of the unknown nodal ordinates and the number of equations (6.3) – equal to the number of the unknown forces. Therefore equations (6.2) and (6.3) allow the unknown variables to be expressed by the main unknowns.

We shall define a polygonal function $\varphi(x)$. The functions' values for the vertical lines with abscissas x_i are:

$$\varphi_i = \varphi(x_i) = h - l_i \quad , \quad (i = 0,1,....,n) \tag{6.4}$$

The lengths of the start and end vertical lines l_0 *and* l_n are in fact the vertical distance between the supports.

The function $\varphi(x)$ is linear between the nodes of the system.

Then from (6.3) and (3.4) it is easily seen that:

$$y_{1i} + y_{2i} = \varphi_i \quad , \quad (i = 0,1,....,n) \tag{6.5}$$

One of the assumptions of the theoretical model is that on the main cables are acting only concentrated forces that are applied in the nodes and are with vertical direction. So we conclude that bending moments between the nodes for the "substituting beam" also change linearly. Then it follows from the relations (6.2) that the ordinates $y_1(x)$ *and* $y_2(x)$ of the main cables also change linearly.

As a conclusion, the relation (6.5) shall be valid for each value of φ_i, and so:

$$y_1(x) + y_2(x) = \varphi(x) \tag{6.6}$$

The function $\varphi(x)$ is ambiguously defined with its nodal values. These values are obtained from (6.4), while at the same time h and l_i do not change even if the loads change. Then according to the non-deformability assumption it follows that the function $\varphi(x)$ does not depend on the loads and remains with constant values in each load state of the cable-truss system.

The bending moment $M_S(x)$ can be expressed from (6.2) as:

$$M_S(x) = -M_1(x) + H_1 y_1(x)$$
$$M_S(x) = M_2(x) + H_2 y_2(x) \tag{6.7}$$

After considering the right sides of (6.7) being equal and some following transformations, we get the relation:

$$M_1(x) + M_2(x) = H_1 y_1(x) - H_2 y_2(x) \tag{6.8}$$

Expression (6.8), except the main unknowns H_1 and H_2, contains also the ordinates $y_1(x)$ and $y_2(x)$ in linear order. That gives us the opportunity using (6.6) and (6.8) to express these ordinates by the main unknowns:

$$y_1(x) = \frac{M(x) + H_2\varphi(x)}{H_1 + H_2} = \frac{M(x)}{H_1 + H_2} + \frac{H_2\varphi(x)}{H_1 + H_2}$$

$$y_2(x) = \frac{-M(x) + H_1\varphi(x)}{H_1 + H_2} = -\frac{M(x)}{H_1 + H_2} + \frac{H_1\varphi(x)}{H_1 + H_2} \tag{6.9}$$

where it is substituted:

$$M(x) = M_1(x) + M_2(x) \tag{6.10}$$

$M(x)$ in equation (6.10) is the bending moment in the substitution simply supported beam caused by the simultaneous application of all nodal loads on both the top and the bottom main cables. It is obvious that $M(x)$ can be accepted as previously known because it is dependable only from the nodal loads.

In expressions (6.9) loading is represented only by the summary bending moment $M(x)$. On the other hand, the bending moment $M(x)$ does not change if some of the loads acting on one of the main cables is transferred to the other main cable (but on to the same vertical line) i.e. if some of the concentrated forces are transferred vertically from one to the other main cable.

Furthermore, the main unknowns H_1 and H_2 and the ordinates y_1 and y_2 remain also unchanged. The reason for that is the previously made assumption for the vertical ties to be non-deformable. The ideally rigid body allows loads to be transferred in that manner while the equilibrium state of the body remains unchanged. But it is important to say, that the transition mentioned above changes the internal forces of the system.

The following expressions show that forces in the vertical ties are dependent of the application place of the loads – whether they are applied over the top or over the bottom cable.

With substitution of (6.9) in (6.7) we obtain the bending moment $M_S(x)$, that is a result of the forces in the vertical ties, now expressed by the main unknowns:

$$M_S(x) = \frac{H_1 M_2(x) - H_2 M_1(x) + H_1 H_2 \varphi(x)}{H_1 + H_2} \tag{6.11}$$

Expression (6.11) does not include the summary bending moment $M(x)$, but the bending moments $M_1(x)$ and $M_2(x)$ instead. The reason is that forces in the

vertical ties change when loads are transferred, even though the equilibrium of the system remains unchanged. So $M_S(x)$ is changing dependently of $M_1(x)\ and\ M_2(x)$, which on the other hand are dependable of the load application place (over the top or the bottom cable), and at the same time the summary bending moment $M(x)$ remains constant.

After differentiating of expressions (6.9) and using the relation $Q(x) = \dfrac{dM(x)}{dx}$ we obtain expressions for the inclination of the simple cables in function of the main unknowns:

$$y_1' = tg\theta_1 = \frac{Q(x) + H_2\varphi'(x)}{H_1 + H_2}$$

$$y_2' = tg\theta_2 = \frac{-Q(x) + H_1\varphi'(x)}{H_1 + H_2}$$

(6.12)

where:

$\theta_1\ and\ \theta_2$ are the angles between the tangent to the simple cables and a horizontal axis pointing to the right. The direction for measuring the angles $\theta_1\ and\ \theta_2$ is from the tangent towards the cable.

If we add and index i for each separate span, then (12) become:

$$y_{1i}' = tg\theta_{1i} = \frac{Q_i(x) + H_2\varphi_i'(x)}{H_1 + H_2}$$

$$y_{2i}' = tg\theta_{2i} = \frac{-Q_i(x) + H_1\varphi_i'(x)}{H_1 + H_2}$$

(6.13)

By using the expressions (6.12) we can obtain the normal forces in the separate simple cables. Inclinations, shear forces and the derivative $\varphi'(x)$ have constant values in the separate spans.

The normal forces in the separate simple cables are:

$$N_{1i} = \frac{H_1}{\cos\theta_{1i}}$$

$$N_{2i} = \frac{H_2}{\cos\theta_{2i}}$$

(6.14)

The forces in the vertical ties can be presented as concentrated forces, acting upon the substituting simply supported beam. Differentiating of (6.11) and taking into

account that bending moment derivatives are constant between the vertical lines i.e in the separate spans, we get:

$$Q_{Si} = \frac{H_1 Q_{2i} - H_2 Q_{1i} + H_1 H_2 \varphi'(x)}{H_1 + H_2} \qquad ,(i = 1,....,n) \qquad (6.15)$$

Now we separate a part of the substituting beam with sections placed on an infinite small distances to the left and to the right from a vertical tie (Fig.6.6). We must also remember that if in the node there is a concentrated load present, that load has already been taken into account in the shear force value.
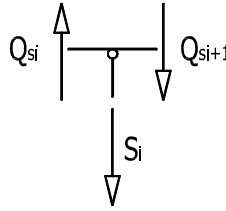

Fig. 6.6. Internal forces in vertical ties

If we write the equation for equilibrium $\Sigma V_i = 0$ we get the relation:

$$S_i = Q_{Si} - Q_{Si+1}. \qquad (6.16)$$

After expressing of Q_{Si} *and* Q_{Si+1} from (6.15), substituting in (6.16) and further transformations, the result for S_i is :

$$S_i = \frac{H_1(Q_{2i} - Q_{2i+1}) - H_2(Q_{1i} - Q_{1i+1}) + H_1 H_2(\varphi'_i - \varphi'_{i+1})}{H_1 + H_2} \qquad (6.17)$$

The same way as for (6.16) we obtain:

$$Q_{1i} - Q_{1i+1} = F_{1i} \quad u \quad Q_{2i} - Q_{2i+1} = F_{2i} \qquad (6.18)$$

Then (6.17) becomes:

$$S_i = \frac{H_1 F_{2i} - H_2 F_{1i} + H_1 H_2(\varphi'_i - \varphi'_{i+1})}{H_1 + H_2} \qquad (6.19)$$

In (6.19) forces in the vertical ties S_i are expressed by the main unknowns.

These forces can also be obtain by using the equation for equilibrium for the upper and/or lower node of the vertical tie (Fig.6.5) :

$$S_i = -F_{1i} + H_1(y'_{1i} - y'_{1i+1})$$
$$S_i = F_{2i} + H_2(y'_{2i} - y'_{2i+1}) \qquad (6.20)$$

In case of stationary supports without displacement, the lengths $\overline{L_1}$ *and* $\overline{L_2}$ of the prestressed main cables are calculated using the following expressions:

$$\overline{L_1} = \int_0^l \sqrt{1 + y_1'^2}\, dx \approx \int_0^l (1 + \frac{1}{2} y_{1i}'^2)\, dx + \frac{1}{2} \int_0^l y_{1i}'^2\, dx$$

$$\overline{L_2} = \int_0^l \sqrt{1 + y_2'^2}\, dx \approx \int_0^l (1 + \frac{1}{2} y_{2i}'^2)\, dx + \frac{1}{2} \int_0^l y_{2i}'^2\, dx$$

(6.21)

We substitute (6.13) in (6.21) and after some simple transformations we get:

$$\overline{L_1} = l + \frac{1}{2} \frac{D + 2BH_2 + CH_2^2}{(H_1 + H_2)^2}$$

$$\overline{L_2} = l + \frac{1}{2} \frac{D - 2BH_1 + CH_1^2}{(H_1 + H_2)^2}$$

(6.22)

where:

$$D = \int_0^l Q^2 dx = \sum_{i=1}^n Q_i^2 a_i \ ; \ B = \int_0^l Q\psi\, dx = \sum_{i=1}^n Q_i \psi_i a_i$$

$$C = \int_0^l \psi^2 dx = \sum_{i=1}^n \psi_i^2 a_i$$

(6.23)

The expressions (6.23) define the geometry and the loading of the cable-truss system. The geometry is defined by $\psi = \varphi'(x)$ and the loading influence is taken into account by the shear force $Q(x)$ in the substituting beam. In (6.23) for simplicity the substitution is:

$$\psi(x) = \varphi'(x) \ , \ \psi_i = \varphi_i' \qquad (i = 1, ..., n)$$

(6.24)

where:

φ_i' is the derivative of φ in separate span i and a_i is the span distance between the vertical ties of the system.

All expressions up to that point are made with the assumption of the supports not allowing displacement.

For the common structural systems support displacements turn out to have small values. That is the reason for them to be ignored in all expressions up to here, except in these for calculating the length of the cables. As we can see, expressions (6.22) consider these variables. Support displacements are small compared to the

cable length. Expressions (6.22) give us the differences between the cable lengths and the distance between the supports (the total span distance). These differences are small quantities.

Support displacements change the distances between the vertical lines and, and as a result, the expressions (6.25). These second members of (6.22) are small compared with the first – the total span distances. The increase of $\overline{d_1}$ and $\overline{d_2}$ are quantities of a higher order than the increase of the first member (the total span distances) and therefore they can be ignored.

If we take into account for supports' displacements, the lengths of the prestressed cables are presented as follows:

$$\overline{L_1} = l - \Delta_{\text{sup},1} + \frac{1}{2} \frac{D + 2BH_2 + CH_2^2}{(H_1 + H_2)^2}$$

$$\overline{L_2} = l - \Delta_{\text{sup},2} + \frac{1}{2} \frac{D - 2BH_1 + CH_1^2}{(H_1 + H_2)^2}$$

$$(6.26)$$

$\Delta_{\text{sup},1}$ and $\Delta_{\text{sup},2}$ are the mutual horizontal support displacements for the corresponding cable.

In this article we assume linearly-elastic supports that allow only horizontal displacements.

In that case we have:

$$\delta_{\text{sup},1} = \delta_{11}H_1 + \delta_{12}H_2$$
$$\delta_{\text{sup},2} = \delta_{21}H_1 + \delta_{22}H_2$$

$$(6.27)$$

where:

➢ δ_{11} is the mutual displacement of the top cable supports caused by thrusts $H_1 = 1$ u $H_2 = 0$

➢ δ_{22} is the mutual displacement of the bottom cable supports caused by thrusts $H_1 = 0$ u $H_2 = 1$

➢ δ_{12} is the mutual displacement of the top cable supports caused by thrusts $H_1 = 0$ u $H_2 = 1$

➢ δ_{21} is the mutual displacement of the bottom cable supports caused by thrusts $H_1 = 1$ u $H_2 = 0$

The Maxwell-Betti theorem states that:

$$\delta_{21} = \delta_{12}$$

$$(6.28)$$

From the cable lengths $\overline{L_1}$ *and* $\overline{L_2}$ when they are prestressed we can easily obtain their lengths L_1 *and* L_2 when they are not prestressed. Elastic changes in length are Δ_{e1} *and* Δ_{e2}. For calculation of L_1 *and* L_2 it is enough to subtract the elastic changes in length Δ_{e1} *and* Δ_{e2} from the prestressed cables' lengths $\overline{L_1}$ *and* $\overline{L_2}$.

The mutual horizontal displacements of the supports $\Delta_{\text{sup},1}$ and $\Delta_{\text{sup},2}$ can be written as:

$$\Delta_{\text{sup},1} = \Delta_{e1} + \delta_{\text{sup},1}$$
$$\Delta_{\text{sup},2} = \Delta_{e2} + \delta_{\text{sup},2}$$

(6.29)

The exact expressions for the elastic changes in lengths Δ_{e1} *and* Δ_{e2} are:

$$\Delta_{e1} = \int_{x=0}^{x=l} \frac{N_1}{E_1 A_1} ds = \frac{H_1}{E_1 A_1} \int_0^l (1 + \frac{1}{2} y_1^{'2}) dx$$

$$\Delta_{e2} = \int_{x=0}^{x=l} \frac{N_2}{E_2 A_2} ds = \frac{H_2}{E_2 A_2} \int_0^l (1 + \frac{1}{2} y_2^{'2}) dx$$

(6.30)

where:
- N_1 *and* N_2 are the normal forces in the main cables;
- E_1 *and* E_2 are the elastic material modulus of the main cables;
- A_1 *and* A_2 are the cross-sectional areas of the main cables.

The squares of the derivatives in (6.30) are small compared to the number 1 and they can therefore be ignored. We obtain the following simple expressions:

$$\Delta_{e1} = \frac{H_1 l}{E_1 A_1}$$
$$\Delta_{e2} = \frac{H_2 l}{E_2 A_2} .$$

(6.31)

After substituting (6.31) in (6.29) and taking into account (6.27), the lengths of the prestressed main cables expressed by (26) transform in:

$$\overline{L_1} = l - \delta_{11} H_1 - \delta_{12} H_2 - \frac{H_1 l}{E_1 A_1} + \frac{1}{2} \frac{D + 2BH_2 + CH_2^2}{(H_1 + H_2)^2}$$

$$\overline{L_2} = l - \delta_{21} H_1 - \delta_{22} H_2 - \frac{H_2 l}{E_2 A_2} + \frac{1}{2} \frac{D - 2BH_1 + CH_1^2}{(H_1 + H_2)^2}$$

(6.32)

On the right side of (6.32) there are variables from different order – the total span distance l is much greater compared to all other members.

We now introduce the variables $\Delta_1 \ and \ \Delta_2$ which are of the same order as the small members in (6.32).

$$\Delta_1 = l - \overline{L_1}$$
$$\Delta_2 = l - \overline{L_2}$$.
(6.33)

It follows from (6.32) and (6.33) that:

$$\Delta_1 = \delta_{11}H_1 + \delta_{12}H_2 + \frac{H_1 l}{E_1 A_1} - \frac{1}{2}\frac{D + 2BH_2 + CH_2^2}{(H_1 + H_2)^2}$$

$$\Delta_2 = \delta_{21}H_1 + \delta_{22}H_2 + \frac{H_2 l}{E_2 A_2} - \frac{1}{2}\frac{D - 2BH_1 + CH_1^2}{(H_1 + H_2)^2}$$
(6.34)

The newly introduced variables $\Delta_1 \ and \ \Delta_2$ have a very simple meaning. If they are positive/negative, they show how shorter/longer are going to be the non-prestressed cable lengths compared to the total span distance, i.e. how much the main cables shall need/lack" to be exactly equal to the total span distance.

It is assumed $\Delta_1 \ and \ \Delta_2$ to be called "insufficiencies" of the main cables for the given total span distance.

6.5. Governing equations for the main unknowns

If for any given load state the thrusts $H_1 \ and \ H_2$ are previously known, then all other variables of the system state can be easily found i.e. the system state is fully defined.

When the thrusts are known expressions (6.34) define the so called "insufficiencies". The case here is of known insufficiencies and solving the problem for obtaining the thrusts.

In that case expressions (6.34) become an equation system for obtaining the thrusts. The system can be written in the following form:

$$r_1(H_1, H_2) = \delta_{11}H_1 + \delta_{12}H_2 + \frac{H_1 l}{E_1 A_1} - \frac{1}{2}\frac{D + 2BH_2 + CH_2^2}{(H_1 + H_2)^2} - \Delta_1 = 0$$

$$r_2(H_1, H_2) = \delta_{21}H_1 + \delta_{22}H_2 + \frac{H_2 l}{E_2 A_2} - \frac{1}{2}\frac{D - 2BH_1 + CH_1^2}{(H_1 + H_2)^2} - \Delta_2 = 0$$
(6.38)

The left sides of $r_1(H_1, H_2)$ and $r_2(H_1, H_2)$ in expressions (6.38) are algebraic expressions of the main unknowns H_1 and H_2.

6.6. Governing equations for the main unknowns

The general problem, the same as in the case of a single cable, can be formulated in the following manner:

One load state, called initial state is fully defined, that is the starting "known state" of the system. Then a change in loads and/or temperature occurs. The goal is to define the new state of the system. That new state is called final state or "wanted state".

All common geometrical and physical variables for the two states are previously known: cross-sectional areas, elasticity modulus, linear temperature coefficients, vertical ties lengths (and so the nodal values of the function $\varphi(x)$. These variables are exactly the same for the two states – the known "initial state" and the wanted "final state".

We are also aware of the loads and temperatures for both states. The "initial state" is fully defined because the thrusts H_{01} and H_{02} are previously known.

The main unknowns for the wanted "final state" are the thrusts H_1 and H_2. Once defined, all other system variables for that state can be ambiguously calculated and so the state shall become fully defined.

All variables that are different for the two cases are named in the previously defined in paragraph 2 way – exactly the same for the "final state", and for the "initial state" - with adding the index "zero".

For composition of the governing equation of the problem we must first of all obtain the relation between the lengths of the two main cables. In general, they are different for the two states because of the temperature difference and the resulting elastic temperature deformations in the main cables:

$$\begin{aligned} L_1 &= L_{01} + \alpha_{t1}(t_1 - t_{01})l \\ L_2 &= L_{02} + \alpha_{t2}(t_2 - t_{02})l \end{aligned}, \qquad (6.39)$$

where:

α_{t1} and α_{t2} - linear temperature deformation coefficients for the main cables

t_{01}, t_{02}, t_1 and t_2 - temperatures of the main cables in the "initial" and "final" states.

When calculating the elastic temperature deformation (increase or decrease of length) with (6.39), instead of the main cable length the total span length is used. It is assumed that both the elastic temperature deformations and the difference

between the main cable and total span lengths are variables of small order. It turns out to be more suitable to solve the problem working with the insufficiencies instead of the main cable lengths. That's because in the following expressions all parts are of the same order. Taking into consideration (6.33), (6.39) easily gives us the relation between the insufficiencies for the "initial" and the "final" states:

$$\Delta_1 = \Delta_{01} - \alpha_{t1}(t_1 - t_{01})l$$
$$\Delta_2 = \Delta_{02} - \alpha_{t2}(t_2 - t_{02})l$$
(6.40)

The insufficiencies for the "initial" state Δ_{01} and Δ_{02} are calculated using (6.34) and with the naming style defined for that state (34) becomes :

$$\Delta_{01} = \delta_{11}H_{01} + \delta_{12}H_{02} + \frac{H_{01}l}{E_1 A_1} - \frac{1}{2}\frac{D_0 + 2B_0 H_{02} + C_0 H_{02}^2}{(H_{01} + H_{02})^2}$$

$$\Delta_{02} = \delta_{21}H_{01} + \delta_{22}H_{02} + \frac{H_{02}l}{E_2 A_2} - \frac{1}{2}\frac{D_0 - 2B_0 H_{01} + C_0 H_{01}^2}{(H_{01} + H_{02})^2}$$
(6.41)

The variables D_0, B_0 and C_0 here are calculated according to (6.23).

$$D_0 = \int_0^l Q^2 dx = \sum_{i=1}^n Q_{0i}^2 a_i \quad ; \quad B_0 = \int_0^l Q\psi\, dx = \sum_{i=1}^n Q_{0i}\psi_i a_i$$

$$C_0 = \int_0^l \psi^2 dx = \sum_{i=1}^n \psi_i^2 a_i$$
(6.42)

After calculating the insufficiencies for the "initial" state with (6.41) and (6.42), the use of (6.40) gives as a result the insufficiencies for the "final" state.

That leads the problem to solving the governing equations system (6.38). The variables D, B and C in (6.38) are also calculated using (6.34) with the characteristics for the "final state". The variables C and C_0 turns out to be exactly the same for both cases because they do not include the loading parameters.

The governing equations system consists of two cubic algebraic equations with both main unknowns included. Solving the system usually demands the use of numerical methods.

Most importantly, the very significant question about the solution being unique, still stays opened.

One of the well-known solutions of this type of systems belongs to Dmitriev and Kasilov (Dmitriev L.G., Kasilov A.V., 1974) The thrust in the main cables is derived

from an algebraic equation of the fifth power. The solution is somewhat easier than solving the (6.38) system, but it does not comply for the uniqueness demand!

6.7. Analysis of the governing equations

The governing equations (6.38) are in fact stationary conditions of a scalar function - $P = P(H_1, H_2)$.

In order for that to be correct it's needed and enough to have the following expressions proven true:

$$\frac{\partial r_1}{\partial H_2} = \frac{\partial r_2}{\partial H_1}$$

$$(6.43)$$

$$\delta_{12} - \frac{CH_1H_2 + B(H_1 - H_2) - D}{(H_1 + H_2)^3} = \delta_{21} - \frac{CH_1H_2 + B(H_1 - H_2) - D}{(H_1 + H_2)^3}$$

Expression (3.28) is assumed and the scalar function $P = P(H_1, H_2)$ can be delivered by an appropriate integration of the expressions r_1 and r_2 for the left parts of the equations.

We get the following:

$$P(H_1, H_2) = \frac{1}{2}\left[\begin{array}{l}(\delta_{11} + C_1)H_1^2 + (\delta_{22} + C_2)H_2^2 + \\ +2\delta_{12}H_1H_2 + \dfrac{D + B(H_2 - H_1) - CH_1H_2}{H_1 + H_2}\end{array}\right] + \overline{C} \quad (6.44)$$

In expression (6.44) $\overline{C}$ is an arbitrary constant. It's here assumed for it to be equal to zero. For simplicity it is assumed that:

$$C_1 = \frac{l}{E_1 A_1} \qquad ; \qquad C_2 = \frac{l}{E_2 A_2} . \qquad (6.45)$$

C_1 and C_2 have the physical meaning of elongations for the specific cable from the thrust. Obviously, by differentiation of (6.44), for the scalar function $P = P(H_1, H_2)$ we get the left parts of the equations (6.38). That proves the statement, that the governing equations (6.38) are in fact stationary conditions of the function $P = P(H_1, H_2)$.

$$r_1(H_1, H_2) = \frac{\partial P}{\partial H_1} = (\delta_{11} + C_1)H_1 + \delta_{12}H_2 - \frac{1}{2}\frac{D + 2BH_2 + CH_2^2}{(H_1 + H_2)^2}$$

$$r_2(H_1, H_2) = \frac{\partial P}{\partial H_2} = \delta_{21}H_1 + (\delta_{22} + C_2)H_2 - \frac{1}{2}\frac{D - 2BH_1 + CH_1^2}{(H_1 + H_2)^2}$$

(6.46)

The type and character of the function's stationarity (if the function has a maximum, a minimum or a stationary point) can be examined with a quadratic form of its second derivatives.

They are as follows:

$$\frac{\partial^2 P}{\partial H_1^2} = \delta_{11} + C_1 + \frac{D + 2BH_2 + CH_2^2}{(H_1 + H_2)^3}$$

(6.47)

$$\frac{\partial^2 P}{\partial H_1 \partial H_2} = \delta_{12} + \frac{D - B(H_1 - H_2) - CH_1 H_2}{(H_1 + H_2)^3}$$

(6.48)

$$\frac{\partial^2 P}{\partial H_2^2} = \delta_{22} + C_2 + \frac{D - 2BH_1 + CH_1^2}{(H_1 + H_2)^3}$$

(6.49)

By the above expressions we can see that their quadratic form can be presented as a sum of three quadratic forms with the following matrices:

$$T_1 = \begin{vmatrix} \delta_{11} & \delta_{12} \\ \delta_{21} & \delta_{22} \end{vmatrix} \qquad\qquad T_2 = \begin{vmatrix} C_1 & 0 \\ 0 & C_2 \end{vmatrix}$$

(6.50)

$$T_3 = \frac{1}{(H_1 + H_2)^3} \begin{vmatrix} D + 2BH_2 + CH_2^2 & D - B(H_1 - H_2) - CH_1 H_2 \\ D - B(H_1 - H_2) - CH_1 H_2 & D - 2BH_1 + CH_1^2 \end{vmatrix}$$

The quadratic form of the first matrix resembles the doubled potential energy of the supports' deformations and is:

$$2U_{\text{supports}} = H_1^2 \delta_{11} + 2H_1 H_2 \delta_{12} + H_2^2 \delta_{22} \geq 0$$

(6.51)

If the supports are horizontally elastic, it is positively determined, and if they're pinned – it's equal to zero.

The quadratic form of the second matrix resembles the doubled potential energy of the deformation of the cables. It is positively determined:

$$2U_{\substack{main \\ cables}} = C_1 H_1^2 + C_2 H_2^2 > 0 \qquad (6.52)$$

The quadratic form of the third matrix is examined with Sylvester's criterion. In order for it to be positively determined, it's enough the first major minors of each row of the matrix to be non-negative. In the case it means that the first element of the major diagonal and the determinant should be non-negative.

The first element of the major diagonal is non-negative, because according to (6.23) it can be represented as follows:

$$\int_0^l (Q + H_2\psi)^2 \, dx \geq 0 \qquad (6.53)$$

That element shall be equal to zero only if $Q + H_2\psi \equiv 0$ and with following the boundary conditions, when

$$y_1 = \frac{M + H_2\varphi}{H_1 + H_2} \equiv 0 \qquad (6.54)$$

The determinant is equal to

$$|T_3| = \frac{DC - B^2}{H_1 + H_2}. \qquad (6.55)$$

By assuming (IV.23), for the numerator we get:

$$(DC - B^2) = \begin{vmatrix} D & B \\ B & C \end{vmatrix} = \begin{vmatrix} \int_0^l Q^2 dx & \int_0^l Q\psi \, dx \\ \int_0^l Q\psi \, dx & \int_0^l \psi^2 dx \end{vmatrix} \geq 0 \qquad (6.56)$$

That's a Gramm's determinant and it's non-negative.

Because all three quadratic forms are proven to be positively determined, their sum is a positively determined quadratic form, also.

So, the scalar function $P(H_1, H_2)$ has a strict downwards convexity in the whole first quadrant, and its stationary point, if it exists, is a minimum.

The proven strict downwards convexity leads to the statement that the function has a single minimum, and by that – the solution of the governing equations' system delivers an unique solution.

6.8. Conclusions

The presented work shows that even complex geometrycally non-linear systems can be sometimes analyzed relatively easy. Article covers all analytical aspects for pre-stressed cable systems with vertical ties.

The methodics accounts for horizontally linear elastic supports and temperature difference.

Using a simple math software for implementing the methodics gives the oportunity to evade using more complex specialized softwares.

Ther most distinct difference with other known methods is the unique solution of the governing equations.

References

Mitashev, D. (2016) 'Static and dynamic analysis of planar cable systems', PhD. Thesis, UACEG, Sofia, Bulgaria

Dmitriev L.G., Kasilov A.V., Cable-stayed roof structures (analysis and construction), 1974, Kiev

7. A UAV-based 3D model for building condition monitoring

Anna Banaszek[1], Sebastian Banaszek[2], Anna Cellmer[3], Vicenç Gibert[4], Carles Serrat[5]

[1] *University of Warmia and Mazury, Faculty of Geodesy, Geospatial and Civil Engineering, Olsztyn, Poland, anna.banaszek@uwm.edu.pl, orcid.org/0000-0002-2744-2023*

[2] *DroneTechCamp Training and Research Center, Olsztyn, Poland, banaszek.sebastian@gmail.com, orcid.org/0000-0001-6470-6270*

[3] *Koszalin University of Technology, Faculty of Civil Engineering, Environmental and Geodetic Sciences, Koszalin, Poland, anna.cellmer@tu.koszalin.pl, orcid.org/0000-0002-7872-6325*

[4] *Universitat Politècnica de Catalunya-BarcelonaTECH, Dept of Architectural Technology, LABEDI-EPSEB, Barcelona, Spain, vicenc.gibert@upc.edu, orcid.org/ 0000-0001-6341-5762*

[5] *Universitat Politècnica de Catalunya-BarcelonaTECH, Dept of Mathematics, IEMAE-EPSEB, Barcelona, Spain, carles.serrat@upc.edu, orcid.org/0000-0002-1504-5354*

Abstract: The aim of the paper is to introduce a tool for the accurate assessment of the technical condition of buildings. The proposed methodology is becoming an efficient strategy for the massive inspection of building stocks, in big residential areas. The authors have developed an utility based on high-performance images captured by Unmanned Aerial Vehicles (UAVs). The flights of the UAVs have been technically protocolized in order to get the proper high-quality information about the real condition of the building. After collecting the images a 3D model is generated and orthophotos of building facades are created. The graphical information is connected with tables of attributes which allow the interactive geo-referenced management and assessment. Main requirements and advantages of this visualization technique will be presented by analyzing a particular case study. The selected example will allow the illustration of the methodology. Ongoing developments and technical details about the information system and the analysis platform connected with the visualization tool will be also reported.

Keywords: Condition monitoring, Unmanned aerial vehicles, inspection methodology, building facades

7.1. Introduction, motivation and background

"*Przybilla and Wester-Ebbinghaus (1979) did the first experiments with UAVs (Unmanned Aerial Vehicles) in photogrammetric applications. At that time, results were not sufficient because of the vibrations caused by the rotor which resulted in image motion. …With this system, it was possible to acquire images of an archaeological area, architecture and building sites…*" (Eisenbeiss, 2004). Twenty years later, Zischinsky, Dorfner and Rottensteiner (2000) used images taken from a model helicopter partly for the generation of a 3D-model of an historical mill. In the last two decades, there has been a growing demand in using UAVs for monitoring, surveillance and information collection tasks. The application contexts and the objectives are different and diverse: marine-oceanic missions (Rubio, Vagners and Rysdyk, 2004), (Reineman, Lenain and Melville, 2016), (Schaub *et al.*, 2018), natural disasters detection and monitoring (Alexis *et al.*, 2009), (Neto *et al.*, 2012), (Popescu, Ichim and Caramihale, 2015), surveillance of complex urban environments (Semsch *et al.*, 2009), among others. In some cases, also the use of multiple UAVs for a persistant surveillance aim has been also considered, and specific optimized algorithms have been studied (Nigam *et al.*, 2012).

Despite the above-mentioned applications and research, the use of UAVs for collecting accurate information in a building, aiming to asses and monitor its technical condition, has not been too much considered. Seminal studies have been developed by Eschmann *et al.* (2012), Hallermann, Morgenthal and Rodehorst (2015), Banaszek, Banaszek and Cellmer (2017) and by Serrat *et al.* (2018, 2019a, 2019b). Within this background, the main aim of this paper is to introduce the preliminary steps for a tool for the accurate assessment of the technical condition of buildings, as an efficient strategy for the massive inspection of building stocks, in big residential areas. The methodology is based on high-performance images captured by UAVs, and it is motivated by authors' previous works in the context of the Building Research Analysis and Information Network (Serrat and Gibert, 2011), (Serrat *et al.*, 2017).

The paper is organized as follows. In Section 7.2 the methodology will be introduced, in particular details on the flights mission and the 3D model will be given. Description of the case study, results and discussion will compose Section 7.3. The paper ends with a summary of the main conclusions.

7.2. Methodology

In recent years, research has developed following use of digital images obtained from the UAVs to monitor the technical condition of buildings and inventories of technical infrastructure. Conventional state-of-the-art inspections are primarily based on visual research methods. New UAV data acquisition technologies offer new opportunities in this field. The method of visual building inspection using UAV is generally divided into two stages: data acquisition (in-flight) and digital post-processing (post-flight) (Eschmann *et al.,* 2012). The type and quality of the data obtained using UAVs depends largely on installed on them sensor, the technical capabilities and planning of photogrammetric flights. The flight mission of the UAVs has been technically protocolized in order to get the proper high-quality information about the real condition of the building.

Based on that, the following methodology of a fully interactive visualization is proposed which is used for building condition assessment.

7.2.1. Data acquisition

7.2.1.1. Assessment of flight conditions (preparation for the flight mission).

Based on the available data sources including project documentation, maps, digital images, video, field vision, etc., the flight area is assessed: density of buildings, overhead lines, directional antennas and masts, height of chimneys, density of the stand, interference (WiFi networks, directional antennas), height of buildings.

For the assessment of meteorological conditions (see Fig. 7.1), the following is checked: a) temperature: average temperature, perceptible temperature, dew point temperature, b) precipitation: relative humidity, rainfall, snowfall, convective precipitation occurrence, sea level pressure, c) wind: average wind speed, maximum gusts of wind, wind direction, d) cloudiness: cloud base, cloud cover, fog.

Evaluation of the possibility of occurrence of undesirable phenomena such as a) downslope winds - arising at the edges of roofs, air collapse, b) turbulence - caused by dense buildings with objects of irregular shapes and a large number of other altitude objects and trees, c) strong wind gusts occurring in the urban canyons, significantly exceeding gusts indicated in local weather forecasts. Analysis based on available sources of national and international data: maps, weather forecasts, field vision.

The last step is checking the legal status of the property and the nearest neighbourhood based on available data sources including project documentation, geoportals, maps, land and mortgage registers, field vision. At this stage, it should

be checked whether the building subject to inspection is not located on or near the statutory prohibition of UAV flying.
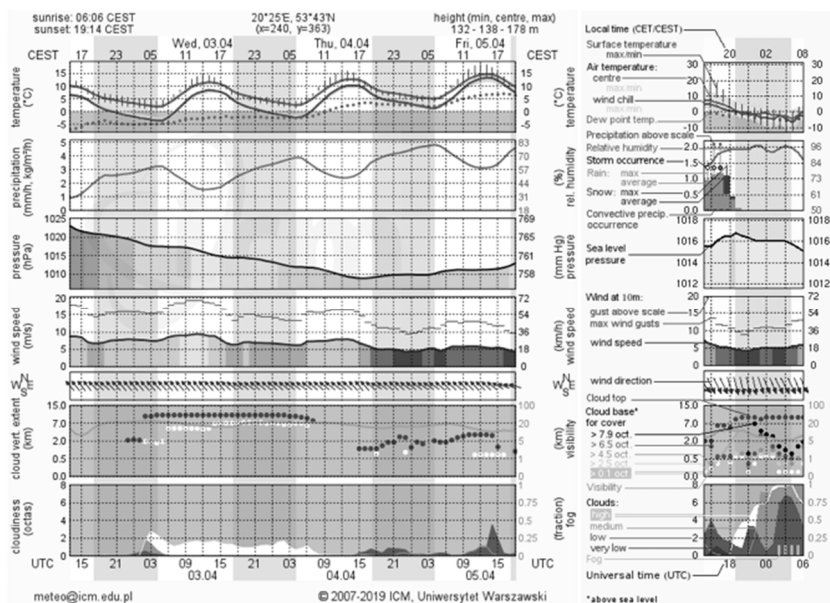

Fig. 7.1. Model UM – meteorogram

7.2.1.2. Law and airspace control (preparation for the flight mission).

The flight mission should be performed in accordance with national law. For example, in this research case study, using UAV for commercial and scientific purposes requires in Poland a qualification certificate of UAVO unmanned aircraft operator (a pilot certificate). This requires Art. 95 of the Law of July 3, 2002, Aviation Law, and the detailed rules for obtaining the certificate are contained in the Regulation of the Minister of Transport, Construction and Maritime Economy of 3 June 2013 on certificates of qualification. It is received by the operator after the completion of theoretical and practical training and passes the state examination, which is conducted by an examiner appointed by the Polish Civil Aviation Office. Civil air traffic in Poland is organized in accordance with international regulations provided by International Civil Aviation Organization (ICAO). Flight operations are performed in controlled airspace (CAS) or uncontrolled airspace. The division contains different approach to flight planning (FP) and group specific types of airspace users (AUs) and aircrafts types (Lichoń, 2017).

7.2.1.3. Selection of a suitable UAV and sensors.

The selection of an appropriate UAV is of key importance to the implementation of the flight mission. Due to the specificity of flights for the purpose of assessing the condition of buildings, the best results are achieved by multirotor (Eschmann *et al.*, 2012), (Nex and Remondino, 2014), (Zhou and Gheisari, 2018). Types of multirotors:

- Super light - weighing up to 0.6 kg (e.g. DJI MAVIC) - the biggest advantage is the weight, such UAVs are subject to simplified legal regulations, the biggest disadvantage is susceptibility to wind and turbulence.
- Lightweight - weighing up to 1.5 kg (e.g. DJI Phantom 4) - the biggest advantage is versatility, it can be used for most applications; the biggest disadvantage is the lack of an interchangeable sensor.
- Medium heavy - weighing up to 5 kg (e.g. DJI Inspire One, Yuneec Typhoon H520) - the biggest advantage is the replaceable sensor, it can be used for most applications; the biggest disadvantage is the short flight time.
- Heavy - over 5 kg (eg DJI MATRICE 600) - the biggest advantage is the possibility of using specialized heavy sensors, they can be used for most applications; the biggest disadvantage is inertia in flight.

The use of light and medium heavy Unmanned Aerial Vehicles is optimal for this type of flight mission. In the case of selecting a UAV with a non-replaceable sensor, a multirotor should be selected in such a way that the sensor RGB parameters allow to get the high-quality information about the real condition of the building. In the case of removable sensor, it should be noted how the installation of the sensor changes the parameters of the UAV which decided on its choice. Examples of technical parameters of sensors RGB according to the price range: a) low - 12 megapixel 1/2.3 inch, fixed lens; b) medium - 20 megapixels 1 inch, fixed lens; c) high - 24 megapixels, 4/3 inch, interchangeable lens.

For data recording, the digital camera is controlled by an automatic photo-firing sequence. Depending on the sensor and distance from the object, you can obtain the resolution of the BRD (Building Resolved Distance) at 0.3 mm BSD (Building Sampling Distance) at the level of 0.1-1.0 cm/pix.

$$BRD = d \cdot \frac{\Delta x_i}{f} \qquad (7.1)$$

where *BRD*: Building Resolved Distance,

  d: distance of the sensor from the facade/roof of the building,

  Δx_i: the size of the smallest detail of the facade/roof depicted in the picture,

  f: focal length of the sensor.

7.2.1.4. Flight mission.

The types of flight operations are: VLOS (Visual Line of Sight) operations in which the pilot or observer maintains direct eye contact with the UAV; FPV (First Person View) operations in which the operator pilots the UAV, not maintaining direct eye contact with him, determining its location in the airspace by the image transmitted in real time to the ground by devices mounted on its board; BVLOS (Beyond Visual Line of Sight) operations in which the UAV pilot does not maintain direct eye contact with unmanned aircraft, including automatic flights.

Due to the specificity of flight mission, VLOS operation flights are preferred. A detailed planning of a flight mission is a fundamental prerequisite for a successful acquisition of UAV data sets. VLOS flights for the purpose of visual building inventory and the creation of 3D model are performed according to standard rules.

The mission is normally planned with dedicated software. Hence manual flight control is currently still the only option to perform when flying close to a building and require from the UAV's operator to be highly skilled in piloting, assessing flight conditions and predicting in-flight abnormalities. According to Eschmann *et al.* (2012) there are two options of flight patterns available when using an UAV for the building inspection in order to have a images allocated to the real object in a structured way: on the one hand, the flight path can be allocated horizontally as a storey-wise scanning of the building, and on the other it can follow vertically aligned slices. Due to the technical aspects of UAV control and legal regulations, the flight close to a building should not be in circular patterns to capture information to ensure consistent overlap. Of course, there are professional photogrammetry and UAV mapping software that facilitate horizontal flight, for example, useful for roof inventory: https://www.pix4d.com/ Dedicated, Universal, and Open source (see Fig. 7.2).

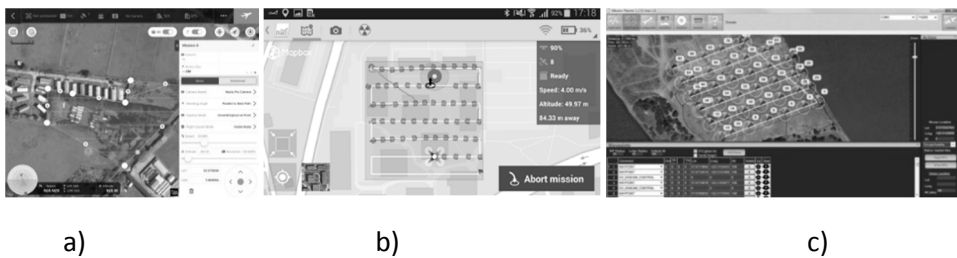a)   b)   c)

Fig. 7.2. UAV mapping software: a) Dedicated (DJI GS Pro app), b) Universal
Pix4Dmapper, and c) Open source APM (ArduPilot Multiplatform) Pilot

In Fig. 7.3 the red line presents the vertical flight plan, made for the purpose of generating the orthophoto facade (the flight is usually performed in manual

mode). The green line presents a horizontal flight plan, made for the purpose of generating the orthophoto roofs. This type of flight can be implemented using professional photogrammetry and UAV mapping software.

According to Nex and Remondino (2014) three primary flight modes have been identified. These are manual, assisted, or autonomous. In connection with the
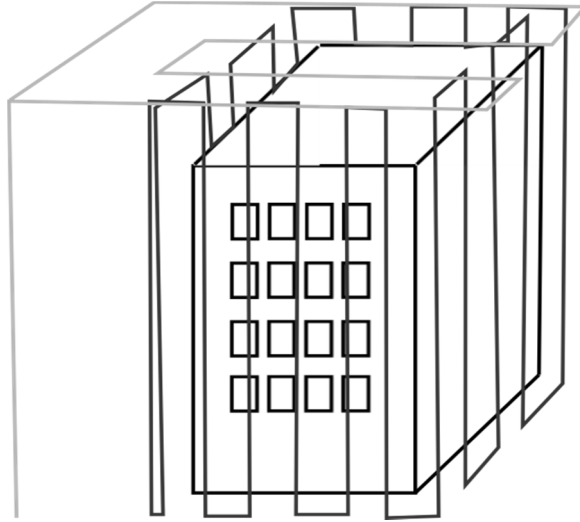

Fig. 7.3. Schematic UAV flight plan

above the flight should be implemented in a mode that provides control in any phase of the flight (GPS mode), however, due to interference near the buildings often should be selected the ATTI mode or manual (excluding some or all electronic flight assistance systems).

7.2.2. Digital Post-processing

7.2.2.1. Control of the data obtained from Unmanned Aerial Vehicles

In the manual flight mode, special attention should be paid to the quality control of the data obtained. During the inspection, the following is checked:

- Geometric accuracy of the flight line. Keeping on the designed flight's line is difficult due to variable wind conditions (including turbulence), interferences in the operation of UAV positioning systems and manual control mode.
- Minimum longitudinal and transverse overlap of digital images. Camera can be controlled manually to set zoom, focus and shutter release if necessary or controlled by an automatic photo-firing sequence and the short distance from the object makes it necessary to maintain a small flight speed. These factors have a negative effect on maintaining the correct parameters.

- Image quality. Better image quality is achieved more easily with larger pixels on sensors. High resolution sensors are required to provide the level of detail needed from an aerial digital image. Factors such as low fixed flight speed in manual mode, small distance to the object and variable lighting conditions have a negative impact on the quality of digital images acquired by UAV.
- Image exposure correctness. Obtaining homogeneous effects in terms of exposure is very difficult to achieve, due to weather conditions (clouds), terrain conditions (high objects casting a shadow), geometry of the object (complex shape), lens parameters (maximum aperture size), time of flight mission (changes in flight altitude and angle of sunlight), a large number of acquired images. Usually aerial images require a radiometric correction in the post-process.

UAV flight mission generates a large amount of data due to the automatic triggering of the camera. The number of photos is much greater than the amount needed for the next visual inspection. In addition, there is often a very large overlap of the area captured on each image, which varies depending on the speed of the hinge parallel to the facade of the building. Therefore, unnecessary records are eliminated if the overlap is too large to avoid double or multiple information in the images and to keep the image database as small as possible without losing quality (Eschmann *et al.*, 2012).

7.2.2.2 Generation of elevation and roof orthophotos

The standard process of generating the orthophoto map is shown in Fig. 7.4. Currently, highly specialized software is used for the generation of orthophoto. This allows the entire process to be performed in automatic mode, using standard processing settings or in supervised mode (supervised images classification) with the possibility of influence on selected processing parameters.
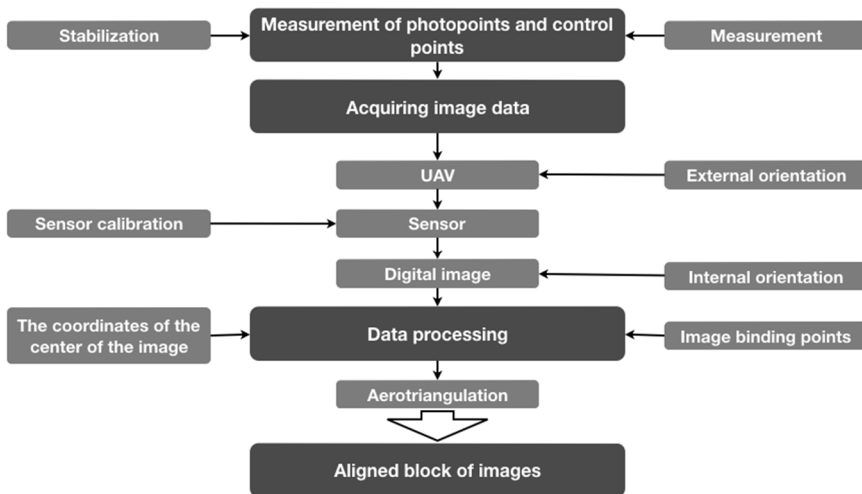

Fig. 7.4. The process of generating an orthophoto map based on UAV images

Regardless of the type of software used, generating a good quality orthophoto of the facade (see Fig. 7.5) is more difficult than generating a good quality orthophoto map or roof plan.

Fig. 7.5. Example of elevation orthophoto generated on UAV images, and enlargements

7.2.2.3. Generating a 3D model

Cleaning the point cloud and recalculating for the purpose of generating orthophotos also has a positive effect on improving the geometry and aesthetics of the generated 3D model. Originally, on the model generated automatically, there are numerous artifacts, especially in the area of roofs, antennas, chimneys, pillars, overhead lines and facade decorative elements. Not all of them can be eliminated by cleaning the point cloud or selecting the appropriate processing parameters. Other artifacts should either be accepted or corrected in a 3D graphics program. Nevertheless, from the authors' point of view, such interference in the material obtained is unacceptable.

7.2.2.4. Vectorization

The next step is vectorization and creation of attributes tables. Among the vector layers, the most commonly used are:

- Image layer (a point layer). A layer indicating the place of release of the shutter, enabling the preview of images taken directly in the analyzed part of the object, without the need to know their location in the catalog or name.
- Grid layer (a polygon layer). A layer containing a grid of squares of the selected size that allows linking the results of the inspections to a specific part of the object. It allows for qualitative and quantitative analysis of the phenomena studied, taking into account spatial and localization attributes.
- Analytical layer (a layer of polygonal most common). Comprising a vectorized content according to the analytical needs.
- Layer of forms (a point layer). A layer containing links to documents referring directly to a selected part of the space, enabling the preview of documents, including forms made during the field vision, without the need to know their location in the catalog or name

The most frequently used software at this stage is the open source QGIS solution; a commercial alternative can be, for example, ArcGIS software.

7.2.2.5. Interactive 3D model

Combination of previously developed elements:

- digital images - in the form of graphic files,
- orthophoto plans - in the form of raster files,
- information and analytical layers - in the form of vector files,
- text documents - in the form of * .pdf files,
- 3D model - in the form of files, e.g. * .obj

on one platform it allows intuitive use and easy access to data of interest to the user without the need to know the structure of names, file directories, databases or the ability to use specialized software.

7.3. Results and discussion

As a research case study, the building was selected taking into account the visible technical wear of the facade, the complicated shape and roof, and its location in a dense urban surrounding. The complex shape of the building caused the need to adjust the flight plan accordingly. The flight plan was developed separately for each of the 6 facades (see Fig. 7.6) and one for the whole roof, and 7 flights were planned and carried out in total. The location in dense urban buildings required great caution during the flight. The location of the sidewalks and the roadway next to the building caused the necessity of interrupting the flight when pedestrians or cars appeared, in particular buses. Despite considerable difficulties, the flight was carried out, which finally confirmed that the proposed solution can be used for the majority of buildings requiring a technical condition assessment.

The experiment uses the DJI Inspire One lightweight quadcopter with the following specifications: weight: 2935g, vertical GPS accuracy: 0,5 m (accuracy determination), horizontal GPS accuracy: 2,5 m (accuracy of X, Y coordinates), Climb speed: 5 m/s, max. drop speed: 4 m s, max. cruising speed: 22m/s (ATTI mode, no wind), maximum flight height: 4500 m ASL (Above Sea Level), max. wind force:10 m/s, flight time: 18 minutes, operating temperature: -10 ° to 40 ° C, size: 438x451x301 mm. Digital camera (RGB sensor) has been used to obtain digital images with the following specifications: 12Mpix resolution (4000x3000), physical size 6.170mm x 4.628mm, focal length: 3.55mm. The flight was carried out at high humidity and transient slight rainfall, the temperature was about +5 degrees, wind at about 5 m/s (in gusts up to 10 m/s).

As can be seen in Fig. 7.6, despite the difficult weather conditions, vertical flight lines, including the assumed longitudinal and transverse overlap, have been preserved.

During the flight, 818 photos with a volume of 4.06 GB were made. As part of the inspection, no blurry photos were found and all of them were included in the processing process performed in the Pix4D software.

A desktop computer with the following parameters was used for processing: CPU: Intel (R) Core (TM) i7-2600 CPU @ 3.40GHz; RAM: 16GB; GPU: NVIDIA GeForce GTX 750 (Driver: 25.21.14.1694). The total processing time in the first iteration with standard processing settings was almost 7 hours:

- Time for Point Cloud Densification - 3 hours. 44 min.
- Time for 3D Textured Mesh Generation - 28 min.
- Time for DSM Generation - 42 min.
- Time for Orthomosaic Generation - 1 hour. 42 min.

The following results of processing have been achieved:

- GSD at the level of 0.36 cm / pix.
- 817 out of 817 images calibrated (100%), 1 images disabled.

- 1.93% relative difference between initial and optimized internal camera parameters.
- Median of 13924.4 matches per calibrated image.

At this stage, it can be confirmed that the coating, despite the difficulties, was made correctly and the material can be used to generate the facade and roof elevation for the purpose of assessing the technical condition of the building. The final effect in the form of a 3D model generated in the 3rd iteration after cleaning the point cloud and recalculating the design is shown in Fig. 7.7.

7.4. Conclusions

In summary, according to the aim of the paper introduced in Section 7.1, in the context of a smart city where the monitoring and prediction on building condition is permanently assessed, a) a comprehensive protocol of flight missions has been established and, b) a full interactive visualization method based on high-quality images from UAVs has been developed.

Specifically, the proposed methodology is an efficient strategy for the massive inspection of building stocks, in big residential areas. The graphical information, collected and processed by the platform, is connected with tables of attributes which allow the interactive geo-referenced management and assessment.

Ongoing developments include the link of the inspection tables as well as the Followup-and-Decision QGIS analysis platform described in Serrat *et al.* (2017) in information and analytical layers, in order to prepare the corresponding monitoring and prediction assessment documents.
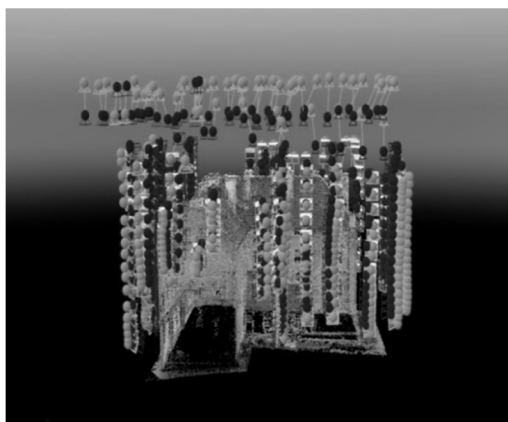
Fig. 7.6. Location of images (view of the west facade)

Fig. 7.7. 3D model generated after three iterations

Acknowledgements

References

Alexis, K. *et al.* (2009) 'Coordination of Helicopter UAVs for Aerial Forest-Fire Surveillance', in Valavanis K.P. (eds) *Applications of Intelligent Control to Engineering Systems. Intelligent Systems, Control, and Automation: Science and Engineering*, 39, pp. 169–193, Springer, Dordrecht.

Banaszek, A., Banaszek, S. and Cellmer, A. (2017) 'Possibilities of Use of UAVS for Technical Inspection of Buildings and Constructions', *IOP Conference Series: Earth and Environment Science*, 95, 032001, pp. 1–6.

Eisenbeiss, H. (2004) 'A mini unmanned aerial vehicle (UAV): system overview and image acquisition', *International Archives of Photogrammetry. Remote Sensing and Spatial Information Sciences*, 36(5/W1), pp. 1–7.

Eschmann, C. *et al.* (2012) 'Unmanned Aircraft Systems for Remote Building Inspection and Monitoring', in *6th European Workshop on Structural Health Monitoring,* Th.2.B.1, pp. 1–8.

Hallermann, N., Morgenthal, G. and Rodehorst, V. (2015) 'Unmanned Aerial Systems (UAS) – Case Studies of Vision Based Monitoring of Ageing Structures*', International Symposium Non-Destructive Testing in Civil Engineering (NDT-CE)*, Berlin, Germany.

Lichoń, D. (2017) 'Analysis of general aviation domestic air traffic structure in controlled airspace of Poland with refer to SESAR 2020, PJ.06-02 project solution', *Journal of KONES Powertrain and Transport, 24(3),* pp. 173–180.

Neto, J.M.M. *et al.* (2012) 'A surveillance task for a UAV in a natural disaster scenario', in *2012 IEEE International Symposium on Industrial Electronics*, pp. 1516–1522, 2012.

Nex, F. and Remondino, F. (2014) 'UAV for 3D Mapping Applications: A Review.' *Applied Geomatics*, 6 (1), pp. 1–15.

Nigam, N. *et al.* (2012) 'Control of Multiple UAVs for Persistent Surveillance: Algorithm and Flight Test Results', *IEEE Transactions on Control Systems Technology,* 20(5), pp. 1236–1251.

Popescu, D., Ichim, L. and Caramihale, T. (2015) 'Flood areas detection based on UAV surveillance system', in *19th International Conference on System Theory, Control and Computing (ICSTCC)*, pp. 753–758.

Przybilla, H.J. and Wester-Ebbinghaus, W. (1979) 'Image flight with remote-controlled small plane. Image Measurement and Aerial Imaging', *Journal of Photogrammetry and Remote Sensing*, Herbert Wichman Verlag, Karlsruhe.

Reineman, B.D., Lenain, L. and Melville, W.K. (2016) 'The use of ship-launched fixed-wing UAVs for measuring the marine atmospheric boundary layer and ocean surface processes', *Journal of Atmospheric and Oceanic Technology*, 33(9), pp. 2029–2052.

Rubio, J.C., Vagners, J. and Rysdyk, R. (2004) 'Adaptive path planning for autonomous UAV oceanic search missions', in *American Institute of Aeronautics and Astronautics 1st Intelligent Systems Technical Conference*, 6228, pp. 1–10.

Schaub, J. *et al.* (2018) 'Using unmanned aerial vehicles (UAVs) to measure jellyfish aggregations', *Marine Ecology Progress Series*, 591, pp. 29–36.

Semsch, E. *et al.* (2009) 'Autonomous UAV Surveillance in Complex Urban Environments', in *2009 IEEE/WIC/ACM International Joint Conference on Web Intelligence and Intelligent Agent Technology*, vol. 2, pp. 82–85.

Serrat, C. and Gibert, V. (2011) 'Survival analysis methodology for service live prediction and building maintenance', in *12th International Conference on Durability of Building Materials and Components*, Porto, Portugal, vol. II, pp. 599−606.

Serrat, C. *et al.* (2017) 'BRAIN: Building Research Analysis and Information Network', in *XIV International Conference on Durability of Building Materials and Components*, Ghent, Belgium, 325, pp. 1−11.

Serrat, C. *et al.* (2018) 'Quantitative comparison between visual UAV-based inspections for the assessment of the thecnical condition of building facades', in *Research and modelling in civil engineering 2018*, Eds J. Katzer, K. Cichocki and J. Domski, Koszalin University of Technology, pp. 19–29.

Serrat, C. *et al.* (2019a) 'Exploring Conditions and Usefulness of UAVs in the BRAIN Massive Inspections Protocol', *Open Engineering*, 9, pp. 1–6.

Serrat, C. *et al.* (2019b) 'Use of UAVs for Technical Inspection of Buildings Within the BRAIN Massive Inspection Platform', *IOP Conference Series: Materials Science and Engineering*, 471, 022008, pp. 1–9.

Zhou, S. and Gheisari, M. (2018) 'Unmanned aerial system applications in construction: a systematic review', *Construction Innovation*, 18(4), pp. 453–468.

Zischinsky, Th., Dorfner, L. and Rottensteiner, F. (2000) 'Application of a new Model Helicopter System in Architectural Photogrammetry', *International Archives of Photogrammetry and Remote Sensing (IAPRS)*, 33, B5/2.

8. Creating a web application to calculate predicted exploitative resistance to frost

Raminta Žurauskaitė[1], Marina Valentukevičienė[2], Ramunė Žurauskienė[3]

[1] *Vilnius Gediminas Technical University, Faculty of Fundamental Sciences, Vilnius, Lithuania, raminta.zurauskaite@stud.vgtu.lt*

[2] *Vilnius Gediminas Technical University, Faculty of Environmental Engineering, Vilnius, Lithuania, marina.valentukeviciene@vgtu.lt*

[3] *Vilnius Gediminas Technical University, Faculty of Civil Engineering, Vilnius, Lithuania, ramune.zurauskiene@vgtu.lt*

Abstract: A new program was created with a goal to ease material researchers' work by calculating predicted exploitation resistance to frost. Resistance to frost, conditional cold season amount and structural sample characteristics are calculated by inputting property values gotten during the experiment into the program's prepared windows – places designated for those values. Programming language Python was used for the new program's creation. In the newly created program user is presented with windows: starting in-formation data input, data gotten during the experiment input, as well as outputted intermediate and final calculation results. After the calculations researchers can generate a .pdf file which contains all the main information about carried out calculations and gotten results. This newly created program allows the simplification and acceleration of material researchers' work, as well as prevents mistakes gotten during calculations. The new program was expanded on by creating a web application for easier access. This application was created by a team using React and a programming language called Java.

Keywords: programming language Python, web application, React, programing language Java, exploitational resistance to frost, prediction of resistance to frost

8.1. Introduction

Predicted exploitational resistance to frost is calculated according to structural sample indicators (Malaiškienė et. al 2012). It is calculated by researching the longevity of ceramic materials and other porous building materials. This characteristic is important while comparing sample longevity, when created products from researched mass will be used in unprotected masonry in especially aggressive environment conditions. Physical sample properties and gotten data determined in the laboratory are used in formulas and sample structural indicators are calculated (Kizinievič et. al 2016). According to these indicators, after putting them into the formulas, it is possible to calculate predicted exploitational resistance to frost, as well as how many conditionally cold seasons from these masses (in determined conditions) created products can stay without disintegrating in these aggressive conditions.

Usually exploitational resistance to frost and other indicators are calculated using Microsoft Excel. Gotten sample property values and structure property calculation formulas are written into the program by hand. Each researcher does that individually. To calculate more precisely and faster structural sample characteristics, exploitational resistance to frost and conditionally cold seasons in this work a program created with Python programing language was used. After creating a new program researchers would not need to do all the calculations by hand. They, while in the laboratory, could input gotten weighing and measuring results directly into displayed input boxes in the window and by clicking the calculation button get both structural sample characteristics and final predicted exploitational resistance to frost results.

The goal of this work is to create a new program using Python programming language, which would be easy to incorporate into each user's device and would be easy and simple to use while doing the calculations. This new program would calculate exploitational resistance to frost and conditional cold season amount. This program was expanded on by creating a web application using React and programing language Java for easier access.

8.2. Used methods

For predictable exploitational resistance to frost calculation a program created with Python programing language was used, together with Tikinter (Roseman, 2007) and PyFPDF (PyFPDF, 2012) libraries and py2exe extension (Retzlaff, 2014). Python programming language is an interpreted, high-level, general-purpose programming language. The program's graphical user interface was written using Tikinter library functions. PDF file generated was created using PyFPDF.

This resistance to frost methodology is based on long-term laboratory research. When first samples were tested, their structural characteristics were determined, which are described in this article. Afterwards samples were tested according to resistance to frost methodology when wet samples were frozen and thawed. Freezing and thawing were on done one of the sides of the samples, this is called a one-sided freezing thawing method, when samples were mounted into a wall fragment and frozen and then thawed by pouring water on this wall fragment from one side. This method imitated façade product usage conditions.

Building ceramics predicted exploitative resistance to frost is calculated with this method, this methodology is sometimes used also in calculating concrete exploitative resistance to frost (Nagrockiene *et al*, 2004).

When predicting exploitational resistance to frost it is first determined if the sample is square shaped or not, then intermediate indicators are calculated.

Sample working surface area is calculated using:

$$S = a_a \cdot b_a, \text{cm}^2 \tag{8.1}$$

Where:
  a_a − sample lower surface area, cm,
  b_a − sample lower surface thickness, cm.

Sample volume is calculated using (when the sample is square shaped):

$$V = \left((a_a + a_v)/2\right) \cdot \left((b_a + b_v)/2\right) \cdot \left((h_1 + h_2)/2\right), \text{cm}^3 \tag{8.2}$$

Where:
  a_v − sample upper surface area, cm,
  b_v − sample upper surface thickness, cm,
  h_1 − sample height (one dimension is measured on the left), cm,
  h_2 − sample height (second dimension is measured on the right), cm.

Sample volume is calculated using (when the sample is non-square shaped):

$$V = \frac{m_4 - m_3}{\rho_V}, \text{cm}^3 \tag{8.3}$$

Where:
  m_3 − impregnated in vacuum sample mass in water, g,
  m_4 − impregnated in vacuum sample mass in air, g,
  q_V − water density, g/cm^3.

Derivative sample structure indicators are calculated (Malaiškienė et. al 2012). Sample effective porousness WE are calculated according to this formula:

$$W_E = \frac{m_0}{V} \cdot \frac{m_1 - m_0}{m_0} \cdot 100, \% \tag{8.4}$$

Where:
  m_0 − dry sample mass, g,
  m_1 − impregnated in normal condition sample mass, g,

V –   calculated sample volume water density, cm^3.

General sample porousness WR is calculated according to this formula:

$$W_R = \frac{m_0}{V} \cdot \frac{m_4 - m_0}{m_0} \cdot 100, \%$$ (8.5)

Structure direction unevenness indicator N is calculated according to this formula:

$$N = \frac{h_{max} - h_{min}}{h_{min}}$$ (8.6)

Where:

h_{max} –   biggest capillary rise after moistening front value, mm,

h_{min} –   smallest capillary rise after moistening front value, mm.

In further calculations intermediate indicators already calculated are used.

Porous space reserve R is calculated according to this formula:

$$R = \left(1 - \frac{W_E}{W_R}\right) \cdot 100, \%$$ (8.7)

Conditional pore and capillary wall thickness D is calculated according to this formula:

$$D = \frac{100 - W_R}{W_R}, \%$$ (8.8)

Capillary mass stream speed in normal conditions g1 is calculated according to this formula:

$$g_1 = \frac{m_2 - m_0}{S}, g/cm^2$$ (8.9)

Capillary mass stream speed in vacuum in freezing direction G1 is calculated according to this formula:

$$G_1 = \frac{m_5 - m_0}{S}, g/cm^2$$ (8.10)

Capillary mass stream speed in vacuum perpendicular to freezing direction G2 is calculated according to this formula:

$$G_2 = \frac{m_6 - m_0}{S}, g/cm^2$$ (8.11)

After calculating sample structural indicators according to sample effective porousness W_E variable an appropriate exploitational resistance to frost conditional cycle prediction formula is chosen.

According to sample effective porousness W_E value exploitational resistance to frost conditional cycles prediction formula is chosen.

Formulas 12-16 were derived by using laboratory research done in research laboratories and calculated structural indicator influence on exploitative resistance frost according to (Maciulaitis and Malaiskiene, 2010).

If $W_E \leq 26\ \%$, then sample disintegration start $F_{RE\ 1}$ is calculated according to this formula:

$$F_{RE1} = 0{,}231 \frac{R^{1,068} \cdot D^{1,345} \cdot G_1^{0,275} \cdot G_2^{0,663}}{N^{0,285} \cdot g_1^{0,830}}, \text{ conditional cycles} \qquad (8.12)$$

while sample disintegration end FRE 2 is calculated according to this formula:

$$F_{RE2} = 0{,}223 \frac{R^{1,465} \cdot D^{0,759} \cdot G_1^{0,383} \cdot G_2^{0,852}}{N^{0,168} \cdot g_1^{1,034}}, \text{ conditional cycles} \qquad (8.13)$$

If $W_E \geq 26$ %, then sample disintegration start $F_{RE\,3}$ is calculated according to this formula:

$$F_{RE3} = 0{,}051 \frac{R^{1,642} \cdot D^{2,332} \cdot G_1^{0,383} \cdot g_1^{0,852}}{N^{0,334} \cdot G_2^{1,145}}, \text{ conditional cycles} \qquad (8.14)$$

while sample disintegration end FRE 4 is calculated according to this formula:

$$F_{RE4} = 0{,}063 \frac{R^{1,813} \cdot D^{2,135} \cdot G_1^{0,179} \cdot g_1^{1,134}}{N^{0,395} \cdot G_2^{0,517}}, \text{ conditional cycles} \qquad (8.15)$$

Porous material longevity is calculated according to the formula which is derived according to 30 year weather observation results. It has been described several times in various scientific articles and are used in calculating product longevity in Lithuania, this methodologist starter is prof. R. Maciulaitis.

Porous material longevity is predicted with this empirical formula:

$$\tau = e^{3,31981 + 0,00524 F_{RE}}, \text{ conditionally cold seasons} \qquad (8.16)$$

Where:

τ –   conditionally cold seasons,

F_{RE} –   exploitational resistance to frost conditional cycles, F_{RE1} or F_{RE3} are used.

8.3. Results and example solutions

A program was created that allows the user to input required data about experiment and samples. Fig. 8.1 shows the program's input window, in which the user inputs starting data.

Fig. 8.1. The window for inputting starting information in the created program

After inputting starting data a second window can be opened, in which you can input values gotten during the experiment – variables (Fig. 8.2).

Fig. 8.2. The window for inputting information gotten from samples when the sample is of square shape (left) is of non-square shape (right)

Result window shows intermediate results and exploitation resistance to frost indicators (Fig. 8.3).

Fig. 8.3. The result outputting window

The program was tested by inputting real sample gotten variables. Two samples were used: square shaped sample exploitational resistance to frost calculation variables were input into appropriate program's variable windows (Fig. 8.4), outputted the results and generated a pdf file.

Fig. 8.4. The square shape sample variable input window with inputted values

The same was done with non-square shaped sample. Exploitational resistance to frost calculation determined variables were inputted into appropriate program windows, results were outputted and a pdf file was generated (Fig. 8.5 and Fig. 8.6).

Fig. 8.5. The generated pdf file of square shape sample

Predicted exploitative resistance to frost calculation

Date:
Sample series number: Non_square_sample
Sample composition:
Sample burning temperature:
Duration of time sample is held in highest burning temperature:
Sample form: Non-square

Starting data:

m0: 227.78   m1: 249.4
m2: 235.64   m4: 256.86
m6: 240.54   m6: 241.32
hmax: 35   hmin: 30
ba: 4.84   aa: 4.89

Results:

$S=23.425$ cm^2 $V=115.0$ cm^3
$WE=18.76$ % $WR=25.287$ %
$N=0.167$ $R=25.653$ %
$G1=0.545$ g/cm^2 $g1=0.336$ g/cm^2
$D=2.963$ $G2=0.578$ g/cm^2
FRE1=96 conditional cycles   FRE2=122 conditional cycles
ti=45 conditionally cold seasons

Fig. 8.6. The generated pdf file of non-square shape sample

After the sample calculation testing the new program is prepared for usage. It can be used by material researchers, predicting exploitational resistance to frost. The program is accessible to both students and researchers. It is presented to VGTU Building material and fire safety department.

For convenience sake the Python language program, with a new team, was recreated as a web application using Java programming language for back-end and React for front-end. Picture below shows the most basic looking version of the web application (Fig. 8.7).

Fig. 8.7. Basic display of the web application

For this application creation a project was initiated. A team was formed that reused the Python application's code (Fig. 8.8). to recreate the program in web application form. To keep track of the progress Github website was used as version control and a Trello board was set up to keep track of current tasks and their status (Github 2018).
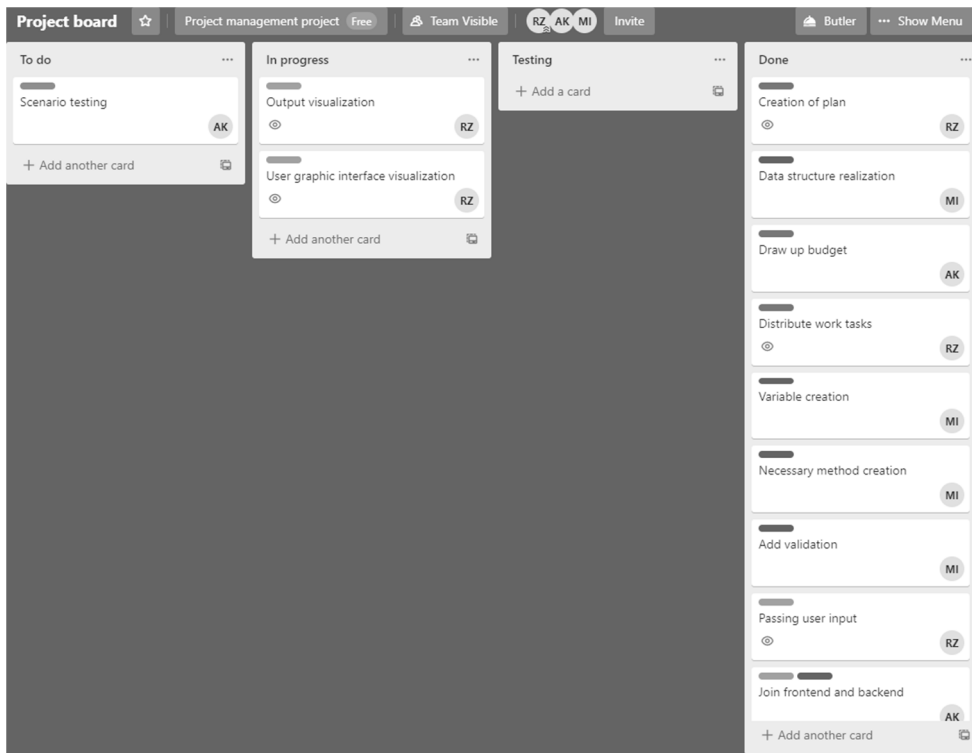
Fig. 8.8. Trello board used during the creation of the web application

8.4. Conclusion

1. Using Python programming language a new program was created. This program helps material science researcher's work with gotten laboratory sample results. Researchers can simply write in their gotten sample results into the program's window. The program displays the main calculation results – predicted exploitational resistance to frost and conditionally cold season amount.

2. Gotten results are more precise and trustworthy because of lower chance of mistakes and it lowers the amount of time used for calculations.

3. The created program allows predicting using both square and non-square shaped samples, which is convenient in the laboratory when a sample or a piece of a sample is being tested.

4. This program was expanded on by creating a web application using React and programing language Java for easier access.

References

Github repository for the project, 2018 [interactive] [last viewed on 2019 May 24th]. Access on the internet: https://github.com/Raminta-Zurauskaite/Projektu-valdymo-projektas

Kizinievič O., Žurauskienė R., Kizinievič V., Yakovlev G., Buryanov A. (2016). Use of sludge from drinking water purification in the production of effective ceramic articles. Glass and ceramics. New York: Springer. Vol. 73, iss. 1-2, p. 58-61.

Mačiulaitis Romualdas; Malaiškienė Jurgita. Frost resistant porous ceramics. Materials science = Medžiagotyra. Kaunas: Technologija. ISSN 1392-1320. Vol. 16, no. 4 (2010), p. 359-364.

Malaiškienė J., Žurauskienė R., Kizinievič O. (2012). Efektyvi statybinė keramika. Vilnius: TECHNIKA, 245 p.

Nagrockienė Džigita; Kičaitė Asta; Mačiulaitis Romualdas. Possibilities to forecast the frost resistance of constructional concrete. The 8th International conference "Modern building materials, structures and techniques" : selected papers : May 19-21, 2004 Vilnius, Lithuania. Vilnius: Technika, 2004. ISBN 9986057574, p. 120-123.

PyFPDF Reference Manual. 2012. [interactive] [last viewed on 2018 January 02nd]. Access on the internet: http://pyfpdf.readthedocs.io/en/latest/ReferenceManual/index.html

Retzlaff, J. 2014. Py2Exe - tutorial. [interactive] [last viewed on 2018 January 15th]. Access on the internet: http://www.py2exe.org/index.cgi/Tutorial

Roseman, M. 2007. TkDocs – Tk Tutorial, [interactive] [last viewed on 2017 December 20th.]. Access on the internet: http://www.tkdocs.com/tutorial/

9. The effect of steel fibres on selected properties of new generation of concrete

Tomasz Ponikiewski[1]

[1] *Silesian University of Technology, Faculty of Civil Engineering, Gliwice, Poland,*
Tomasz.Ponikiewski@polsl.pl, orcid.org/ 0000-0003-0535-2454

The paper presents results of tests on self-compacting mixtures with the addition of steel fibers (Steel Fiber Reinforced Self-Compacting Concrete). Considered are four types of steel fibers at 3 levels of the volume ratio. The results include studies on samples belonging to classes of slump flow SF, classes of viscosity T_{500}, and to rheological tests. The studies were based on two rheometers for rheological properties of concrete mixtures - BT2 Rheometer and Viskomat XL. Additionally, a study of compressive strength $f_{cm,28}$ and the flexural strength f_{fl} was carried out on concrete SFRSCC. These studies have confirmed the possibility of using steel fibers in concrete SCC while maintaining the assumed technological parameters for concrete mixtures and - above all - their workability. The long fibres (30 mm) are mostly oriented parallel to the flowability direction, vertically to the loading direction, and hence, they can operate efficiently under flexural loading. The orientation of fibers connected with the direction of the SFRSCC mix flow during moulding was confirmed.

Keywords: steel fibre, self-compacting concrete, rheology, flexural strength, X-ray

9.1. Introduction

The use of fibres in a cementitious system has led to many advantages in construction technology. It has been reported that fibres are effective in many ways, such as (Boulekbache *et al.*, 2010): (i) fibre reinforcement has been shown to improve the ductility, toughness, flexural strength and shear strength of cementitious materials; (ii) fibres bridge cracks during loading and transfer the load, arresting the growth and coalescence of cracks, playing the role of energy absorber; (iii) the fibres reduce the shrinkage, cracking and permeability of concrete; (iv) the fibres enhance fatigue and impact resistance; (v) the fibres take up internal stresses through their tension resistance and hence ensure the transfer of the loads, provided that a good bond exists between the fibres and the hardened cement matrix.

Analysis of the influence of fibers on the self-compacting and mechanical properties of concrete is one of the new tendencies in investigations of cement composites (Barragán *et al.*, 2004),(Ding *et al.*, 2004). The general improvement in the hardened self-compacting concrete properties with increased fiber volume is accompanied by lowered workability on casting. Other problems present themselves while dealing with the production of steel fiber modified SCC and their application. Therefore the workability of SFRSCC as well as the effect of fibres on the properties of fresh and hardened concrete mixture should be well recognized. The SCC mix design is not a simple task; every decrease in precise dosage of components, variable materials and curing conditions can result in manufacturing of material with no assumed properties: fluidity, ability to flow between the reinforcing bars as well as the resistance to segregation (Kaszyńska, 2003).

Short fibres with lengths of 10–30 mm are generally adopted in fibre reinforced concrete. These fibres are dispersed randomly in all directions so as to exhibit isotropic behavior. However, the real fibre distribution is strongly influenced by various factors such as fibre characteristics (diameter, length, and volume fraction), the fluidity of the matrix, placing method, and shape of the form (Kang *et al.*, 2011). The previous studies on random distribution of steel fibres in SFRSCC have not provided systematic experimental data to enable their design for their assumed mechanical parameters as well as the distribution and orientation of the dispersed reinforcement (Zerbino e*t al.*, 2012), (Kim *et al.*, 2008), (Ding *et al.*, 2012). This causes the discrepancy between the projected and obtained mechanical parameters of the modified concretes (Ding *et al.*, 2008), (Kang and Kim, 2011). It is important to determine the degree of variation in the mechanical properties of SFRSCC caused by the location and orientation of the dispersed reinforcement (Pająk and Ponikiewski, 2013), (Kang and Kim, 2011), (Tanikella and Gettu, 2008). Other studies have confirmed the variable and directional when using steel fibres in SCC during technological processes (Pająk and Ponikiewski,

2013), (Torrijos *et al.*, 2008), (Vandewalle *et al.*, 2008), (Yardimci *et al.*, 2008). The problems, also in the case of fiber reinforced cement composites, appear as technological difficulty during their production as well as with the formed concrete elements (Grünewald, 2004), (Rudzki et al., 2013), (Ponikiewski and Gołaszewski, 2012). Recognition of the real nature of workability and a definition of the impact that added fibers have on the phenomena occurring in fresh and hardened cement composites are needed. With the use of different type, shape, and strength of fibres, SCC can be tailored for more possible applications (Akcay and Tasdemir, 2012). At this point, however, it is vital to determine the effect of fibres on workability properties of SCC. The rheology parameters of the flowing material, particularly the yield stress and the wall effect generated by the geometry of the formwork, are the greatest influences on the orientation of the fibres within the fresh concrete. The distribution and orientation of fibres is, in turn, the parameter which influences the most the ductility of fibre concretes (Boulekbache *et al.*, 2010).

The current technological problems when applying cement composites modified with steel fibers as dispersed reinforcement are being discussed in the article. An analysis of fiber randomness influencing the workability and mechanical properties of fiber reinforced cement composite is dealt with as well. The concrete mixture was modified with steel fibers of various length and volume ratio. The results of workability tests of fiber reinforced cement mixes in the rheological context will be also presented. Research carried out by the rheometrical workability test was conducted with a new rheometer for concrete mixes Viscomat XL. The approximation of measurable results was done by the two-parameter Bingham rheological model, which allowed determination of two basic rheological parameters – yield value g and plastic viscosity h. The flexural tensile and compressive strengths of SFRSCC will be presented as well.

Self-compacting concrete technology allows one to form engineering structures in a faster and safer way than in the case of concrete with traditional characteristics. The technological procedures for forming structures from the self-compacting concrete are simpler by far with the final results enabling a broad display of hardened structures.

Equally important is the problem of uneven distribution of fibers in the volume of hardened concrete after completing the technological processes, indicated in the literature (Pająk and Ponikiewski, 2013), (Kang and Kim, 2011), (Grünewald, 2004). The problem with the application of mixtures using modified binders - fiber-cement, lies in the need to ensure even distribution of fibers in the volume of the molded component.

Past studies have shown the impact that the dimensions of a formed element have on the direction of fibers in the concrete mix. Uneven and directional deployment of reinforcements in the technological process brings some problems tied to the

randomness of fiber distribution in the volume of concrete. The analysis of mutually exclusive factors occurring with the addition of steel fibers to self-compacting concrete, namely the deterioration of workability, or even a complete loss of self-compatibility from one side to an increase in compressive concrete strength on the other, is discussed in this paper. The present work aims at investigating experimentally the relation between rheology, fibre distribution and mechanical properties of SFRSCC.

9.2. Experimental Procedure

The basic problem of the SCC, including those containing fibres, is their workability. From numerous studies which have considered the workability of mixture, it appears that it behaves under load as a viscoplastic Bingham body (Ponikiewski and Gołaszewski, 2012). The yield stress g and plastic viscosity h, called the rheological parameters are material constants, characterizing the rheological properties of the mixture according the formula:

$$\tau = \tau_o + \gamma\, \eta_{pl} \qquad\qquad (9.1)$$

where τ (Pa) is the shear stress at shear rate γ (1/s), τ_o (Pa) is the yield value and η_{pl} (Pa·s) is the plastic viscosity (Tattersall and Banfill, 1983). The physical interpretation of yield value is that of the stress needed to be applied to a material in order to start flowing. When the shear stress is higher then yield value the mix flows and its flow resistance depends on plastic viscosity. Rheological parameters of fresh mortar, like those of fresh concrete, can be measured using Two Point Workability Test (TPWT), by applying a given shear rate and measuring the resulting shear stress. Because of the nature of the rheological behaviour of cement mixtures, the measurements should be taken at no less than two considerably different shear rates. The rheological parameters are determined by regression analysis according to the relation:

$$T = g + N\, h \qquad\qquad (9.2)$$

where T is the shear resistance of a sample measured at rotation rate N and *g* (Nmm) and *h* (Nmms) are constants corresponding respectively to yield value τ_o and plastic viscosity η_{pl}. By suitable calibration of the rheometer, it is possible to express g and h in fundamental units. The principles of TPWT and rheological properties of fresh cement mortars and concretes are presented in existing literature (Tattersall and Banfill, 1983). The uniformity of distribution of steel fibers has been studied in SFRSCC molded as bars with dimensions of 600x150x150 mm.

9.3. Assumptions And Methodology Of Research

Results of workability tests of self-compacting cement mixes modified with steel fibres in rheological context are presented in this paper. Research was carried out with the rheometrical workability test (RWT) conducted with a rheometer for mortars and concrete mixes - Rheometer BT2 and Viskomat XL. RWT method was discussed in detail in literature (Tattersall and Banfill, 1983). An approximation of measurement results conducted by two-parameter Bingham rheological model. It allowed two basic rheological parameters - yield value *g* and plastic viscosity *h* to be determined by use of a two-parameter model. The composition of SFRSCC is shown in Table 9.1. Four types of steel fibres were used in the study (Table 9.2, Fig. 9.1). The self-compacting behavior was met by all tested concretes, according to adopted mixing procedure (Fig. 9.2). The obtained results are presented for samples with the fiber content 0.5 to 2.25% (40 to 180 kg/m^3). The self-compacting behavior was verified by the time and flow diameter measurements with Abrams cone as well as by the measured rheological parameters. The research used superplasticizers based on polycarboxylen ether. Fibers used for testing were chosen from a relatively large group of all those available on the market. The selection was aimed at demonstrating the effect of fibers with various geometric parameters on the workability of self-compacting mixtures. A procedure for the preparation of concrete mixes was developed and implemented which allowed for maintaining the technological reproducibility of the results. The sequence applied during the preparation of concrete mixes are presented in Figure 9.2.

Table 9.1. Composition of SFRSCC mixture, kg/m^3

Component	Symbol	Content kg/m3
CEM I 42,5 R	C	490,0
Sand 0–2 mm	S	756,0
Aggregate 2–8 mm	B	944,4
Water	W	226,4
Steel fibres – kg/m3 (% by volume)	F	20 – 160 (0.25 – 2.0)
Superplasicizer Glenium ACE 48 (3.5 % m.c.)	SP	17,0
Stabilizer RheoMatrix (0.4 % m.c.)	ST	1,6
W/(C+SF)	-	0,42
Slump-flow (SF)	-	SF1 – SF2

Table 9.2. Characteristics of applied steel fibres

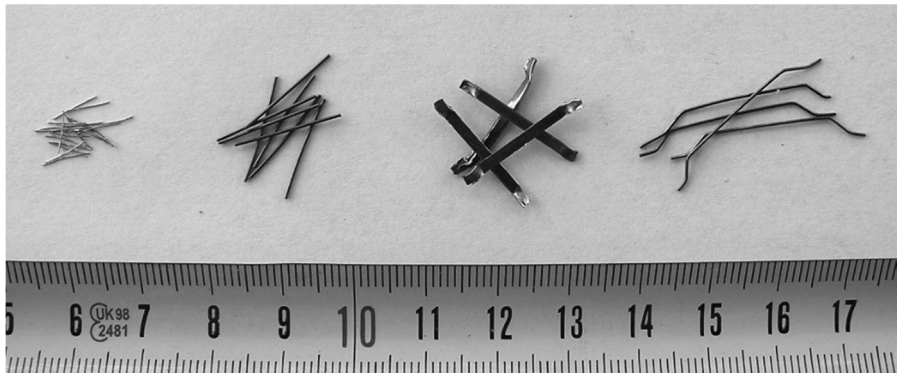| Name	Length (mm)	Diameter (mm)	Cross-section	Shape	Material	Tensile strength (N/mm^2)
DM 6/0.17	6±10%	0.17±10%	round		low-carbon steel	2100±15%
DG 12.5/0.4	12.5±10%	0.40±10%	round		low-carbon steel	1250±15%
KE 20/1.7	20±10%	1.70±10%	rectangular		DC01	770±15%
ST 30/0.5	35±10%	2.30±2.95	part of circle		low-carbon steel	800±15%

Fig. 9.1. Type of steel fibres used in the study: DM 6/0.17 ; DG 12.5/0.4 ; KE 20/1.7 ; ST 30/0.5
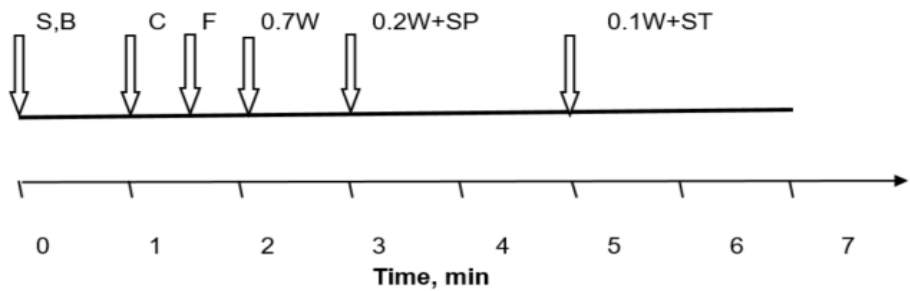
Fig. 9.2. Mixing procedure of SFRSCC

The basic problem of the new generation of concretes, including those containing fibres, is their workability. From the numerous studies which considered the workability of mixture it appears that it behaves under load as a viscoplastic Bingham body. The yield point g, plastic viscosity h, called the rheological parameters are material constants, characterizing the rheological properties of the mixture. Once the stress exceeds the yield point, the mixture will flow at a speed proportional to the plastic viscosity. The smaller the plastic viscosity of the mixture, the higher the velocity of flow at a given load. It is assumed that yield point g corresponds to the diameter of the maximum Slump-flow *SF*, while plastic viscosity h propagation time corresponds to a diameter of 500 mm T_{500}, both parameters were measured in the propagation test (Slump-flow) according to standard EN 12350-8:2009. The uniformity of distribution of steel fibers has been studied in SFRSCC molded and tested as bars with dimensions of 600x150x150 mm (RILEM TC162-TDF, 2000). The static flexural strength tests were conducted on a 200 kN servo-controlled actuator and the specimens were loaded at third points. A minimum of two samples were tested for each combination of fibers.

9.4. Study on the effect of dosage of steel fibers into SCC

Workability and rheological properties

The paper also presents selected research on self-compacting concrete with steel fibers. Figure 9.3 shows the effect of the type and volume ratio of steel fibers on the diameter of the SF propagation and on the propagation time T_{500} of SFRSCC mixtures. Based on the study carried out, it can be concluded that an increase in the content of steel fibres in the mixture reduces the diameter of the SF propagation and prolongs the propagation T_{500}. The shorter fibres in the mix, the greater the scope of change. Generally, the effect of deterioration on the workability of SFRSCC mixes with the addition of steel fibers is small, in the range of research 40-80 kg/m^3. The mixture is easy to apply, workable, but there is a phenomenon of an uneven distribution of fibers in the concrete. This effect is greater when the volume ratio of fibers in the mixture SCC increases and greatest in the SCC mix containing 100 kg/m^3 of steel fibers.
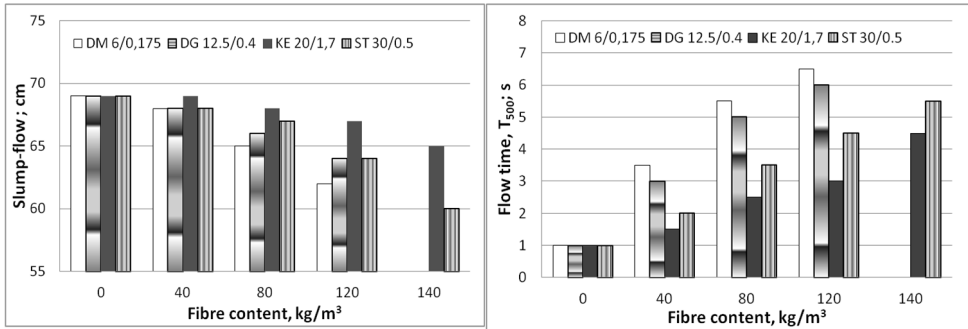
Fig. 9.3. Effect of steel fibres type and volume on slump-flow properties of SFRSCC; a) - slump-flow *SF* value; b) - flow time T_{500} value

Figure 9.4 shows the effect of the type and volume ratio of steel fibers on the rheological properties of SFRSCC according Viskomat BT2 research. It has been found that there is increasing rheological parameters yield value *g* and plastic viscosity *h* of self-compacting mixtures with increasing fiber content in the mixture. This effect is greatest for the SCC mixtures with ST 30/0.5 and DM 6/0.17 fibres. Increasing the content of KE 20/1.7 fibres showed no major changes in the values of *g* and *h* of SFRSCC with their addition.
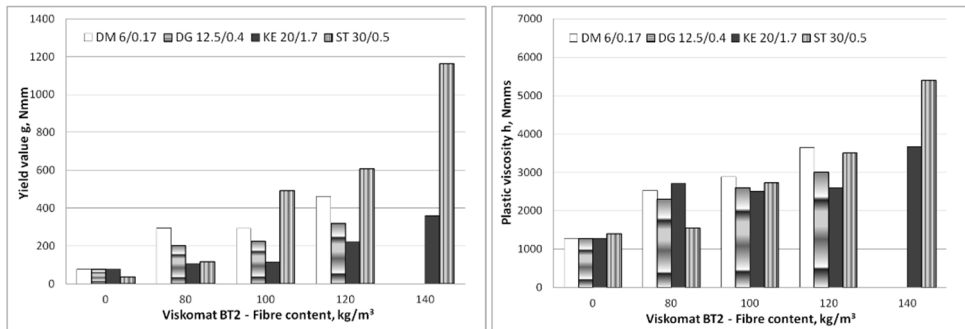
Fig. 9.4. Effect of steel fibres type and volume on rheological properties of SFRSCC according Viskomat BT2 research; a) - yield value g; b) - plastic viscosity h

Figure 9.5 shows the effect of the type and volume ratio of steel fibers on the rheological properties of SFRSCC according Viskomat XL research. It has been found that there is increasing rheological parameters yield value *g* and plastic viscosity *h* of self-compacting mixtures with increasing fiber content in the mixture as well. This effect is greatest for the SCC mixtures with DM 6/0.17 fibres.

Increasing the content of KE 20/1.7 fibres showed no major changes in the values of *h* of SFRSCC with their addition.
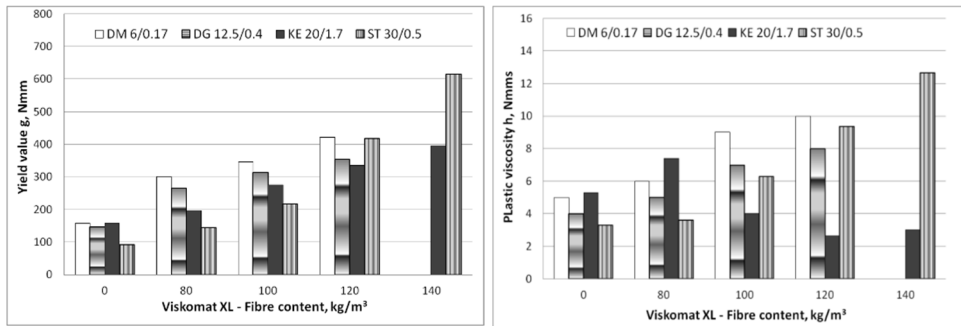

Fig. 9.5. Influence of steel fibres kind and volume on rheological properties of SFRSCC according Viskomat XL research; a) yield value g; b) plastic viscosity h

Flexural Strength Test and Compressive Strength Test Results

Flexural strength f_{fl} results for SFRSCC mixes with different type of fibres at different fibre volume fractions are shown in Fig. 9.6. The load-deflection curves obtained in this investigation for SFRSCC with different type of fibres at different fibre volume fractions are presented in Fig. 9.7 – 9.10. Figure 9.7 presents the load-deflection curves and compressive strength tests for SFRSCC with 40-80-120 kg/m³ of DM 6/0.17 fibres. Figure 9.8 presents the load-deflection curves and compressive strength tests for SFRSCC with 40-80-120 kg/m³ of DG 12.5/0.4 fibres. Figure 9.9 presents the load-deflection curves and compressive strength tests for SFRSCC with 100-140-160 kg/m³ of KE 20/1.7 fibres. Figure 9.10 presents the load-deflection curves and compressive strength tests for SFRSCC with 40-80-120 kg/m³ of St 30/0.5 fibres.

It can be seen from Fig. 9.7-9.10 that the maximum increase in flexural strength with respect to plain concrete was obtained for SFRSCC with St 30/0.5 fibres.

Figures 9.7 – 9.10 show the effect of the type and volume ratio of steel fibers on the compressive strength $f_{cm,28}$ of SCC. The effect of the fiber being tested on the value of $f_{cm,28}$ is small and with the increase their volume ratio, it is even negative. In the case of SCC concrete, such an effect can be explained by the irregular distribution of fibers in the matrix of concrete. Low fiber content does not cause such problems and the value of $f_{cm,28}$ for the tested concrete SCC increased. With

higher fiber content the effect of unevenness in their distribution became larger and resulted in a decline in the value of $f_{cm,28}$ in the tested SCC concrete.
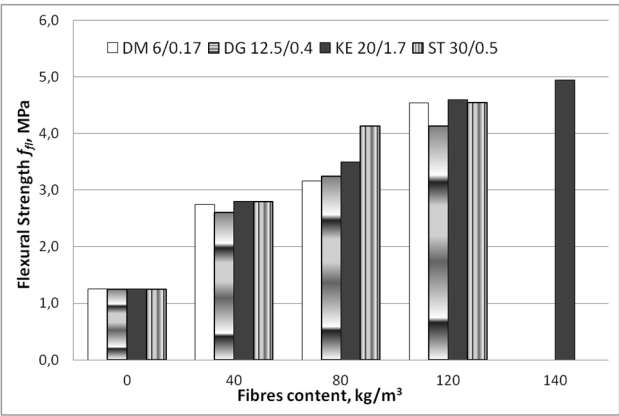

Fig. 9.6. Flexural strength ffl of SFRSCC with different fibres type and volume fractions
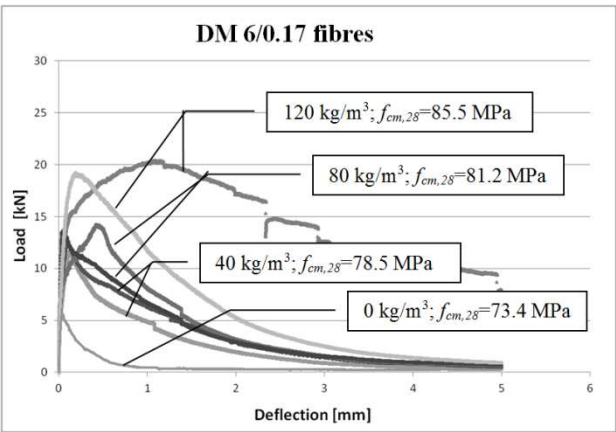

Fig. 9.7. Load-deflection curves and compressive strength tests for SFRSCC with DM 6/0.17 fibres (0 - 40 - 80 - 120 kg/m³)
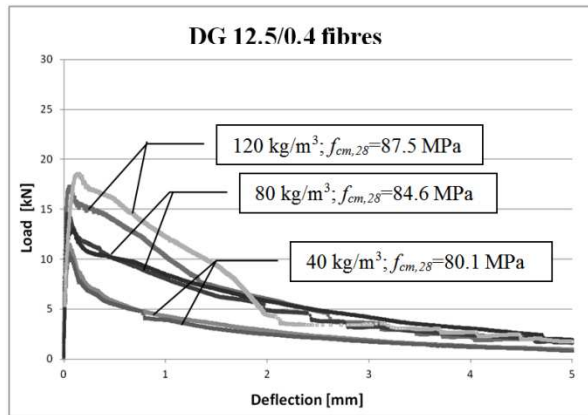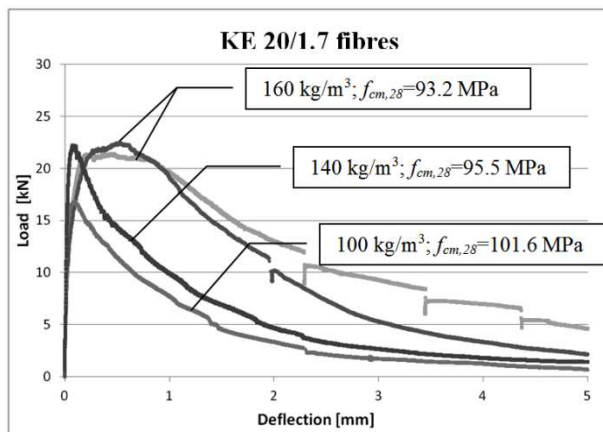
Fig. 9.8. Load-deflection curves and compressive strength tests for SFRSCC with DG 12.5/0.4 fibres (40 - 80 - 120 kg/m3)

Fig. 9.9. Load-deflection curves and compressive strength tests for SFRSCC with KE 20/1.7 fibres (100 - 140 - 160 kg/m3)
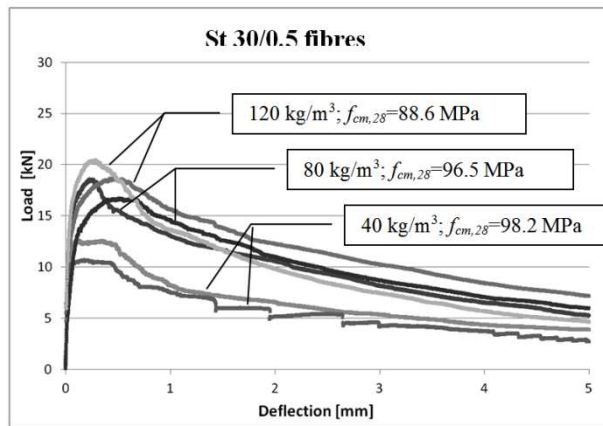
Fig. 9.10. Load-deflection curves and compressive strength tests for
SFRSCC with ST 30/0.5 fibres (40 - 80 - 120 kg/m³)

Figure 9.11 presents the flexural strength f_{fl} - yield value g curves for SFRSCC with
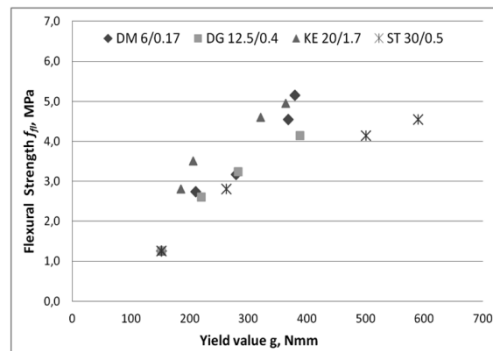all detected steel fibres.

Fig. 9.11. Flexural strength f_{fl} - yield value g curves for SFRSCC with steel fibres

In general, increasing yield value g causes linear increase of flexural strength f_{fl} of
SFRSCC but the increasing number of fibres affects the rheological properties of
the mix and its strength, while there is no cause and effect relationship between
these properties. So, the optimal fibre content and type according rheological and
mechanical can be used.

The computed tomography X-ray of 2D sections of SFRSCC beams, with F 30x0.7
mm fibres are presented in Figures 9.12 and 9.13. The 2D cross-section of the
concrete with ST 30x0.5 fibres, located at 0 - 10 - 20 - 30 - 40 cm from concreting
places is shown in Figures 9.12. In general, increasing distance between forming
places causes the trend of the orientation of fibres and irregular distributed in

SFRSCC. Fig. 9.13. X-ray 2D images of SFRSCC beams sections with ST 30x0.5 fibres located at 1 - 3 - 7 - 10 - 14 cm from its down surface.

The 2D image confirms the trend of the orientation of fibers in a matrix of concrete. The fibres are generally evenly distributed in concrete, with the exception of selected sections of the edge of the concrete.
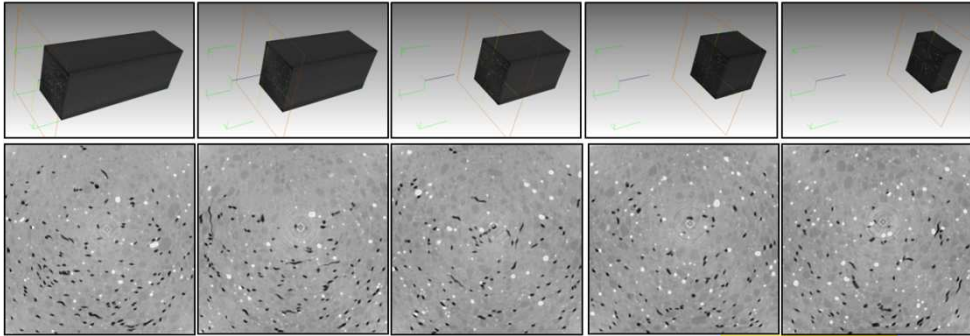

Fig. 9.12. X-ray 2D images of SFRSCC beams sections with ST 30x0.5 fibres; located at 0 - 10 - 20 - 30 - 40 cm from concreting places
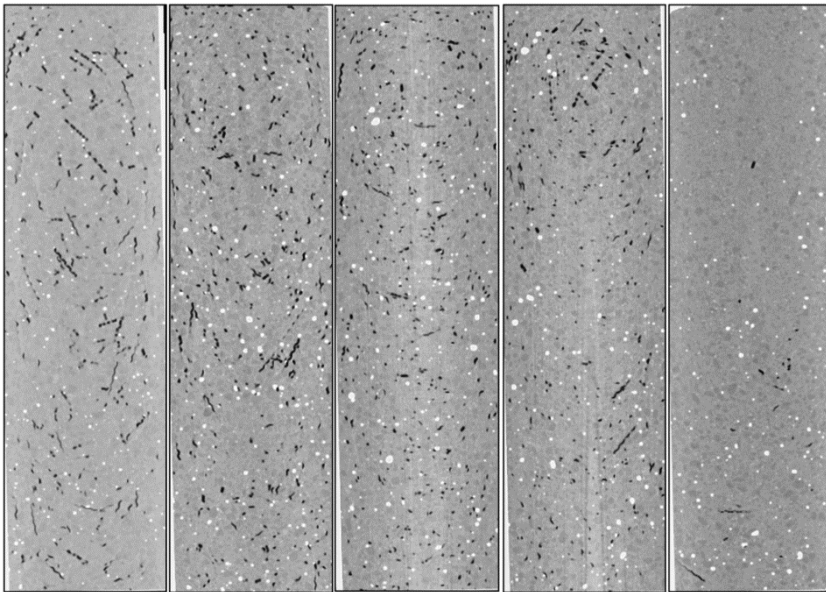

Fig. 9.13. X-ray 2D images of SFRSCC beams sections with ST 30x0.5 fibres; located at 1 - 3 - 7 - 10 - 14 cm from its down of beam

The 3D cross-section of the concrete with KE 20/1.7 fibre, laying between 400-500 mm from the surface of the sample, is shown in Figures 9.14. 3D image confirms the trend of the orientation of fibres in a matrix of concrete. The fibres are generally evenly distributed in concrete, with the exception of particular sections on the edge of the concrete.
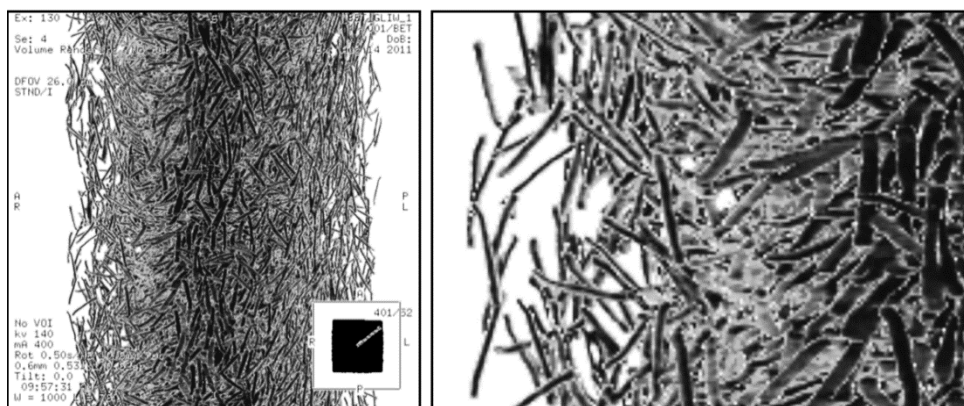

Fig. 9.14. X-ray 3D image of SFRSCC bars sections with KE 20/1.7 fibres located at 400 ÷ 500 mm from its surface

3.5. Conclusions

The main scope of the paper was to examine the characterization of rheology and mechanical properties of SFRSCC and to establish the optimal relationships between rheology and mechanical properties. Rheological properties, slump-flow workability, compressive strength and flexural strength of SFRSCC were investigated. Basing on experimental research, with application of the new rheological equipment and computed tomography, some preliminary results were obtained in the undertaken realm of investigation.

Decline in workability of concrete mixtures occurs, but to a certain extent the properties of self-compatibility are maintained.

The self-compatibility of concrete mixtures deteriorates with an increasing volume ratio of fibers in the mixture of self-compacting concrete. Despite the deterioration in the workability, it is possible to attain self-compatibility for mixtures with the addition of steel fibers and with good mechanical properties.

It was also shown that using the rheological properties of matrix with the content and geometry of fibre it is possible to predict the flexural strength of SFRSCCs.

The orientation of fibers connected with the direction of the SFRSCCs mix flow during moulding was confirmed. Proved as well was the uniform distribution of fiber in the produced concrete element.

References

Akcay B., Ali Tasdemir M. (2012) Mechanical behaviour and fibre dispersion of hybrid steel fibre reinforced self-compacting concrete. Construction and Building Materials 28, pp. 287–293.

Boulekbache B., Hamrat M., Chemrouk M., Amziane S. (2010) Flowability of fibre-reinforced concrete and its effect on the mechanical properties of the material. Construction and Building Materials 24, pp. 1664–1671.

Barragán B., Zerbino R., Gettu R., Soriano M., De la Cruz C., Giaccio G., Bravo M. (2004) Development and application of steel fibre reinforced self-compacting concrete. 6th RILEM Symposium on Fibre Reinforced Concrete FRC – BEFIB, Varenna, Italy, pp. 457–466.

Ding Y., Thomaseth D., Niederegger Ch., Thomas A., Lukas W. (2004) The investigation on the workability and flexural toughness of fibre cocktail reinforced self-compacting high performance concrete. BEFIB, Varenna, Italy, pp. 467–478.

Ding Y., Azevedo C., Aguiar J.B., Jalali S. (2012) Study on residual behavior and flexural toughness of fibre cocktail reinforced self compacting high performance concrete after exposure to high temperature. Construction and Building Materials 26, pp. 21–31.

Ding Y., Liu S., Zhang Y., Thomas A. (2008) The investigation on the workability of fibre cocktail reinforced self-compacting high performance concrete. Construction and Building Materials 22, pp. 1462–1470.

Grünewald S. (2004) Performance-based design of self-compacting fibre reinforced concrete. PhD thesis Delft University of Technology.

Kang S.T., Lee B.Y., Kim J.-K., Kim Y.Y. (2011) The effect of fibre distribution characteristics on the flexural strength of steel fibre-reinforced ultra high strength concrete. Construction and Building Materials 25, pp. 2450–2457.

Kang S.-T., Kim J.-K. (2011) Investigation on the flexural behavior of UHPCC considering the effect of fiber orientation distribution. Construction and Build. Mat. 28, pp. 57–65.

Kang S.-T., Kim J.-K. (2011) The relation between fiber orientation and tensile behavior in an Ultra High Performance Fiber Reinforced Cementitious Composites (UHPFRCC). Cement & Concrete Research 41, pp. 1001–1014.

Kaszyńska M. (2003) Mix design of the self-compacting concrete. in: Proc. Int. Symp. `Brittle Matrix Composites 7`, A.M.Brandt, V.C.Li, I.H.Marshall, Warsaw, pp. 331–338.

Kim DJ, Naaman AE, El-Tawil S. (2008) Comparative flexural behavior of four fiber reinforced cementitious composites. Cement & Concrete Composites 30, pp. 917–928.

Zerbino R., Tobes J.M., Bossio M.E., Giaccio G. (2012) On the orientation of fibres in structural members fabricated with self compacting fibre reinforced

concrete. Cement & Concrete Composites 34, pp. 191–200.

Pająk M., Ponikiewski T. (2013) Effect of the shape of steel fibers on the mechanical properties of reinforced self-compacting concrete. Cement Wapno Beton, Issue 6, November-December, pp. 335-342.

Ponikiewski T., Gołaszewski J. (2012) The new approach to the study of random distribution of fibres in high performance self-compacting concrete. Cement Wapno Beton, Vol. XVII/LXXIX, No. 3, pp. 165 - 176.

RILEM TC162-TDF (2000) Test and design methods for steel fibre reinforced concrete, Recommendations: Bending test, Materials and Structures, 33, Jan.-Feb.

Rudzki M., Bugdol M., Ponikiewski T. (2013) Determination of steel fibers orientation in SCC using computed tomography and digital image analysis methods Cement, Wapno, Beton, Issue 5, September – October, pp. 257-263.

Tanikella P.N.D., Gettu R. (2008) On the distribution of fibers in self compacting concrete. 7th RILEM Symposium on Fibre - Reinforced Concretes - BEFIB, RILEM Publications S.A.R.L Chennai, India., pp. 1147–1153.

Tattersall, G H, Banfill, P F G. (1983) The Rheology of Fresh Concrete. Boston, Pitman Books Limited.

Torrijos M.C., Tobes J.M., Barragán B.E., Zerbino R.L. (2008) Orientation and distribution of steel fibres in self-compacting concrete. ibid., pp. 729 – 738.

Vandewalle L., Heirman G., van Rickstal F. (2008) Fibre orientation in self-compacting fibre reinforced concrete ibid., pp. 719 - 728.

Yardimci M.Y., Baradan B., Taşdemir M.A. (2008) Studies on the relation between fiber orientation and flexural performance of SFRSCC. ibid., pp. 711-718.